May 2020

Effectiveness of Ground Improvement Around Piled-Raft for Tall Wind Turbines in Weak Soil: Analytical and Finite Element Analyses

Saphal Phuyal
Clemson University, saphalphuyal22@gmail.com

EFFECTIVENESS OF GROUND IMPROVEMENT AROUND PILED-RAFT FOR TALL WIND TURBINES IN WEAK SOIL: ANALYTICAL AND FINITE ELEMENT ANALYSES

A Thesis
Presented to
the Graduate School of
Clemson University

In Partial Fulfillment
of the Requirements for the Degree
Master of Science
Civil Engineering

---

by
Saphal Phuyal
May 2020

Accepted by:
Dr. Nadarajah Ravichandran, Committee Chair
Dr. Ronald D. Andrus
Dr. Kalyan R. Piratla

ABSTRACT

The generation of sustainable energy from wind has received global recognition in recent years. Large-scale wind farms with tall towers are required to meet the renewable energy demands. Taller towers produce higher power due to steady wind with higher speeds at higher altitudes. The site for building a wind farm is primarily selected based on wind conditions, accessibility to the site, and subsurface conditions. In cases where available land consists of soil with poor geotechnical properties, the construction of foundation can become expensive primarily when the foundation must sustain a substantial horizontal and moment loads induced by a tall wind turbine. In such a circumstance, the soil near the ground surface may be improved to enhance the strength and deformation properties of the soil to achieve substantial economic benefit. The study conducted shows the analytical design, 3D finite element analysis, and cost analysis for a piled-raft foundation for a tall wind turbine on in-situ and improved clays.

Initially, the analytical design of the piled-raft foundation for 80 m tall wind turbine on the in-situ soil was completed using the contemporary geotechnical design methods. The final design of the piled-raft foundation in the unimproved ground for design mean wind speed of 80 mph, consisted of 24 auger cast piles each 48.4 m long and 0.457 m in diameter. The raft was designed to be a circular raft, 8 m in diameter and 1 m in thickness. Then, five depths of ground improvement using cement soil mixing (CSM) around the piled-raft foundation were considered, and analytical design was performed for each case. The five successive depths of ground improvement correspond to 0.25, 0.3, 0.35, 0.4, and

0.45 times the diameter of the raft. Two design approaches were used: the first one was to determine the effectiveness of the ground improvement and the second to evaluate the performance. For the first design approach, the length of the piles was adjusted while keeping the number of piles, the diameter of the raft, and the cross-section of pile constant to meet the safety and serviceability requirements. The length of the pile decreased by 79.64 % for the highest depth of ground improvement in comparison with the unimproved case. On the other hand, the differential settlement increased by 73.91 %, and lateral deflection increased by 57.57 % due to the shortening of piles, but these deformations were within the design requirements. For the second approach, the length of the pile was kept constant at 48.4 m, and the deformation behavior of the piled-raft was studied. The differential settlement decreased by 12.9 %, and lateral deflection decreased by 33.05 %. The factor of safety against axial load increased by 104.9 %, and the factor of safety against the moment increased by 126.4 %.

To gain further insights into the performance of the piled-raft foundation, three-dimensional finite element models for the piled-raft foundations and supporting soil were created and analyzed using ABAQUS. The FE model created adopting the design outcome from the first approach from analytical design (length of pile varies with ground improvement) lead to a 16.37 % increase in horizontal deflection and 56.67 % increase in differential settlement for the highest level of ground improvement. The FE model created adopting the design outcome from the second approach from analytical design (length of the pile remains constant with ground improvement) leads to a 29.38 % decrease in horizontal deflection and a 1.1 % decrease in the differential settlement.

A parametric study was performed by varying the undrained shear strength of soil by ±1standard deviation (σ). The length of the pile increased by 24.38 % with positive variation in undrained shear strength and decreased by 17.36 % with negative variation in undrained shear strength soil. Cost analysis performed by adopting the length of the pile for various cases of ground improvement led to the conclusion that ground improvement reduced the total cost of the foundation.

Keywords: wind turbine, piled-raft foundation, ground improvement, renewable energy

DEDICATION

To my loving late grandmother Mrs. Subha Kumari Phuyal

and

to all the victims of the pandemic Covid-19.

ACKNOWLEDGMENTS

I would like to express my utmost gratitude to my advisor **Dr. Nadarajah Ravichandran** for the invaluable knowledge and insights provided for the completion of this thesis. I am hugely indebted to him for the encouragement, guidance, support, and criticism to help me achieve my academic goals. Not only his research guidance but his spirited mentorship on life during my time in graduate school has equipped me with essential life-lessons.

I would also like to thank the defense committee members **Dr. Ronald D. Andrus** and **Dr. Kalyan R. Piratla,** for their support and for taking their valuable time in reviewing my thesis.

Thank you to all the faculties and staff at Glenn Department of Civil Engineering for making my study smooth and pleasant. Thank you, all my friends, for your love, support, and making my journey enjoyable.

My parents Subarna and Sudha, thank you for the endless love and affection, encouragement, support, and opportunities you have provided for my entire life. Sandhya and Sagar for being the best siblings and always having my back.

TABLE OF CONTENTS

Page

Table of Contents (Continued)

Page

Table of Contents (Continued)

Page

Table of Contents (Continued)

Page

LIST OF TABLES

LIST OF FIGURES

List of Figures (Continued)

Page

List of Figures (Continued)

Page

List of Figures (Continued)

Page

List of Figures (Continued)

Page

CHAPTER 1

INTRODUCTION

1.1 Global energy demand and supply

The global energy demand has been escalating quickly in recent times and has grown by 2.9 % in 2018 alone (BP, 2019). The energy demands are met from sources like oils, natural gases, coal, nuclear energy, hydroelectricity, wind, solar, biofuels, geothermal sources, etc. The bulk share of energy is derived from fossil fuel, which has contributed to global warming and climate change because of large carbon emissions. The Emission Gap Report 2019, published by the United Nations Environment Program (UNEP), showed greenhouse gases (GHG) emissions have been rising at an alarming rate of 1.5 % annually in the past decade. The GHG emissions attained an unprecedented 55.3 $GtCO_2e$ in 2018. The CO_2 emissions increased by 2.0 % in 2018, to a record-high 37.5 % $GtCO_2e$ per year (UNEP, 2019). The global GHG should be lowered by 25 % and 55 % of emissions in 2018, to constrain global warming to under 2˚C and 1.5°C, respectively, by 2030 (UNEP, 2019). Nuclear energy is another popular source of primary energy and can provide an uninterrupted generation of power. However, the proper disposal of nuclear waste has been a genuine concern, and the consequences of nuclear power plant failures are catastrophic, as observed from nuclear tragedies in Fukushima and Chernobyl. The best possible way to overcome such long-term issues is to develop sustainable and renewable energy sources.

The production of energy from renewable sources to reduce the usage of fossil fuels to limit GHG emission is today's necessity. Figure 1.1 shows the share of consumption of

energy by sources in the past and the predictions for the future. This figure reveals the decrease in the use of fossil fuel and the subsequent increase in the use of renewable energy over the forthcoming years.

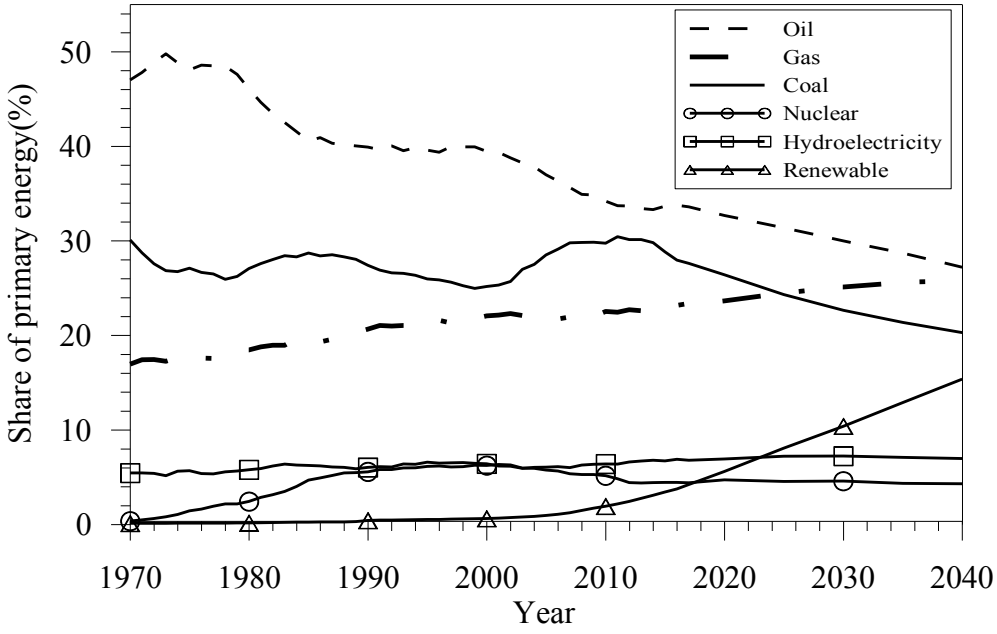

Figure 1.1. Percentages of global energy consumption by source type and data forecast (Data source: BP, 2019)

1.2 Growth of wind and other renewable energy

Wind energy production is swiftly growing as one of the most popular renewable sources of energy globally. Construction of many small and large-scale windfarms has increased in recent years to boost the generation of wind energy. Figure 1.2(a) shows the percentage of total energy generated by the wind, solar, and biomass and geothermal sources globally in the past and the prediction for the future. Wind and solar energy are predicted to meet around 14% and 12% of the global energy production, respectively, by

2040 (BP, 2019). Approximately 11% of the total energy generated in the USA in 2018 was from renewable sources (U.S. EIA, 2018). Figure 1.2(b) shows the percentage share of renewable energy consumed in the USA. This figure shows wind energy to be one of the primary renewable energy sources contributing to 22 % of total renewable energy consumption.

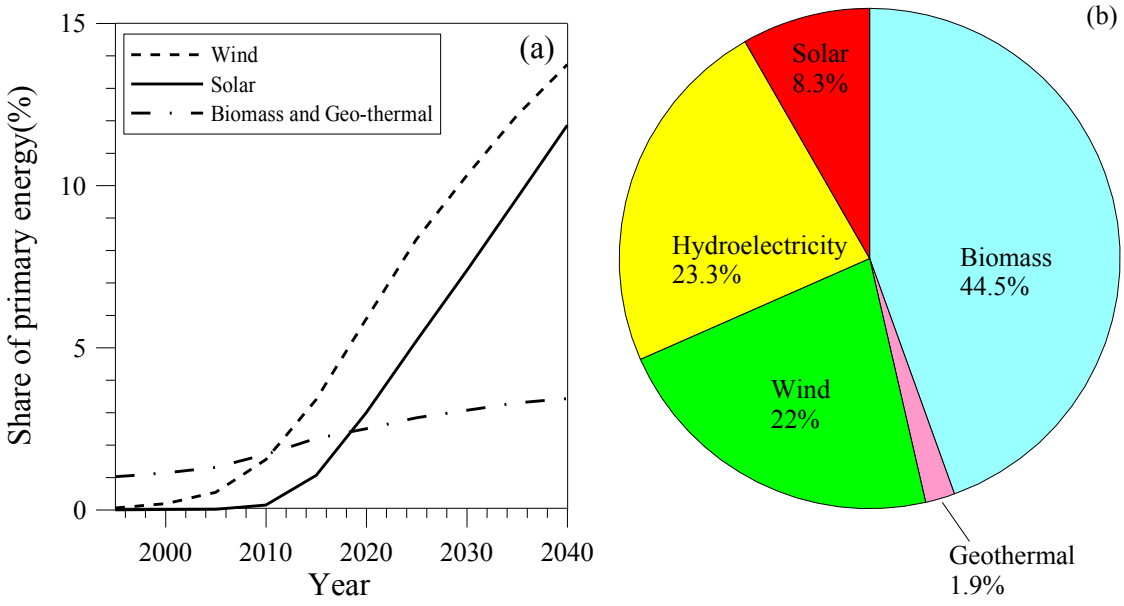

Figure 1.2. Renewable energy consumption (a) Global renewable energy consumption by source type and data forecast (BP, 2019) and (b) USA renewable energy consumption by source (U.S. EIA, 2018)

The wind became the second most important contributor to renewable energy generation in Europe in 2017 (Eurostat, 2018). Wind accounted for 13.8 % of total renewable energy production (Eurostat, 2018). A similar trend in the rise of wind energy can be seen in the USA. Figure 1.3 shows the total contribution made by wind and hydroelectricity to the total electricity production in the USA. The wind is becoming increasingly popular and will overtake hydroelectricity soon. (U.S. EIA, 2018). This

positive trend in the rise of wind energy has inspired the authors to investigate the ways to enhance wind energy generation and to explore the challenges of building a wind farm on weak soil and suggest a suitable solution.

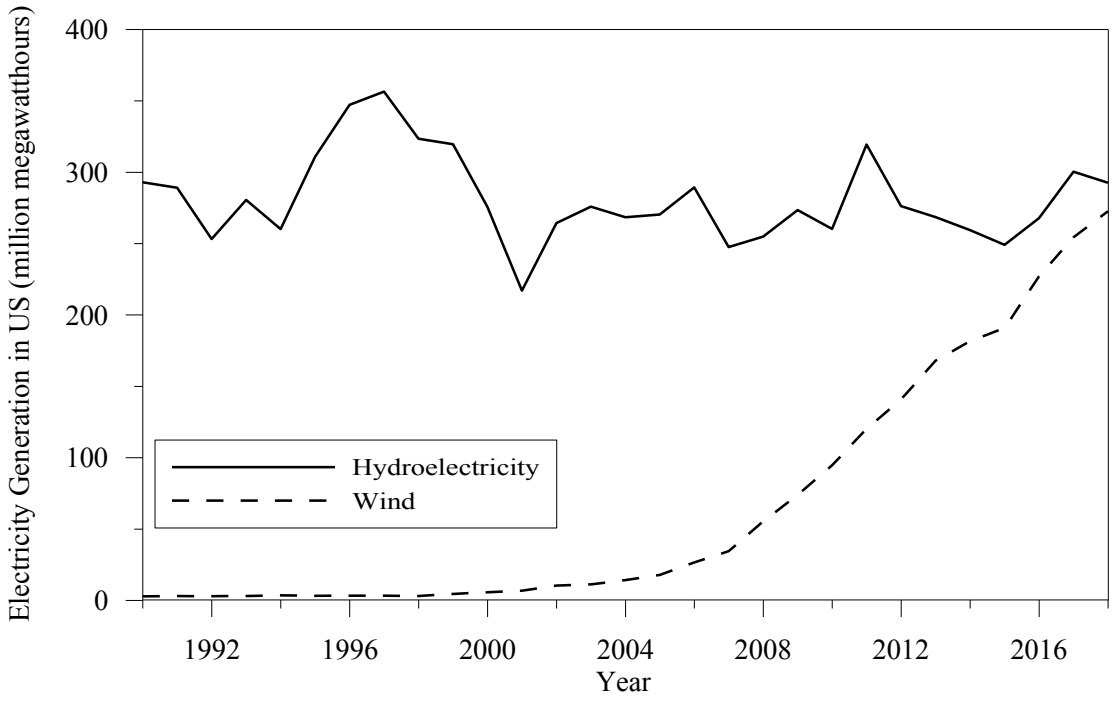

Figure 1.3. Comparison of electricity generation from wind and hydro in the USA (U.S. EIA, 2018)

1.3 Motivation

To address the increasing renewable energy demand and to counteract climate change, which is becoming an existential threat to humanity, renewable energy production from sources like the wind has received a surge in recent decades. The trend in harvesting wind potential for energy generation is encouraging, and this process should be implemented on a large scale to meet renewable energy demands.

Optimum utilization of available land and other resources is necessary for increasing the construction of large-scale wind farms. The efficiency of the wind farm project fundamentally rests on the wind conditions at the wind farm site. The wind farm should receive sustained winds with optimum wind speed for higher efficiency. Offshore wind farms have right wind conditions, but the construction and operation & maintenance of large-scale offshore wind farms is costly. The development of onshore wind farms is cheaper, but obtaining the vast area of land suitable for the construction of large-scale wind farms is a challenge. Availability of enormous expanse of land with good subsurface conditions, accessibility, and steady wind, essential for the construction of wind farm, is scarce. This can lead to wind farms being constructed in areas with poor soil not suitable for supporting tall wind turbines with large loads.

The energy generation has a direct relationship with steady wind and higher wind speed, which is encountered at higher altitudes. Taller the tower, the higher the energy output. According to Lantz et al. (2019), with every meter increase in height, the annual energy output increases by 0.5 to 1.0 % because of lower turbulence and higher wind speed at higher elevations. For exploiting the steady winds with higher wind speed, extremely tall towers have become mainstream. Tall towers and large turbines consequently increase the vertical design load, the horizontal load, and the bending moment on the foundation. Depending on the loads from the tower and the subsurface condition, different types of foundations like raft, pile-group or piled-raft can be used to support wind turbines. Piled-raft foundation can be efficiently used for counteracting eccentric load from wind turbines due to the load sharing between piles and the raft. Shrestha and Ravichandran (2017)

showed that a piled-raft foundation, a hybrid foundation that takes advantage of higher bearing capacity of shallow foundation (raft) and higher settlement resistance of deep foundation (pile), is economical for supporting tall wind turbines.

If the subsurface soil subjected to large bending moment is weak in nature, a larger raft with many long piles is needed to meet the safety and serviceability requirements, which makes the foundation expensive. However, the in-situ soil can be improved using existing ground improvement techniques to decrease the foundation dimensions and, eventually, its cost. This study investigates the economic advantage of improving the ground for constructing foundations for supporting a tall wind turbine tower. Among several ground improvement methods available, the method of cement soil mixing (CSM) was adopted for the study. The specifics of the ground improvement technique and the methodology used to explore the benefits of constructing a piled-raft foundation for a tall wind turbine in poor soil are presented in the following chapters. The primary objectives of the study are as follows.

(i) To complete the analytical design of piled-raft foundation for supporting wind turbines in unimproved and improved soils.

(ii) To perform comprehensive finite element analysis of piled-raft foundation in unimproved and improved ground and to compare with results from analytical design.

(iii) To conduct a parametric study to investigate the effect of the variation in soil properties in the design outcome.

(iv) To perform a cost analysis of the construction of foundation in unimproved and improved grounds and to investigate the economic advantage of ground improvement.

1.4 Outline of the thesis

The thesis is comprised of 9 chapters. The first chapter is the introduction to the study, which presents the motivation and objective of the study. Chapter 2 is the literature review section, which discusses different types of foundation, ground improvement measures, and history on numerical modeling of piled-raft foundation. Chapter 3 discusses the problem in hand: the soil profile and properties, the wind turbine, and the design loads from the turbine. In Chapter 4, the process of obtaining the properties of the improved ground and the approach of the application of proposed ground improvement in the field is discussed. The analytical design method of the piled-raft foundation and the results obtained from the design and analysis of piled-raft foundation in the unimproved and improved ground is presented in Chapter 5. The numerical model creation procedure, constitutive models, and the results obtained from the finite element analysis of the piled-raft foundation is discussed in detail in Chapter 6. Chapter 7 presents the parametric study conducted to evaluate the performance of the piled-raft foundation with variation in shear strength. The comparative cost calculation between the unimproved ground and different levels of ground improvement is shown in Chapter 8. This Chapter also presents comparative cost with variation in shear strength for various levels of ground improvement. Chapter 9 includes the conclusion and recommendations of the study.

CHAPTER 2

LITERATURE REVIEW

2.1 History of wind energy

Wind energy was utilized for navigation, agriculture, mills, etc., for centuries, but its utilization for electricity generation has only evolved around the past century. Electricity generation from the wind for the first-time dates to the 19th century. The first wind turbine to produce electricity was developed in 1886 in Scotland by Prof. James Blyth. The tower was 10 m high and consisted of cloth sailed turbine. Charles F Brush developed a larger, more functional wind turbine in 1887-1888 in Ohio, USA. The wind turbine consisted of an 18 m high tower with a rotor 17 m in diameter mounted at the top of the tower. The wind turbine produced 12 kW of power. (https://en.wikipedia.org/w/index.php?title=History_of_wind_power&oldid=935936215). The following Figure 2.1 shows the historical wind turbine designed by Mr. Brush.

Over the years, the size of the wind turbines has increased, the turbines have become more efficient and consequently produce a large amount of power. The turbines can stand hundreds of meters high and produce megawatts of electricity. The following Figure 2.2 shows a modern wind turbine.

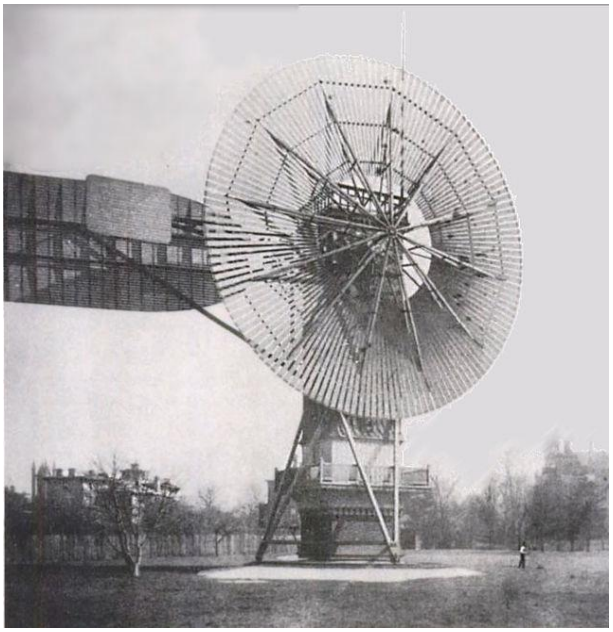

Figure 2.1. Historical wind turbine developed by Charles F. Brush (Righter, 1996)

Figure 2.2. A 178 m tall wind turbine with 3.4 MW capacity installed in Germany (Weaver, 2017)

2.2 Location of wind farms and types of wind turbine foundation

Depending on the suitable wind conditions, accessibility, and availability of land, the wind farms can either be constructed on land (onshore) or in the large bodies of water (offshore). Offshore wind farm receives steady wind with higher wind speed than their onshore counterparts due to no topographical restriction. However, the cost of construction of offshore wind farms is more elevated, and its operation and maintenance are costly too. The selection of the type of wind farm depends mainly on the topography, functionality, and economy.

2.2.1 Offshore wind farm

Large scale wind farms can be built in the sea or ocean due to lack of physical restrictions like mountains, glaciers, forest, residential, and commercial areas. Most European countries with smaller land areas have resorted to the sea to install wind farms. The challenging part with the offshore wind farm is the cost to build such massive structures in water. The cost could easily be multiple times the value of the same scale onshore wind farm. The cost of operation and maintenance of offshore wind turbines is also high due to corrosion by seawater, wear and tear due to high tides and waves and requirement of the highly facilitated workforce for maintenance. The common types of foundation used in an offshore wind turbine are monopiles, gravity-based structures (GBS), suction bucket, tripods, and jackets.

Monopile is the most used foundation for offshore wind turbines. It consists of a large steel pile 3.5 m to 4.5 m and driven 10 to 25 m into the soil. GBS foundation is used

in shallow water, and the basic principle is to obtain a stable structure supported by its weight. It consists of a conical or cylindrical shaped foundation with a large bottom diameter ranging from 30 to 40 meters. GBS is made of precast concrete blocks and installed on firm soil or a concrete platform. The suction bucket consists of a bucket with an open bottom. The bucket is embedded into the sediments with the open end facing down and sealed at the top resulting in the lifting forces to create a differential pressure that holds the structure. These foundations are used for the installation of turbines in water less than 25 m deep (close to the shore).

Tripods and jackets are used when the turbine sizes are massive and exposed to large loads and extreme conditions. Tripods consist of three steel piles driven into the ground. The three steel piles are welded together by small-diameter steel tubes. The piles are also welded to the tower using steel tubes. The jacket foundation consists of three or four piles driven into the soil. The piles are connected to a latticed intermediary structure, which can rise above the water surface. This latticed structure provides required stiffness against large loads and supports the tower. Figure 2.3 shows different types of foundations for an offshore wind turbine.

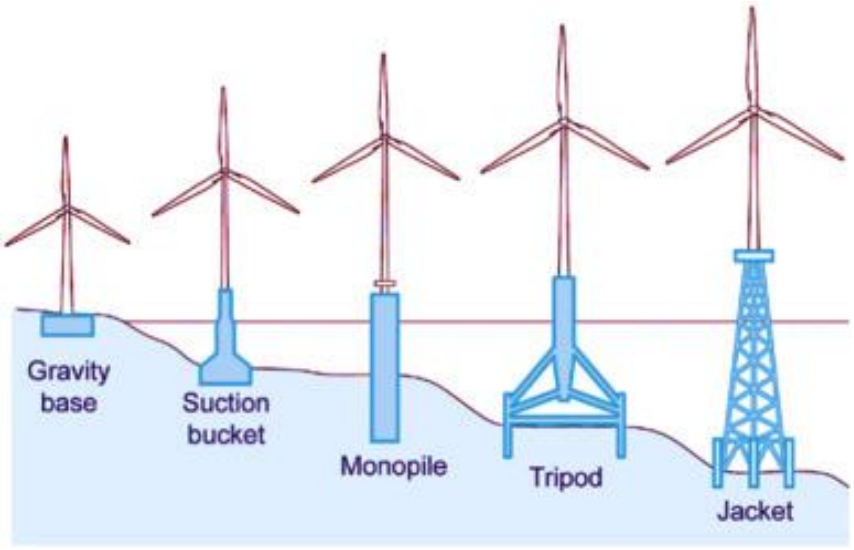

Figure 2.3. Different types of conventional foundation for offshore wind turbines (Moulas et al., 2013)

When the wind farms must be installed in water more than 40-50 m deep, the foundation mentioned above would not be feasible to construct. Thus, floating foundations are used in such a circumstance. Three types of floats generally in use are the Tension leg platform (TLP), semi-submersible, and spar-buoy. The TLP consists of buoyant columns that are tied to the suction/piled anchors at the seabed using highly tensioned cables. The spar-buoy comprises a large cylinder filled with weights keeping the center of gravity below the center of buoyancy. These various types of floating foundations are shown in Figure 2.4.

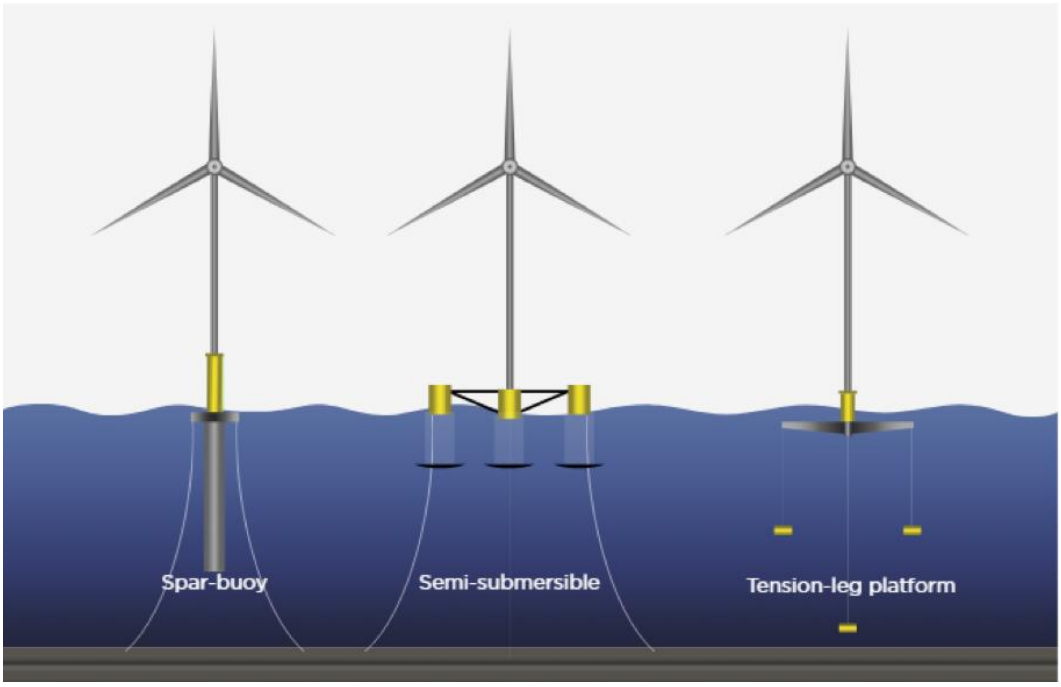

Figure 2.4. Types of the floating foundation for offshore wind turbine (Source: https://cph.world/2017/01/27/falling-costs-tech-innovations-will-drive-offshore-wind-power-boom/)

2.2.2 Onshore wind farm

The onshore wind farm is more common among the two types. The site selection plays an essential role in onshore windfarm construction. Different factors like topography, wind condition, transportation, and geotechnical property of subsurface soil play a critical role in onshore wind farm construction. Different types of foundations are used for onshore wind turbines, depending on the property of the soil at the site, wind conditions, and load from the tower. Shallow foundations are used when the wind turbine has small loads and located in a site with strong topsoil. A deep foundation that transmits the load to bedrock or firmer soil is necessary for supporting tall wind turbines, especially in weak soil. Some commonly used onshore foundations are discussed below.

2.2.2.1 Mat foundation

The mat foundation for a wind turbine can be circular or octagonal. It consists of three parts: a central pillar, mat, and the basement. The tower sits at the top of the foundation around the central pillar. The diameter of the mat can range from 15 to 22 m, and the thickness can be around 0.6 to 0.8 m at the edges and 2.5 to 3.5 m at the center. The mat is a widely used foundation for smaller wind turbine towers, and the construction is simple and consumes less time. A shallow mat foundation is shown in Figure 2.5.

Figure 2.5. Shallow mat foundation for onshore wind turbine (Source: http://www.steelwindtower.com/wind-turbine-foundation-5-foundation-types-explained-for-onshore-wind-turbine)

2.2.2.2 Ribbed beam basement foundation

The ribbed beam basement type of foundation can also be circular or octagonal. The diameter of the mat can range from 15 to 22 m. This foundation also consists of three parts: a central pillar, mat, and the basement. Unlike the mat foundation, this foundation

consists of beams originating from the central pillar and extending to the edge of the foundation. The ribbed beam foundation is shown in Figure 2.6. These beams are designed to counteract the overturning moments.

Figure 2.6. Ribbed beam basement foundation (Source: http://www.steelwindtower.com/wind-turbine-foundation-5-foundation-types-explained-for-onshore-wind-turbine)

2.2.2.3 Uplift anchors

This type of foundation is used in the sites with stable rock at or near the ground surface. The foundation takes advantage of the higher bearing capacity of the rocks. Several high strength prestressed anchors are fixed to the rock, which transfers load and prevents the uplift of the foundation. An uplift anchor foundation is shown in Figure 2.7.

Figure 2.7. Uplift anchor (Source: Norwegian Geotechnical Institute, 2017)

2.2.2.4 Pile group foundation

Pile group is one of the types of deep foundation used when the soil near the surface is of inferior quality, and thus the loads are required to be transferred to firm soil at greater depths or the bedrock. The piles in a group usually consist of a pile cap that transfers the load from the superstructure to the piles and provides structural rigidity to the foundation. The loads in the pile group are carried entirely by the piles alone. Piles in a pile group can either be end-bearing piles, friction piles, or a combination of both. The end bearing piles derives the resistance from the toe of the pile, generally lodged into hard stratum. The friction piles develop resistance from the skin friction between the circumference of the pile and the soil. The following Figure 2.8 shows the pile group foundation.

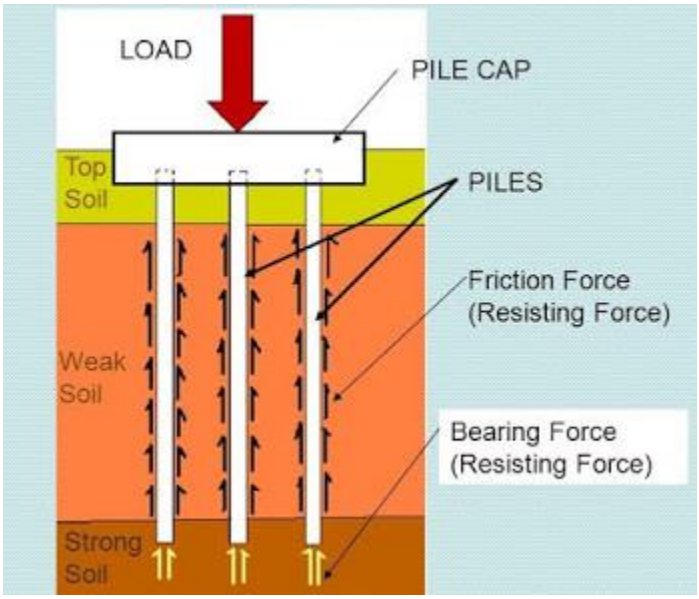

Figure 2.8. Pile group in action (Mohammed, 2019)

2.2.2.5 Piled-raft foundation

Piled-raft foundation is a hybrid foundation that comprises of piles drilled or driven into the ground and a raft resting on top of piles. A piled-raft foundation can support massive structures with large loads. The piles and the raft in the piled-raft foundation share the load-induced from the superstructure. The sharing of loads between the piles and the raft depends on the stiffness of piles and the raft and the interaction of the parts with the soil and with each other. Ravichandran and Shrestha (2018) formulated a performance and cost-based robust design optimization for raft, pile group, and piled- raft for tall wind turbines and concluded piled-raft foundation to be the most economical among the three foundations in clayey soil. Piled-raft was used as the foundation for this study, and its design has been discussed in detail in Chapter 5. The following Figure 2.9 shows a comparison of a typical raft and a piled-raft foundation.

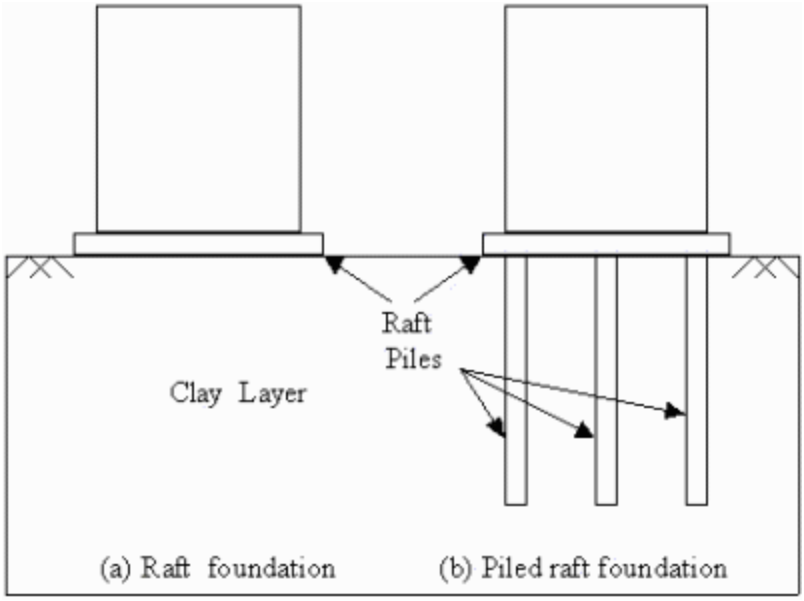

Figure 2.9. Raft and piled-raft foundation (Maharaj, 2004)

2.3 Methods of ground improvement

When the site condition for the construction of a project is unsuitable due to poor soil properties, the in-situ soil can be improved using various geotechnical methods. Various ground improvement methods serve one or many of the purposes like increasing shear strength and bearing resistance, accelerating consolidation, decrease in permeability, deformation control, increased horizontal stability, and increased resistance to seismic load and liquefaction. The choice of adopting a ground improvement method depends on the soil property, site conditions, scale of construction, loads on the foundation, desired level of strength after improvement, and cost of the improvement. Rollins et al. (2010) investigated the effectiveness of different ground improvement methods like compaction, soil mix wall, and jet grout treatment for increasing the horizontal resistance of pile groups. From the analysis, they concluded that mass soil mixing led to a 65 % increase, and jet

grouting led to a 400 % increase in horizontal resistance and initial stiffness of the soil. They concluded ground improvement techniques like soil mixing and jet grouting could provide an economical solution to lowering the cost of deep foundations. Different methods of ground improvement applicable to varying site conditions are discussed below.

2.3.1 Ground improvement by vibration

In this method, vibration is used to densify the ground either by the introduction of an elevated intensity of energy at the ground surface or by penetrating the ground with a vibrator. This type of improvement is suitable for cohesionless or low cohesive soils. Different methods of ground improvement using vibration are listed below.

2.3.1.1 Vibro-compaction

It is the most common method of ground improvement by vibration and involves the insertion of a vibrator to the desired depth. The vibrator (also called vibro-float or float) generates horizontal vibrations into the ground, which breaks the frictional contact and decreases effective stress between the soil structures, thereby creating a denser soil. The process of vibro-flotation is shown in Figure 2.10.

Figure 2.10. Vibro-flotation in action (Source: https://civildigital.com/vibro-compaction-vibro-flotation-ground-improvement-principle-images)

2.3.1.2 Vibro-stone columns

Vibro-stone columns are used to increase the load-bearing capacity of the soil and fills. The process involves the creation of holes in the ground using vibration and compressed air jet. The vibrator is then withdrawn, and a certain amount of stone is placed into the hole and compacted. This process is repeated until the stone column reaches the ground surface. Figure 2.11 shows a schematic construction of a stone column using top-feed vibro-compaction.

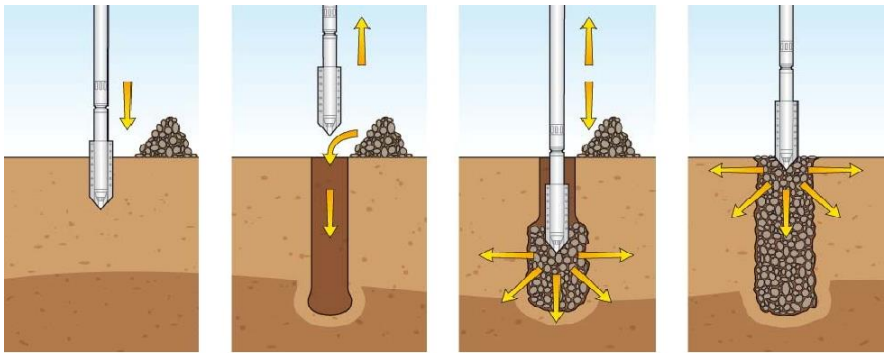

Figure 2.11. Top-feed vibro-stone column construction (Mokhtari and Kalantari, 2011)

2.3.1.3 Dynamic compaction

It is a ground improvement technique carried out by dropping a weight from a height to densify soil and fills. The drop weight usually made of steel is lifted to the desired height by a crane and repeatedly dropped to the ground surface. The impact of the drop densifies the soil. This method can is best applied in non-organic soils, reclaimed lands, and soils with high porosity such as poor fills and landfill sites. The following Figure 2.12 shows dynamic compaction being performed at a site.

Figure 2.12. Dynamic compaction in action (Source: https://civildigital.com/dynamic-compaction-ground-improvement-principle-images)

2.3.2 Ground improvement by loading

The process is based on the principle of consolidation, i.e., dissipation of excess pore water pressure. Soils with high permeability, particularly unsaturated fills, consolidates rapidly, but soft, saturated clays take a long time to consolidate as the

porewater pressure dissipates slowly. Preloading and vertical drains are conventional methods of ground improvement, which are discussed below.

2.3.2.1 Pre-loading

Pre-loading is obtained by placing a tremendous amount of earth over the allocated construction site. The soil under the fill undergoes consolidation due to the weight of the fill. Usually, soils with large voids, have a substantial immediate settlement. The fill is removed once the desired consolidation is attained and often reused in the construction process. The following Figure 2.13 shows pre-loading and surcharging.

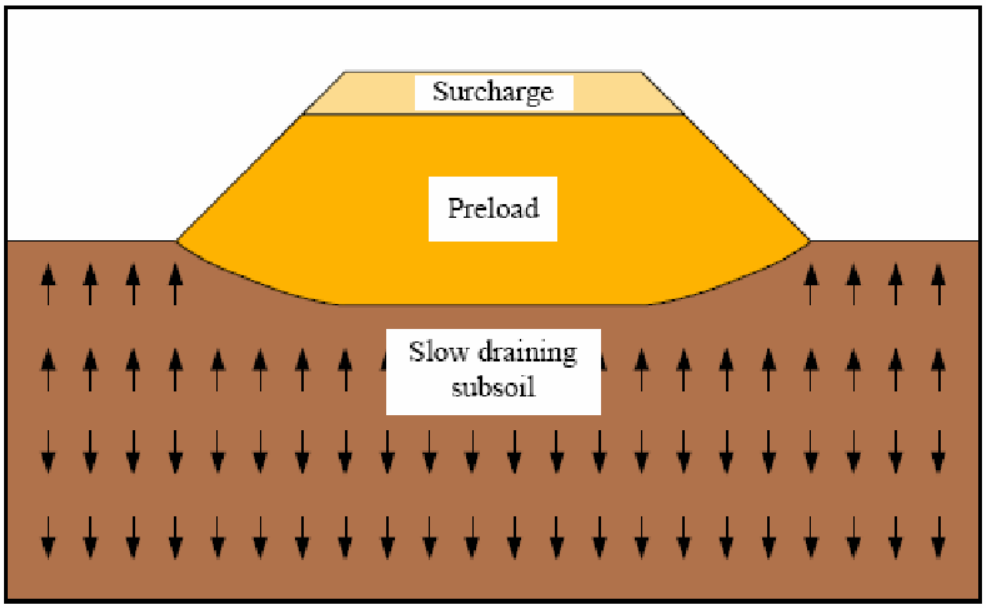

Figure 2.13. Preload and surcharging (Bilal and Talib, 2016)

2.3.2.2 Vertical drains

The rate of consolidation of soils depends on how quickly the excess pore water can be removed from the ground. Vertical drains installed in the ground provide

unobstructed movement of water and accelerates the consolidation. The vertical drains can be made of sand drains, or prefabricated vertical drains called wick drains. The wick drains are highly porous and sufficiently flexible to withstand horizontal loads. The following Figure 2.14 shows the vertical drain.

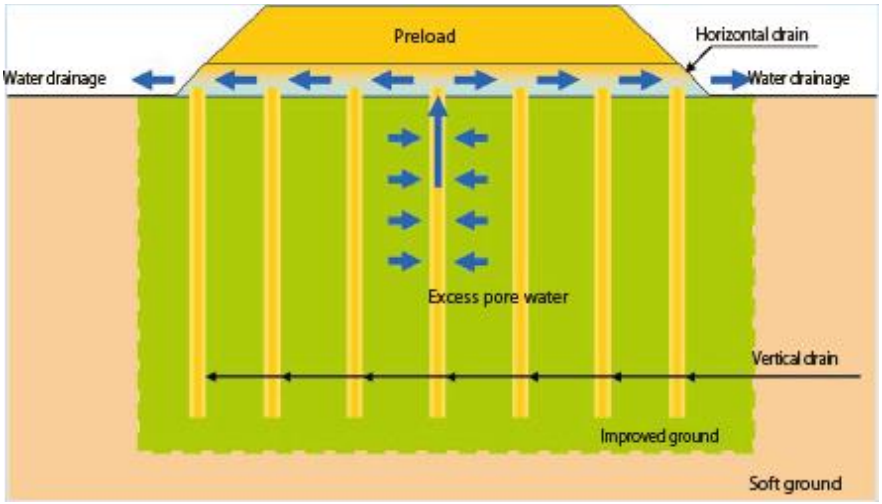

Figure 2.14. Preloading with installed vertical drains (Source: www.wakachiku.co.jp/en /technologies/various _vertical_drain _methods)

2.3.3 Ground improvement by reinforcement

Various types of reinforcements, such as geotextile, geogrid, and geonet, are used for strengthening soil. These are usually used in the construction of pavement, retaining walls and embankments. Geogrids, geotextiles, and geonets allow drainage. They possess high tensile strength and stiffness. The openings in geonets, geotextiles, and geonets allow interaction with soil and aggregates and reinforce the earth. One of the applications of geosynthetics is shown in Figure 2.15.

Figure 2.15. Geosynthetics as the lining of cut slopes (Varpe, 2018)

2.3.4 Ground improvement by grouting

The injection of slurry or liquid can improve the soil. The injected material is referred to as grout, and the grout can be in the form of suspension, emulsion, or solution. The grout fills the voids in the soil or rock and bonds with it to create a resilient, impervious mass. Some of the methods of grouting are available, which are listed below.

2.3.4.1 Displacement-compaction grouting

The injected grout is a thick, less mobile grout which remains as a homogeneous mass. The grout is infused through a small diameter pipe, and the grout expands to form a grout bulb that displaces the surrounding soil, thereby densifying the soil. This form of grouting is used in settlement control and fixing of sinkholes. The process of displacement-compaction grouting is shown in the following Figure 2.16.

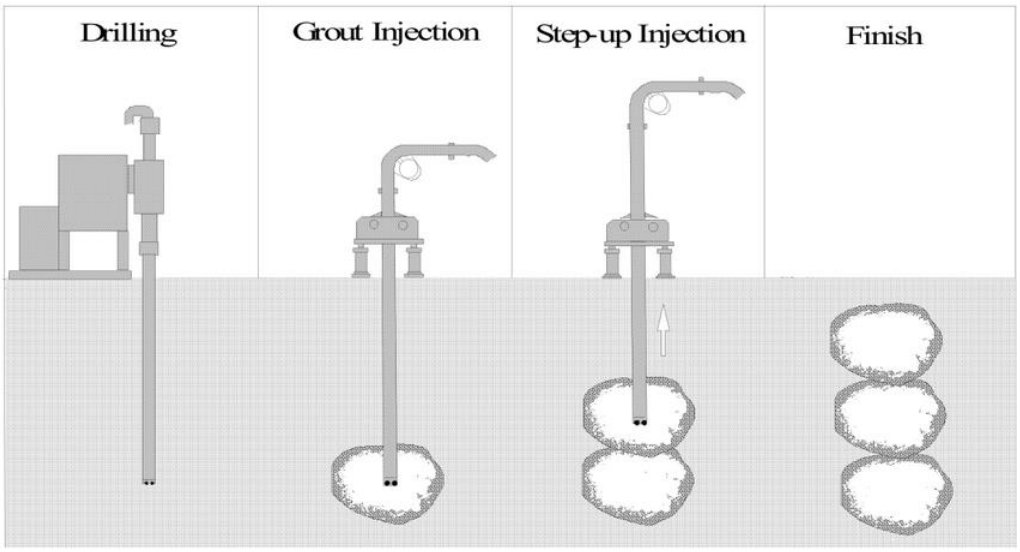

Figure 2.16. Compaction grouting process (Sayehvand and Kalantari, 2011)

2.3.4.2 Permeation grouting

Permeation grouting is the method of infusion of thin chemical grouts into the soil or fractured rocks. The infused grout fills the voids in the ground by replacing water and air but does not displace the soil particles or widens the cracks in the rock. Upon curing, the grout coalesces with the soil or rock to form a solid mass. It is used to control seepage in water storage facilities and preparing ground before tunneling. Figure 2.17 shows permeation grouting in soil and rock.

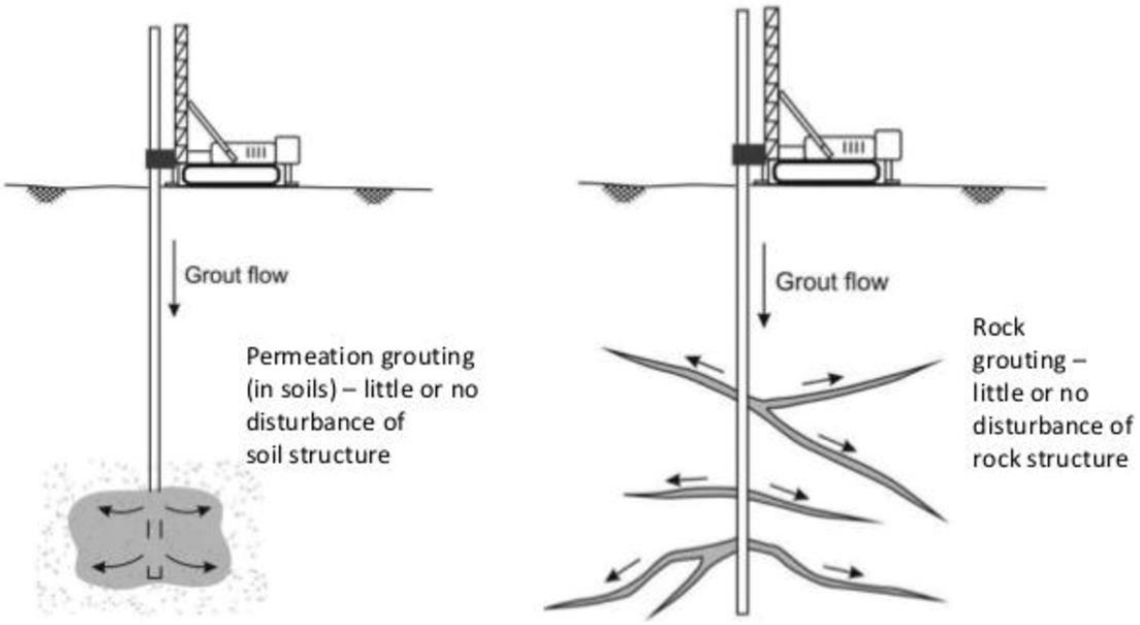

Figure 2.17. Permeation grouting in soil and rock (Rahman, 2016)

2.3.4.3 Jet grouting

It is a method of soil stabilization by injection of grout into the ground under high pressure. The process of jet grouting, as shown in Figure 2.18, involves drilling a small diameter hole and injecting the grout at elevated pressure through a nozzle of small diameter (1-10 mm). The pipe is raised and rotated slowly to seal the surface of the column. The soil particles dislodged due to the pressure rise to the surface, leaving a fully sealed column of the soil-grout mix at the bottom.

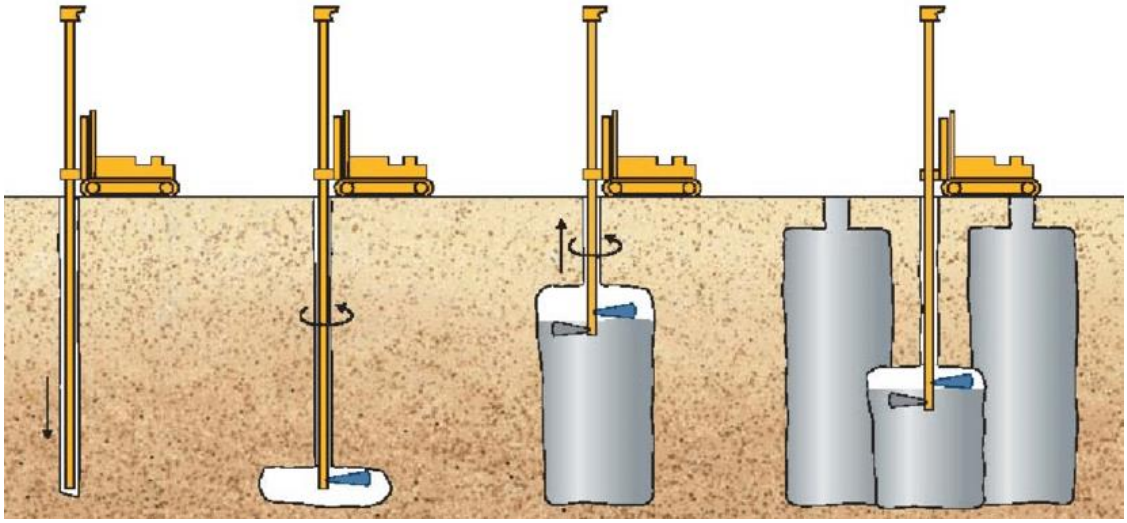

Figure 2.18. Jet grouting procedure (Source: https://www.pilebuck.com/foundation/soil-improvement)

2.3.5 Ground improvement by admixtures

Different additives and admixtures like cement, lime, fly ash, bitumen can be used to the soil to improve the soil. This method of ground improvement is a conventional method of ground improvement and widely used in pavement design. Highly plastic clays can be enhanced by mixing it with a proper amount of cement or lime. The types of ground improvement by admixtures are discussed below.

2.3.5.1 Cement soil mixing

The process involves mixing of soil with cement using special rotatory or shaft like apparatus. The process can be a wet or dry mixing. Wet mixing uses slurry as the binder, whereas the dry method uses dry cementitious binder. Cement soil mixing can be done to

create a column of improved soil, which can range meters deep and also be used to mass stabilize soil to a shallow depth.

Grzyb-Faddoul (2014) performed a numerical analysis of the strengthening of existing shallow and deep foundations by cement soil mixing technique. The shallow foundation was supported on a single column of improved soil or by four small soil columns. The soil columns in the group were found to provide a relatively better solution and reduced the rotation of the foundation significantly. The installation of soil columns led to doubling the bearing capacity of the unsupported shallow foundation. For deep foundations, soil columns were either installed around the deep foundation or beneath the deep foundation. The installation of soil columns under the pile foundation drastically increased the bearing capacity of the foundation due to the increase in toe resistance. Taghavi et al. (2015) used Cement Deep Soil Mixing (CDSM) method to improve the soil and studied the efficiency of ground improvement on the horizontal resistance of pile groups using centrifuge tests.

Deep soil mixing: The method consists of lowering the mixing shafts or cylindrical tool with rotatory blades in the tip, into the soil to the desired depth. While withdrawing the tool, the cementitious binder is injected through a pipe that runs through the shaft and mixed with the soil by the rotatory blades or shaft to obtain a consistent cement-soil mix (soilcrete) column. Several individual or overlapping columns are created depending on the requirement at the site. The following Figure 2.19 shows the deep soil mixing process.

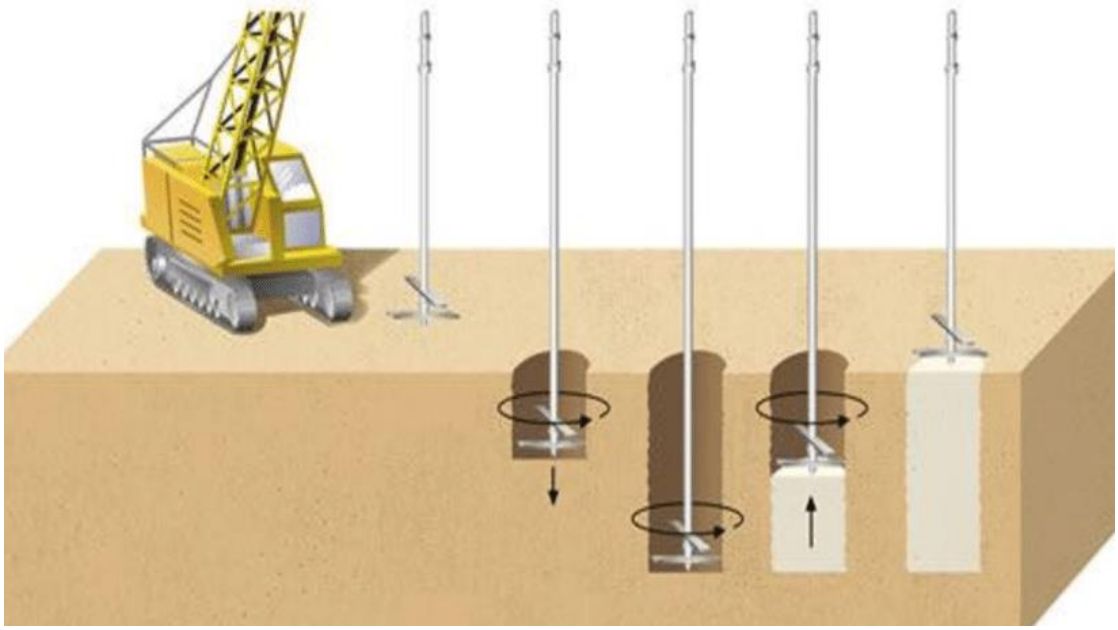

Figure 2.19. Deep soil mixing procedure (Muhammad, 2014)

Mass Stabilization: When the ground surface consists of weak soil with high water content and a large area of the ground needs to be improved, mass stabilization by shallow mixing is adopted. The soil can be improved to a depth of up to 4 m using this method. The stabilization is performed in parts, with each part typically comprising an area around 10 m^2. This method uses a special apparatus with rotatory blades to mix the soil with cement supplied through an auger. The following Figure 2.20 shows the mass stabilization of weak soil using cement. This method was used for soil stabilization in our study and explained in detail in Chapter 4.

Figure 2.20. Mass stabilization of soil (Source: https://grounddevelopments.co.uk/ground-improvement/deep-soil-mixing/mass/)

2.3.5.2 Lime column

This method is a variation of deep soil mixing and uses quicklime instead of cement as the binder material. The exothermic reaction between the quicklime and the soil moisture helps in reducing the water content and increases the strength of the soil. The construction procedure is similar to that of cement deep soil mixing. The lime columns are used as excavation supports or to stabilize slopes.

2.4 A brief review of numerical analysis of piled-raft foundation

Several authors have used three-dimensional (3D) finite element (FE) software to analyze a piled-raft foundation. Ruel et al. (2000) carried out a 3D FE analysis on an over-

consolidated clay. They performed numerical analysis considering contact between the soil and structure as perfectly rough, and the loads were uniformly distributed over the raft. A good agreement was achieved with the comparable model from Katzenbach et al. (1997b). Non-linear FE analysis of piled-raft foundation using ANSYS was performed by Maharaj and Gandhi (2004). They analyzed the effect of soil modulus and raft thickness on load settlement behavior of piled-rafts. They concluded that the load settlement curve for rafts of varying thickness was almost the same in soft clay citing soil-structure interaction causing the raft to exhibit rigid behavior.

Roshan and Shooshpasha (2013) performed a static numerical analysis of piled-raft foundation in soft clays using Plaxis 3-D. They conducted a parametric study with variation in the length of piles, the spacing of piles, the number of piles, and raft thickness to obtain economical and effective design. They found out the total settlement and differential settlement in soft clay decreased with an increase in raft thickness. They also concluded that with the increase in the length of the pile, the settlement decreases, but the decrease in differential settlement stops after a certain length. Sinha and Hanna (2016) created a 3D FE model on a piled raft foundation and carried out a parametric study. They found out that when piles are closely placed, piles take a larger portion of the load, and rafts carry a more significant share when piles are placed far apart. They also suggested pile spacing more than 7D is ineffective. They found out thicker raft is effective in reducing differential settlement, meanwhile indicating that it would contribute to higher maximum settlement due to an increase in the self-weight of the raft. Though the above method considered the pile-raft-soil interaction but did not take in to account the influence of the bending moment

on the differential settlement, which is an essential factor in causing differential settlement. This study is concerned with the development of a comprehensive 3D FE models of the piled raft foundation to simulate unimproved and improved ground conditions and analyze the performance of the foundation in those conditions.

CHAPTER 3

WIND TURBINE AND SUBSURFACE PROPERTIES

3.1 Problem definition

The wind turbine tower considered in this study was 80 m tall and made of prestressed concrete. The tower had a base diameter of 6.75 m and a top diameter of 3.0 m. A piled-raft foundation with reinforced concrete raft supported by several auger cast piles was used in this study. The properties of the tower and wind turbine were obtained from Lyrner et al. (2010). The location for the wind turbine was hypothetical, and the horizontal load on the foundation was calculated using a mean wind speed of 80 mph. The following Figure 3.1 shows the outline of the wind turbine tower used in the study.

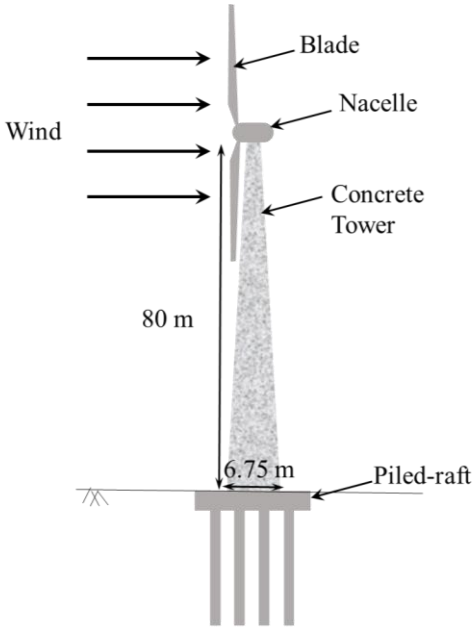

Figure 3.1. Wind turbine tower with piled-raft foundation (not to scale)

3.2 Design loads

The total vertical/axial load (A) was the weights of the tower and other wind turbine components such as the nacelle and rotor. The total vertical load calculated was 8819.19 kN. The spreadsheet used for the calculation of vertical load is shown in Appendix A.

The horizontal load on the tower was due to the wind load on the tower and turbine components. The total horizontal load was computed following the design guidelines from ASCE 7-10 (2010). The rotor is subjected to drag force, which is included in the horizontal load and moment load calculations. The total horizontal load (L) was computed as 579.49 kN and bending moment (M) as 30223.70 kNm. The spreadsheet used for the calculation of wind load and moment load is shown in Appendix A.

3.3 Soil properties

The profile consisted of a homogeneous clay layer. The properties of the clay are listed in Table 1 and were obtained from Quiroga et al. (2017). The in-situ soil is considered as the unimproved case in this study, and the near-surface soil surface is improved later to evaluate the effectiveness of ground improvement on the performance of the piled-raft foundation. Quiroga et al. (2017) performed a series of geotechnical tests on the unimproved soil and developed a stress-strain curve. The stress-strain curve for the unimproved clay shown in Figure 4.1(a) was recreated using the data obtained by Quiroga et al. (2017). The undrained shear strength calculated is considered as the mean shear strength, and a parametric study with the variation in shear strength is presented in Chapter 7.

Table 3.1. Properties of clay (Quiroga et al., 2017)

Geotechnical Properties	Values
Saturated unit weight (kN/m^3)	19.20
Liquid limit (%)	32
Plastic limit (%)	17
Specific gravity	2.69
Average water content (%)	0.22
Young's modulus (kPa)	30,500
Undrained shear strength (kPa)	41

CHAPTER 4

GROUND IMPROVEMENT

4.1 Mix design and properties

The ground improvement method adopted in the study is cement soil mixing (CSM). Quiroga et al. (2017) used cement soil mixing in the laboratory and performed tests on the improved soil to obtain the properties of the improved soil. A mix design created by Quiroga et al. (2017) using CSM was adopted in this study. The mix design properties obtained from Quiroga et al. (2017) are listed in Table 2, and Figure 4.1(b) shows the stress-strain curve of improved clay. The unit weight of the improved clay was calculated to be 18.38 kN/m^3. The enhancement in strength and deformation properties of the improved clay compared to unimproved in-situ soil can be seen by comparing Figure 4.1 (a) and Figure 4.1 (b). The Young's modulus increased from 30,500 kPa in the unimproved ground to 120,000 kPa in improved soil, which is a 394 % increase. Similarly, the undrained shear strength for CSM improved increased from 41 kPa to 360 kPa, respectively, which is 878 % higher than in unimproved clay. So, a piled-raft foundation with a smaller dimension can be used for supporting the tall wind turbine because of an increase in the bearing capacity of soil.

Table 4.1. Properties of cement-soil mix design (Quiroga et al., 2017)

Mix design Properties	Values
Water to cement ratio by weight	1
Cement Content (%)	10
Cement Factor	270
Total water to cement ratio by weight	4.4

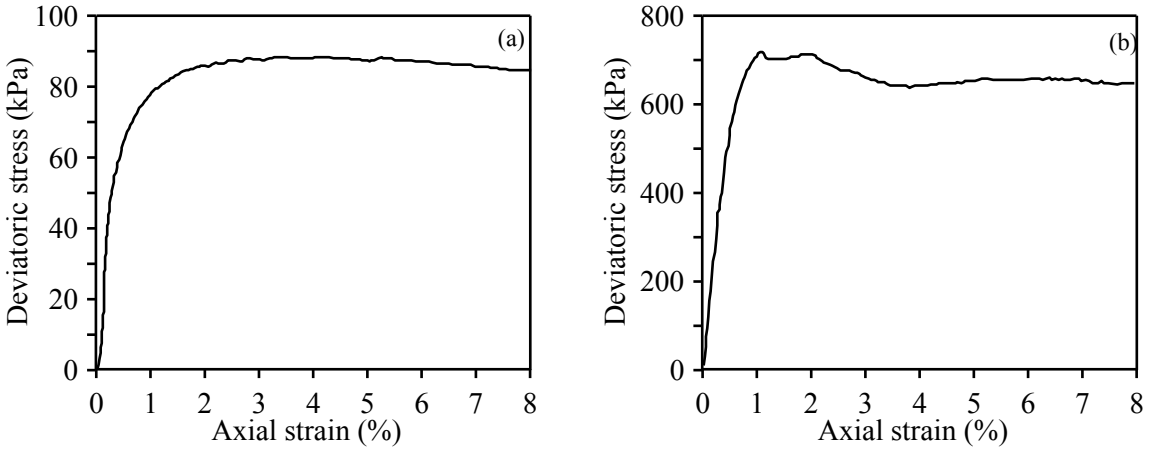

Figure 4.1. Stress-strain curve from consolidated undrained compression test (recreated from Quiroga et al., 2017) (a) soft poor clay and (b) CSM improved clay

4.2 Field procedure

The field procedure involved improving the ground around the foundation using mass mixing. As discussed in Chapter 2, the ground improvement using cement soil mixing can be deep soil mixing (where columns of improved soils are created), or mass stabilization through shallow mixing. Since the depth of ground improvement in this study is shallow, mass stabilization using cement soil mixing was adopted. The mass stabilization/mixing is achieved by using the rotation of a shaft or rotatory blades to mix the cement with in-situ soil forming a uniform soil-cement mixture.

A total of five different levels of ground improvement (V_1 to V_5) were considered in this study. A cylinder represents the volumetric improvement with the height of the cylinder equivalent to the depth of vertical improvement (V_i, i= 1 to 5) and the radius of the cylinder is the sum of raft radius and the depth of improvement (H_i= R + V_i, i= 1 to 5). The vertical depths of improvement considered are 2.0 m, 2.4 m, 2.8 m, 3.2 m, and 3.6 m, which are equivalent to 0.25, 0.3, 0.35, 0.4 and 0.45 times the diameter of the raft, respectively. The horizontal radius of improvement considered is 6.0 m, 6.4 m, 6.8 m, 7.2 m, and 7.6 m. The different levels of ground improvement considered for the geotechnical design are presented schematically in Figure 4.2.

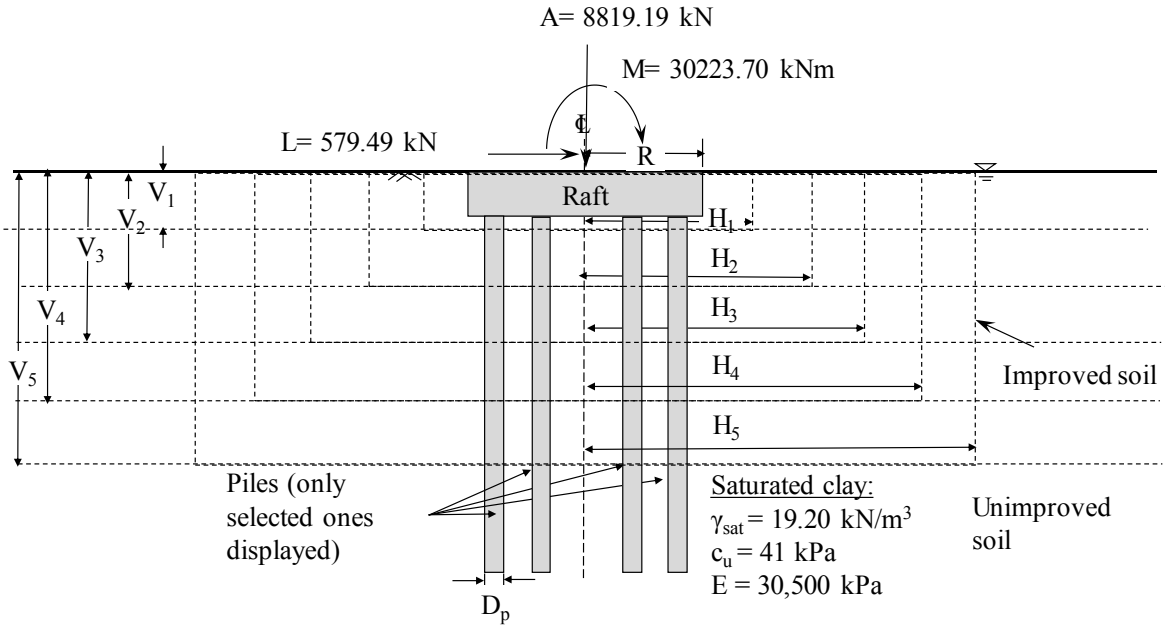

Figure 4.2. Soil profile with horizontal and vertical variations in levels of ground improvement (measurements not to scale)

However, the analytical design method cannot incorporate ground modification in the horizontal direction. Hence, the analytical designs were performed by considering the

ground improvement in the horizontal direction (H) to be infinite. To supplement the analytical design and to overcome this limitation, a comprehensive FE analysis was performed, with models having variations of ground improvement in both horizontal and vertical directions.

CHAPTER 5

ANALYTICAL DESIGN AND ANALYSIS OF PILED-RAFT FOUNDATION

The geotechnical design method of the piled-raft foundation exposed to combined vertical load, horizontal load and bending moment are not well documented in the literature owing to the uncertainty in the ratio of the loads (especially the bending moment) carried by the raft and the piles. The initial design of the piled-raft foundation was carried out using the method proposed by Hemsley (2000). The procedure used by Hemsley (2000) is based on simplified methods suggested by Poulos and Davis (1980) and Randolph (1994). This study also uses a new approach proposed by Shrestha et al. (2017) to calculate the differential settlement due to the bending moment. It is an iterative procedure of distribution of bending moment among the piles and the raft such that the differential settlements of the raft and the piles are equal. Stability and serviceability requirement checks were performed on the piled-raft to obtain the final design results. The stability checks consist of vertical load capacity, moment capacity, and horizontal load capacity. The serviceability checks involved checks on total and differential settlements and the rotation of the foundation and displacement of tower top. The design procedure involved assuming the dimensions of the raft and the dimension and number of piles and varying the dimension or the number until both the stability and serviceability criteria were satisfied. For the stability requirements, a factor of safety of 2.5 was considered to be sufficient. For the serviceability requirement, a design method proposed by Grunberg and

Gohlmann (2013) was used. This method suggests a vertical misalignment of 3 mm per meter height of the tower to be secure against rotation. An allowable differential settlement of 24 mm and an allowable rotation of 0.171° were obtained from the study.

5.1 Bearing capacity design of raft

Initially, a raft 8 meter in diameter and 1 m in thickness was considered to support a tower with the base of 6.75 m in diameter. The bearing capacity of the raft was determined using the method proposed by Vesic, along with the adjustment for eccentricity using Meyerhoff's method (Coduto, 2001). Vesic's bearing capacity equation is shown in Equation (5.1).

$$q_u = c'N_c s_c d_c i_c b_c g_c b_c + q'N_q s_q d_q i_q b_q g_q b_q + 0.5B\gamma'N_\gamma s_\gamma d_\gamma i_\gamma b_\gamma g_\gamma b_\gamma \tag{5.1}$$

where N_c, Nq, N_γ are the bearing capacity factors and, s_c, s_q, and s_γ are shape factors. Similarly, d_c, d_q and d_γ are depth factors and i_c, i_q and i_γ are load inclination factors. Also b_c, b_q and b_γ denote base inclination factors and g_c, g_q and g_γ are ground inclination factors. B is the width of foundation, c' is effective cohesion, γ' and q' is the effective unit weight and effective overburden pressure, respectively. The following Equation (5.2) shows the bearing capacity factors.

$$\begin{aligned} &N_c = (N_q - 1)\cot(\phi') \; for \; \phi' > 0 \text{ and } N_c = 5.14 \text{ for } \phi' = 0 \\ &N_q = e^{\pi \tan(\phi')} \tan^2\left(45 + \phi'/2\right) \\ &N_c = 2(N_q + 1)\tan(\phi') \end{aligned} \tag{5.2}$$

The shape factors are calculated using the following Equation (5.3).

$$
\begin{aligned}
s_c &= 1+\left(\frac{B}{L}\right)\left(\frac{N_q}{N_c}\right) \\
s_q &= 1+\left(\frac{B}{L}\right)\tan(\phi') \\
s_\gamma &= 1-0.4\left(\frac{B}{L}\right)
\end{aligned}
\tag{5.3}
$$

The depth factors are calculated based on the following Equation (5.4).

$$
\begin{aligned}
d_c &= 1+0.4k \\
d_q &= 1=2k\tan\left(\phi'\right)\left(1-\sin\left(\phi'\right)\right)^2 \\
d\gamma &= 1
\end{aligned}
\tag{5.4}
$$

where $k = D/B$ for $D/B \le 1$ and $k = tan^{-1}\left(D/B\right)$ for $\left(D/B\right) > 1$

The load inclination factors are calculated by using the following Equation (5.5).

$$
\begin{aligned}
i_c &= 1-\frac{mV}{Ac'N_c} \ge 0 \\
i_q &= 1-\left(\frac{V}{P+Ac'/\tan(\phi')}\right)^m \ge 0 \\
i_q &= 1-\left(\frac{V}{P+Ac'/\tan(\phi')}\right)^{m+1} \ge 0 \\
m &= \frac{2+B/L}{1+B/L}, \text{when inclined in direction of B}
\end{aligned}
\tag{5.5}
$$

where V is horizontal load, P is applied vertical load, and A is base area.

The base inclination factors are calculated using Equation (5.6).

$$b_c = 1 - \frac{\alpha}{147}$$
$$b_q = b_\gamma = \left(1 - \frac{\alpha \tan(\phi')}{57}\right)^2 \quad (5.6)$$

α is the inclination of the base with the horizontal

The ground inclination factors are calculated using Equation (5.7)

$$g_c = 1 - \frac{\beta}{147} \geq 0$$
$$g_q = g_\gamma = (1 - \tan)^2 \quad (5.7)$$

α is the inclination of the base with the horizontal

When the foundation is eccentrically loaded, like the foundation of the wind turbine, Vesic's equation should be modified. The method proposed by Meyerhoff was used to account for the eccentricity in this study. This method calculates the effective dimension of the foundation due to eccentricity and adopts the values in bearing capacity equation. An ellipse represents the circular raft under eccentric load with effective dimensions, as shown in Figure 5.1. The area of the ellipse is calculated by using Equation (5.8).

$$A_{eff} = 2\left[R^2 \cos^{-1}(e/R) - e\sqrt{R^2 - e^2}\right]$$
$$b_e = 2(R - e) \quad (5.8)$$
$$l_e = 4\,A_{eff} / \pi b_e$$

The effective dimension of the rectangle (l' and b') of the equivalent area of the ellipse is calculated using Equation (5.9). These values (l' and b') were used in Equation

(5.1) to compute the bearing capacity. The raft with the design dimension did not satisfy the design requirement for unimproved soil. However, the same dimension (8 m diameter and 1 m thick) was still considered as the deficit was compensated by the piles. After ground improvement, the bearing capacity of the raft improved substantially.

$$l' = \sqrt{A_{eff}\frac{l_e}{b_e}}$$
$$b' = \frac{l'}{l_e}b_e \tag{5.9}$$

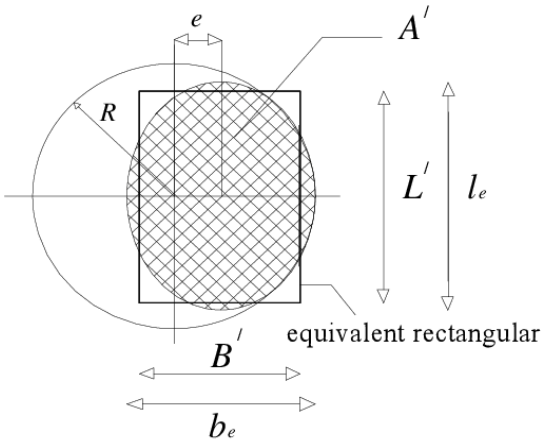

Figure 5.1. Effective area of the eccentrically loaded circular raft

5.2 Ultimate pile capacity calculation

The ultimate upward $\left(P_{ult-up}\right)$ and ultimate downward (P_{ult-dn}) capacity of a single pile were calculated. The ultimate capacity (P_{ult}) of a single pile was calculated as the sum of ultimate skin friction (P_s) and ultimate toe resistance $\left(P_t\right)$, i.e. ($P_{ult} = P_s + P_t$). For calculation of the skin friction, the API method was used, and O'Neil and Reese's (1999)

method was used for the calculation of toe resistance. The total capacity of the pile group was calculated by multiplying the single pile capacity by the entire number of piles. The piles are arranged around the raft with enough spacing to avoid the group effect. The detailed design and calculation of the ultimate pile capacity are shown in Appendix B.

5.3 Stability check

5.3.1 Vertical capacity

Two different cases were considered for calculating vertical capacity. The sum of the ultimate capacities of the individual components (piles and the raft) was considered for the first case, i.e. $(P_{ult})_{pr} = (P_{ult})_{raft} + (P_{ult})_{pile}$. The ultimate capacity of the piled-raft foundation (raft, pile, and the soil) as a block $(P_{ult})_{block}$ was considered for the second. The lower of the two was considered for further design. The factor of safety $(FOS_{vertical})$ against vertical capacity failure was calculated using Equation (5.10). A factor of safety of 2.5 was deemed to be enough for the vertical capacity.

$$FOS_{vertical} = \frac{\min\left[(P_{ult})_{pr}, (P_{ult})_{block}\right]}{P} \tag{5.10}$$

The factor of safety $(FOS_{vertical})$ of 2.88 was obtained for unimproved ground for the assumed foundation size, which meets the factor of safety requirement of 2.5. In calculating the vertical capacity of piles in improved ground, a similar method was used but with the adjustment of skin friction provided by the improved layer. The detailed calculation of vertical capacity in unimproved soil is shown in Appendix B.

5.3.2 Moment capacity

The moment capacity was also obtained to be the smaller of (i) the summation of the ultimate capacities of the individual parts (piles and the raft), i.e., $\left(M_{ult}\right)_{pr} = \left(M_{ult}\right)_{raft} + \left(M_{ult}\right)_{pile}$ and (ii) the ultimate capacity as a block $\left(M_{ult}\right)_{block}$. The moment capacity of the raft $\left(M_{ult}\right)_{raft}$ was calculated using the Equation (5.11).

$$\left(M_{ult}\right)_{raft} = M_m \frac{27}{4}\frac{P}{p_u}\left[1-\left(\frac{P}{p_u}\right)^{0.5}\right] \text{where,}$$
$$M_{\mathrm{m}} = \frac{\left(P_{ult}\right)_{raft} D^2}{4}\left[\frac{\pi}{4}-\frac{1}{3}\right] \tag{5.11}$$

where p_u is the centric load applied to the raft in the absence of moment load, P is applied vertical load, D is the raft diameter and M_m is the highest moment the soil can support.

The moment capacity of the piled raft as a block was calculated using the Equation (5.12).

$$\left(M_{ult}\right)_{block} = \alpha_B \overline{p_u} B_B {D_B}^2 \tag{5.12}$$

where α_B is the factor whose value ranges from 0.2 to 0.25 depending on the distribution of horizontal pressure, $\overline{p_u}$ is average horizontal resistance of soil along the block, B_B is the width of the block, and D_B is the depth of block. The factor of safety against the

moment (FOS_{moment}) is calculated, as shown in the Equation (5.13). A factor of safety equal to 2.5 was deemed to be safe against moment capacity failure.

$$FOS_{moment} = \frac{\min\left\lfloor (M_{ult})_{pr}, (M_{ult})_{block} \right\rfloor}{M} \tag{5.13}$$

Moment capacity governed the design of the piled-raft foundation in the case of unimproved ground. In the case of improved ground, moment capacity was obtained using a similar procedure as in the unimproved ground, but it also included the skin friction from the improved layer. The detailed moment capacity calculation of piled-raft in unimproved soil is shown in Appendix B.

5.3.3 Horizontal (lateral) capacity

Brom's (1964a) method designed for the calculation of the horizontal capacity of piles in cohesive soil was used. The method is principally intended for the calculation of the deflection of a single pile. However, this method was used presuming that the piles in a piled-raft will have deformation behavior like that of the individual piles. The Equation (5.14) gives the factor of safety against the horizontal load.

$$FOS_{horizontal} = \frac{n(P_m)_{horizontal}}{L} \tag{5.14}$$

where n is the total number of piles in a piled-raft, L is the horizontal load, and $(P_m)_{horizontal}$ is the maximum allowable horizontal load capacity of a single pile. The detailed calculation procedure of horizontal deflection for a single pile in cohesive soil is shown in Appendix

B. The horizontal capacity of a single pile in unimproved soil was calculated to be 342.51 kN. Similarly, the horizontal deflection was calculated to be 4.69 mm. The factor of safety against the horizontal load was found to be 15.40.

The calculation of horizontal deflection in the improved ground is a little complicated. Firstly, the ground was considered to be improved hypothetically to a depth of 48.4 m (equivalent to the length of the pile in the unimproved ground). The horizontal deflection, in that case, was noted as 1.68 mm. Then, the horizontal deflection of various ground improvement levels was computed by taking the weighted average of the deflection in the unimproved ground (4.69 mm) and the deflection in the improved ground (1.68 mm) depending on the depths of improvement carried out (2.0 to 3.6 m). The horizontal deflections in the improved ground with different levels of ground improvement led to horizontal deflections between 1.68 mm and 4.69 mm.

5.4 Serviceability check

5.4.1 Vertical settlement

Randolph's (1994) method was used for calculating the vertical settlement. This method was based on the idea of load distribution between the piles and the raft in the piled-raft foundation. The following Equation, (5.15) developed by Randolph (1994), calculates the stiffness of the piled-raft foundation and the fraction of the load taken by the piles and the raft.

$$K_{pr} = \frac{K_p + \left(1 - 2\alpha_{rp}\right) K_r}{1 - \alpha_{rp}^2 \left(K_r / K_p\right)} \tag{5.15}$$

where the stiffness of piled-raft is represented by K_{pr}, K_r is the stiffness of the raft, K_p is the stiffness of the pile group, and α_{rp} is the pile-raft interaction factor. The pile-raft interaction factor α_{rp} varies on the spacing between piles, slenderness ratio, and the value varies between from 0.65 to 0.8. However, Clancy (1993) suggested a constant value of 0.8 for a larger pile group, and the α_{rp} does not depend on the pile spacing and the slenderness ratio. The stiffness of the raft is calculated using the Equation (5.16)

$$K_r = \frac{2.25GB}{(1-\nu)} \tag{5.16}$$

where B is the width of the raft, G is the shear modulus of the soil and ν is the Poisson's ratio of the soil.

The method outlined by Poulos (2001) was adopted to calculate the stiffness of the piles. In this procedure, a target stiffness of the piled-raft system was established, assuming an allowable settlement $(S_{allowable})$. The vertical load P, when divided by the allowable settlement, gives a target stiffness (K_{pr}). The value of K_{pr} when back substituted to Equation (5.15), the equation takes a quadratic form and solving the resulting equation; the stiffness of the pile group K_p can be calculated.

The load at which the pile capacity is completely mobilized is denoted by P_M and given by the Equation (5.17).

$$P_M = \frac{(P_{ult})_{pile}}{\beta} \tag{5.17}$$

where $(P_{ult})_{pile}$ is the ultimate capacity of piles and β is the fraction of load shared by the pile. The Equation (5.18) indicates the stiffness of the piled-raft will be fully functional until the bearing capacity of the pile gets completely mobilized at P_M and beyond that point, the raft takes the remaining load.

$$For\ P < P_M; S = \frac{P}{K_{pr}}\ and\ For\ P > P_M; S = \frac{P_M}{K_{pr}} + \frac{P - P_M}{K_r} \tag{5.18}$$

A vertical load settlement curve, as shown in Figure 5.2, can be designed using the relation shown in Equation (5.18). The load settlement curve was assumed to be hyperbolic to introduce inelasticity of soil. The inelasticity of the curve was obtained by replacing initial raft stiffness K_{pi} and the initial raft stiffness K_{ri} with secant pile and raft stiffness K_{pf} and K_{rf} respectively. These secant pile and raft stiffness were obtained using the following Equation (5.19).

$$K_{pf} = K_{pi}\left(1 - \frac{R_{fp}P_p}{(P_{ult})_{pile}}\right) \text{ and } K_{rf} = K_{ri}\left(1 - \frac{R_{fr}P_r}{(P_{ult})_{raft}}\right) \tag{5.19}$$

where R_{fp} and R_{fr} are the hyperbolic factors for piles and raft respectively, P_p and P_r are loads carried by the piles and raft respectively.

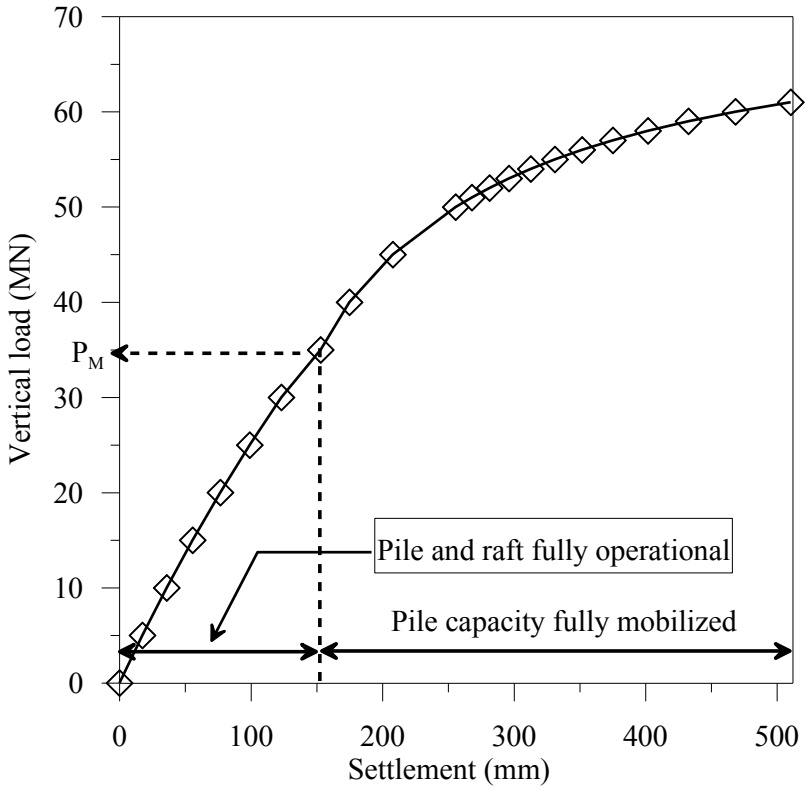

Figure 5.2. Vertical load-settlement curve for the unimproved soil

For the allowable vertical settlement of 30 mm, the vertical design load on the piled-raft foundation in unimproved soil was determined to be of 8.81 MN. The pile capacity is not entirely mobilized as the design load is smaller than the permissible load P_M . A vertical settlement of 9.87 mm was calculated for a vertical load of 8.81 MN. The piles and the raft shared 59.97 %, and 40.03 % of the vertical load for the unimproved ground. The procedure of load settlement calculation for the piled-raft foundation in unimproved soil is shown in Appendix B. The vertical settlement calculation in the improved case involved a similar method but with the modification in the modulus of elasticity of the system. The

modification was made by taking the weighted average of the modulus of elasticity for different depths of layers of improvement.

5.4.2 Differential settlement and rotation

The differential settlement calculation for piled-raft foundation subjected to bending moment is not well documented in the literature. This study is based on the method of calculating the differential settlement caused by the moment load proposed by Shrestha et al. (2017). In this method, the raft and the piles share the moment applied to the piled-raft in such a percentage, resulting in the equal differential settlement of the piles and the raft. The differential settlement governed the design in the case of improved ground. The calculation of the differential settlement of specific parts of the piled-raft foundation (piles and raft) is presented in the following section.

5.4.2.1 Differential settlement of raft

The differential settlement of the raft was calculated based on the rotation (θ) caused by the wind. The wind load rotates the tower by an angle (θ) that is equivalent to the rotation of the raft. The rotation of the raft was determined using Equation (5.20) (Grunberg and Gohlmann 2013).

$$\theta = \frac{M_{foundation}}{c_s I_{foundation}};\ c_s = \frac{E_s}{f'\sqrt{A_{foundation}}} \tag{5.20}$$

where c_s is the modulus of the foundation, $M_{foundation}$ represents the fixed-end moment at the interface of the soil and structure, E_s is the equivalent modulus of elasticity of soil,

$I_{foundation}$ symbolizes the second moment of inertia of the foundation, $A_{foundation}$ is the area of the foundation, and f' is the shape factor for overturning. The differential settlement was calculated using trigonometry once the raft rotation (θ) was established.

5.4.2.2 Differential settlement of piles

The differential settlement of the piles in a piled-raft was calculated by considering the portion of the total vertical load and bending moment carried by the piles. Initially, the vertical load on every pile head was approximated, and the settlement of every pile was determined using the method described by Fellenius (1999). The same procedure was repeated by adjusting the bending moment shared by the raft and piles until the settlement profiles of the raft and the piles matched, which was considered as the differential settlement of the piled-raft. The process of matching the differential settlement of the raft and the piles is an iterative method. After numerous iterations, it was discovered that for the case of unimproved ground, the piles carried 80.62 % of the total bending moment, and the rest was carried by the raft to produce an equal differential settlement. For unimproved ground differential settlement was calculated to be 13.80 mm and the rotation to be 0.098°. The rotation displaces the top of the 80 m tower by 138.05 mm, which is within the tolerable limit (<240 mm for 80 m tall tower). The calculation procedure of differential settlement of the piles and the raft in unimproved soil is shown in Appendix B. A similar method was adopted for the determination of differential settlement of the piled-raft foundation in the improved ground. Figure 5.3 shows the proposed approach in graphical form.

$$M_{PR} = M_P + M_R$$
$$\delta_{PR} = \delta_P = \delta_R \tag{5.21}$$

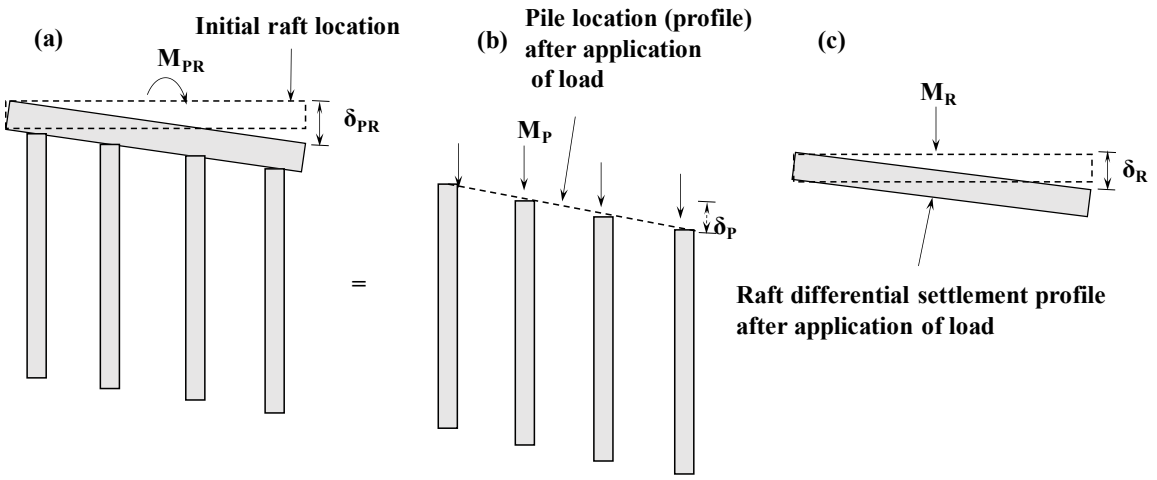

Figure 5.3. Diagrammatic representation of differential settlement calculation (a) piled-raft foundation (b) piles and (c) raft

5.5 Final design of the piled-raft foundation

The final design comprised a raft of 8.0 m in diameter and 1.0 m in thickness. The top of the raft was level with the soil surface. For in-situ soil (without ground improvement), a total of 24 auger cast piles with an outside diameter of 457 mm (18 inches) and 48.4 m in length was needed to meet the design requirements. The arrangement of the piles was in two circles of 12 piles, each around radii of 3.37 m and 2.23 m, respectively. For the design of the foundation in improved soil, the dimensions of the raft were kept constant, the same number of piles were used, and only the length of the piles was varied. The plan view of the layout of the piles around the raft is shown in Figure 5.4.

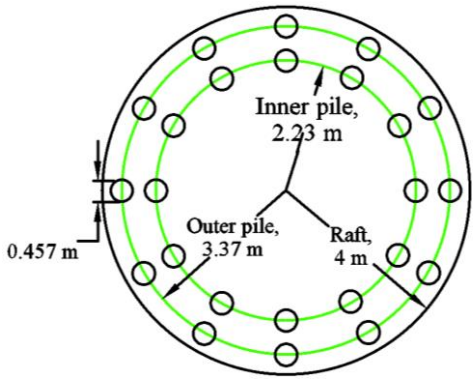

Figure 5.4. Plan view of the piled-raft designed for the wind turbine.

5.6 Results and discussion

5.6.1 Effectiveness of ground improvement in the design outcome

To calculate the effectiveness of ground improvement, initially, the analytical design of the piled-raft foundation was done for the unimproved case (shown in the earlier section). It was then followed for improved cases, where the length of piles was decreased under 48.4 m (the length in the unimproved case) until the critical design for either the stability or the serviceability requirement was reached. The stability requirement (moment capacity) governed the design in case of unimproved ground. However, the serviceability requirement (differential settlement) governed the design in case of improved ground. The critical differential settlement for both improved and unimproved cases was set at 24 mm.

Figure 5.5(a) shows the decrease in the length of the pile for various levels of ground improvement in the vertical direction. The decrease in the length of the pile from 48.40 m to 9.85 m was seen when the ground improvement was applied to unimproved soil to the most significant depth of 3.60 m (level V_5). The huge decrease in the length of the

pile is possible due to variation in the total vertical and bending moment loads shared by the piles and the raft for each case of ground improvement. The raft carried 19.38 % of the bending moment in the unimproved ground. However, the percentage of moment carried by the raft for the various ground improvement levels V_1, V_2, V_3, V_4, and V_5, increased to 46.08 %, 48.58 %, 51.17 %, 53.47 %, and 55.93 %, respectively. It can be seen from Figure 5.5(b) the horizontal deflection decreases initially from the unimproved case (4.69 mm) to the shallowest (level V_1) depth of ground improvement (4.36 mm). However, the horizontal deflection increased with a further rise in levels of ground improvement. The increase in horizontal deflection is possibly due to the decrease in pile length not being sufficiently compensated by a corresponding increase in depth of ground improvement. Ultimately, a horizontal deflection of 7.69 mm was noted for the most profound ground improvement depth (level V_5). The analysis showed the vertical load capacity, and the bending moment capacity increased with ground improvement, as shown in Figure 5.6.

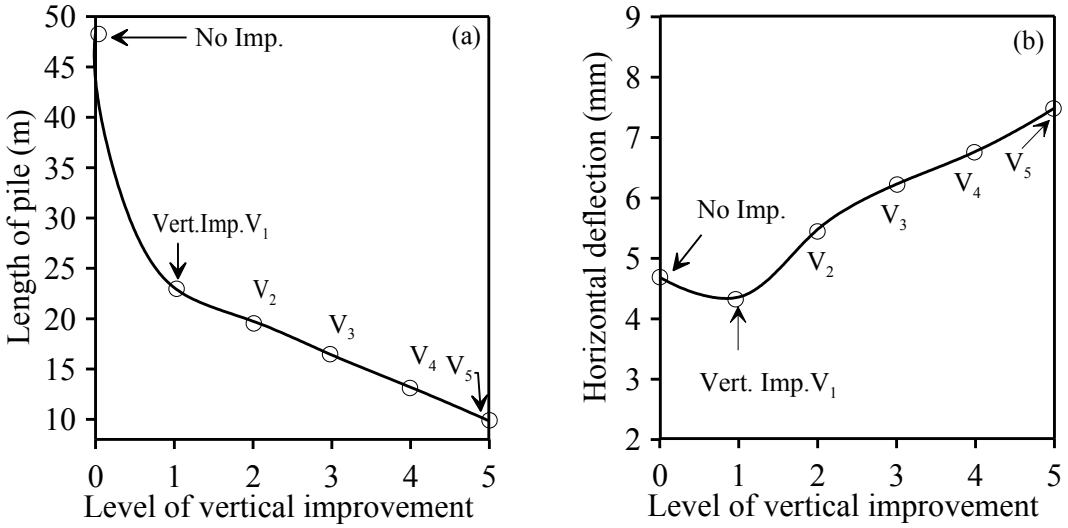

Figure 5.5. Analytical design results on (a) length of the pile and (b) horizontal deflection

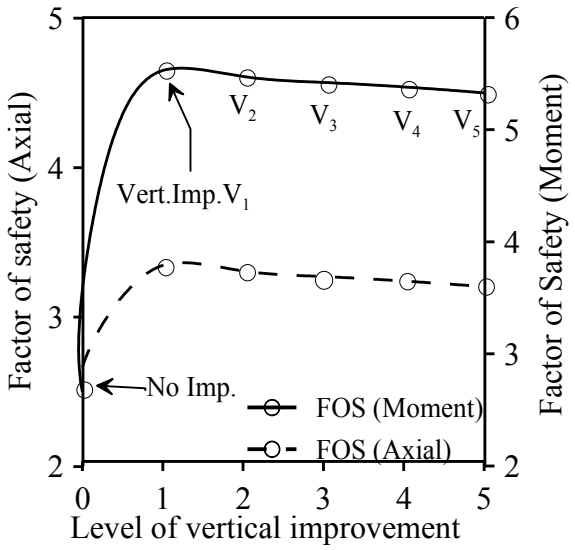

Figure 5.6. Variation of the factor of safety for vertical load and moment capacities with various level of ground improvement (pile lengths were adjusted to meet the minimum design requirements, controlled by differential settlement)

5.6.2 Performance evaluation of piled raft

The results shown in the previous section illustrate the effectiveness of ground improvement on the length of the pile. However, the performance of a piled-raft foundation can be truly assessed by only varying the depths of ground improvement, meanwhile keeping the dimensions of the piled-raft constant. By only applying ground improvement (keeping foundation dimensions the same as in the unimproved case), the differential settlement, horizontal deflection, and the rotation were observed to decrease. Figure 5.7(a) shows the change in horizontal deflection with the various levels of ground improvement when the pile length is 48.40 m (pile length in the unimproved case). Figure 5.7(a) shows the horizontal deflection reduced to 3.10 mm when the depth of ground improvement was 3.6 m (level V_5) as compared to 4.69 mm in the case of unimproved ground. Similarly, Figure 5.7(b) shows the change of differential settlement with the variation in the level of

ground improvement with the pile length being fixed at 48.4 m. The differential settlement reduced from 13.80 mm to 12.02 mm when the ground was improved from an unimproved case to a depth of 3.6 m (level V_5).

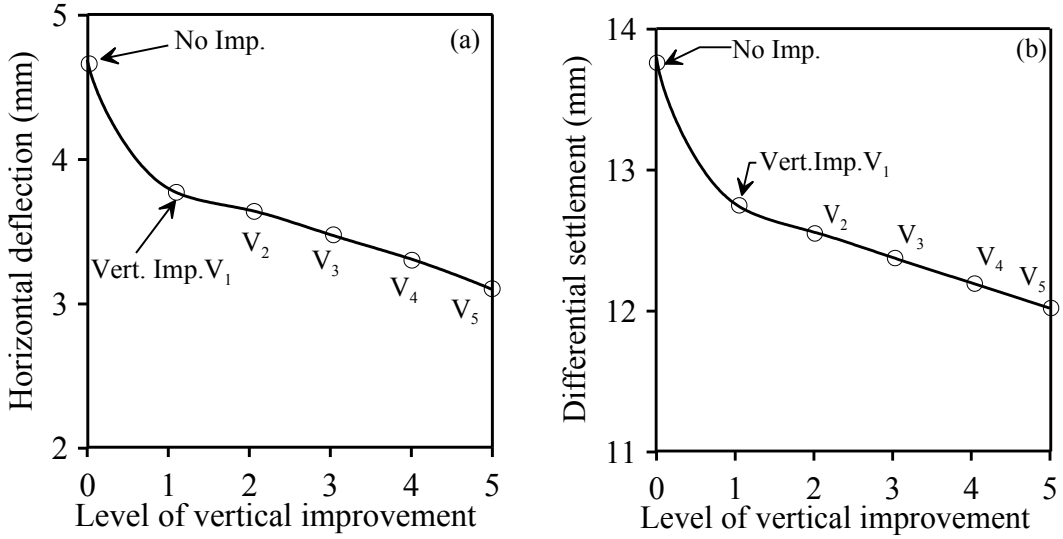

Figure 5.7. Effect of ground improvement on the deflection behavior (pile length = pile length in the unimproved ground) (a) horizontal deflection and (b) differential settlement

Figure 5.8 shows the increase in the factor of safety for vertical and moment load capacities with the application of ground improvement. The increase in the factor of safety against both vertical and moment load capacities are not consistent with levels of ground improvement. The factor of safety increases substantially from unimproved ground to the first ground improvement level, but the increase is minor after that.

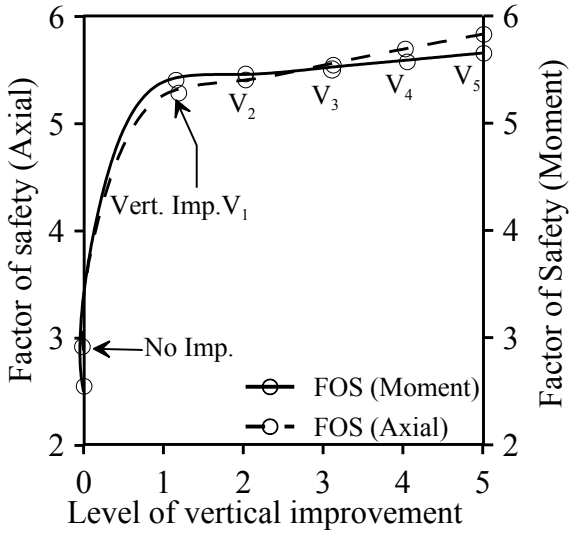

Figure 5.8. Variation of the factor of safety for vertical load and moment capacities with various levels of ground improvement (length of piles= length of piles in the unimproved soil)

The analytical design of the foundation led to findings of a substantial reduction in the length of the pile with ground improvement. The safety and serviceability criteria were satisfied after the ground improvement, even with a large decrease in the pile length. The performance evaluation study showed that the ground improvement after a certain level of improvement would not increase the performance proportionally as the initial level of improvement, which could be an essential factor in deciding on the most economic depth of ground improvement.

CHAPTER 6

FINITE ELEMENT ANALYSIS OF PILED-RAFT FOUNDATION

Because of the limitations in the analytical design, the analytical design only dealt with the variation in the depth of ground improvement. The width (horizontal distance from the center of the raft) of ground improvement was considered infinite, which does not portray the real field conditions. The variation in ground improvement along the width and depth must be incorporated in the design to replicate the real-world scenario. Analysis of models with both horizontal and vertical variations in ground improvement is necessary for developing the most effective and economical ground improvement configuration. The analytical design is obtained from the simplified method and lacks standard design procedure, especially for differential settlement due to the bending moment. Also, complex soil-structure interaction in the foundation design can be better incorporated using advanced FE algorithms. Thus, to get further insight into the performance of piled-raft foundation with realistic ground improvement approach, 3D FE simulation domains (models) representing unimproved ground and various levels (both vertical and horizontal variations) of ground improvements were created and analyzed. This chapter discusses the 3D FE model creation, constitutive models, and FE analysis and the results.

6.1 Finite element model properties

Three-dimensional (3D) FE simulation domains (models) of the soil-pile-raft system based on the outcomes of the analytical design was created using the software ABAQUS v2018. The problem under discussion requires the ability to develop models that

can simulate ground improvement in 3D, illustrate combined loads acting asymmetrically on the foundation and the soil-pile-raft interaction. The 3D FE software ABAQUS has an extensive library of various material modes to represent the soil and the structure accurately. Besides, this software is capable of illustrating the interaction between soil and structure and structure to structure precisely.

6.1.1 Simulation domain and boundary condition

Numerous simulation domains were needed to be created to analyze the effectiveness of ground improvement on design outcomes (variation in pile length), the performance of the piled-raft foundation (constant pile length), and parametric study (variation in cohesion values). Two different simulation domain sizes were used for the analysis. The configuration with pile length equal to 48.4 m used a simulation domain 30 m in diameter and 60 m in height. Similarly, the other configurations with reduced length of piles used a simulation domain 30 m in diameter and 40 m in height. Size sensitivity analysis was performed under various loading conditions to choose the size of the simulation domain to reduce the effect of simulation size on the computed results. Based on this, the dimensions mentioned above were considered suitable for the simulations. The thickness and diameter of the raft were 1 m and 8 m, respectively. As observed from the analytical design, various configurations with varying depth of ground improvement had varying lengths of the pile, and FE simulation domains were created for each of the cases.

The simulation domain (model) for each analysis was developed by creating separate 3D components individually. The individual components (parts), for example,

raft, piles, and soil, are then combined using the assembly module. A soil-pile-raft assembly was conceived and cut instance applied to the assembly to core the soil for adjusting piles and raft. This process of coring creates a new soil component (part) with spaces for the pile and raft to slot in. This process is required to identify independent surfaces in the structures that come in contact with the soil surface and to define the interaction properties between these surfaces in contact. The following Figure 6.1 shows the pile-raft and the soil domain with spaces cut to adjust the raft and pile assembly.

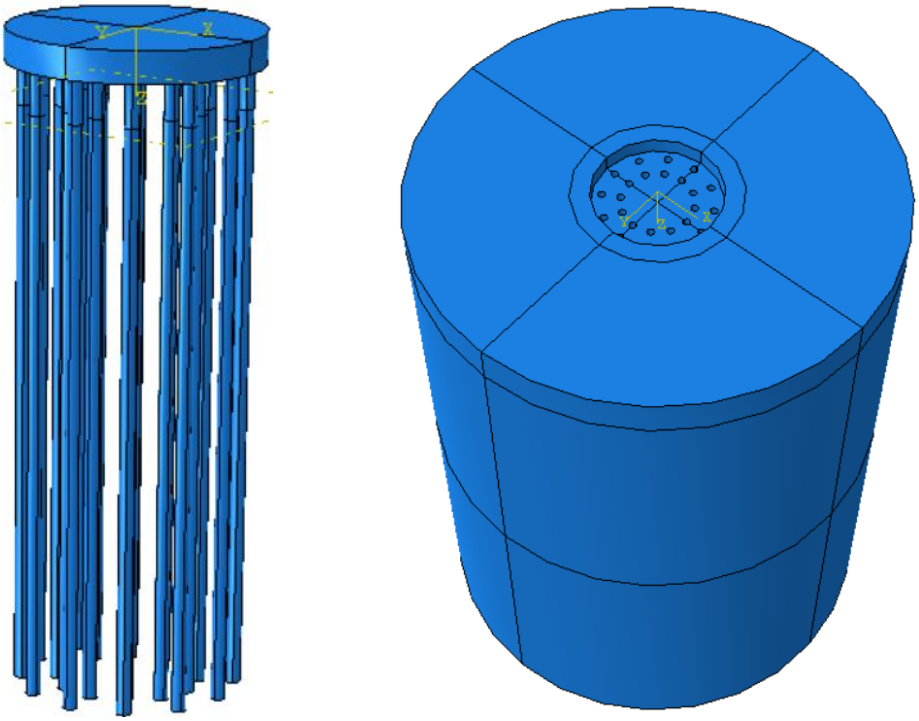

(a) (b)

Figure 6.1. (a) Pile-raft assembly and (b) soil domain with space cut to adjust the pile and the raft

The boundary condition was applied to the simulation domain. The base of the domain was fixed in all x, y and z directions, and the sides fixed only in x and y directions. This boundary condition allows the soil and structure to move along z-direction to illustrate the settlement of the foundation and the interaction (slip) of the piles along the soil surface. The following Figure 6.2 shows the 3D FE simulation domain for the case with the unimproved ground, and Figure 6.3 shows the 3D FE simulation domain for the case with the improved ground with the level of improvement V_1H_1 (depth of improvement = 2 m and width of improvement = 14 m).

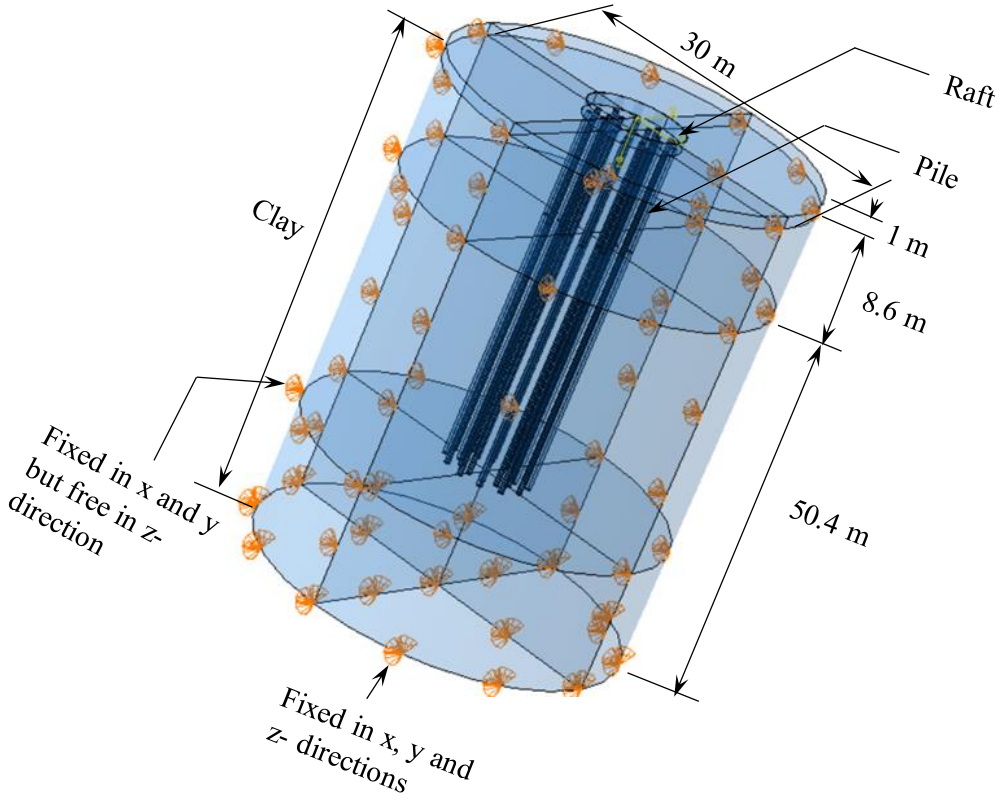

Figure 6.2. A 3D simulation domain of piled-raft foundation for unimproved ground

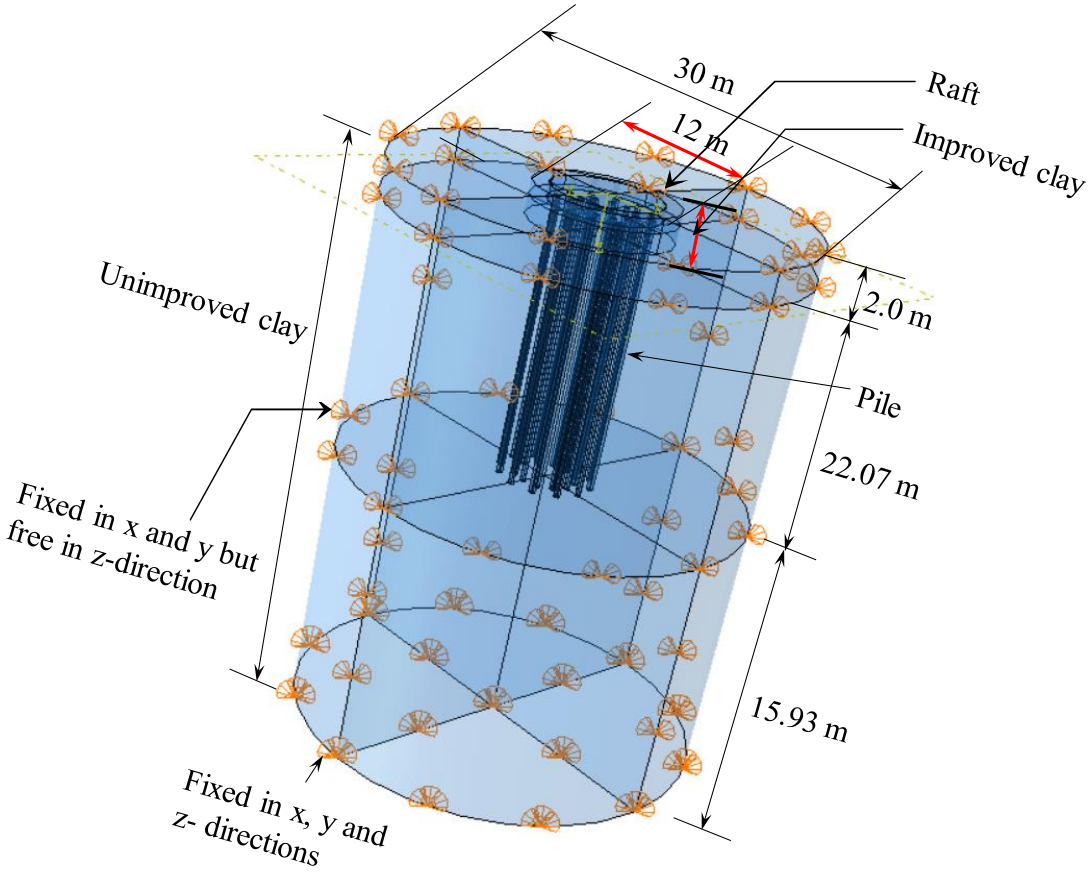

Figure 6.3. A 3D simulation domain of piled-raft foundation for improved ground (V_1H_1)

6.1.2 Mesh generation

Mesh was generated in the simulation domain using the linear eight-noded hexahedral brick element (C3D8R) with reduced integration and hourglass control. The eight-noded hexahedral brick element (C3D8R) element used in the study is shown in the following Figure 6.4.

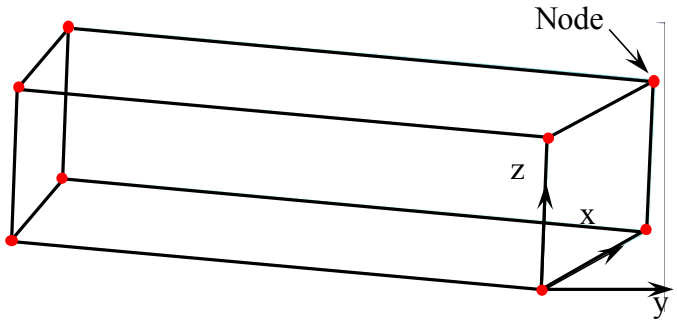

Figure 6.4. Linear 8-noded hexahedral brick element (C3D8R)

Various partitioning techniques available in ABAQUS was used to divide different parts in order to create a suitable mesh. The number of elements assigned to the surfaces in contact was proportionate to ensure node to node contact between them. A coarser mesh was used in the areas with lower stress concentration, such as the soil towards the bottom and side boundaries. Finer mesh towards the piles, raft, and the soil near piles and the raft. Using the bias feature available in ABAQUS, it was possible to designate varying element sizes, which enabled generating increasing or decreasing element sizes in the desired direction. The partition of the simulation domain and the FE mesh generated is shown in Figure 6.5. A total of 109,770 nodes and 98,174 elements were generated in the mesh for the case with improvement level V_1H_1. The unimproved case had a larger soil domain and thus had a total of 705,898 nodes and 638,224 elements in the generated mesh. The total number of elements for each simulation domain varied due to the variation in the dimension of the piles and the dimension of ground improvement.

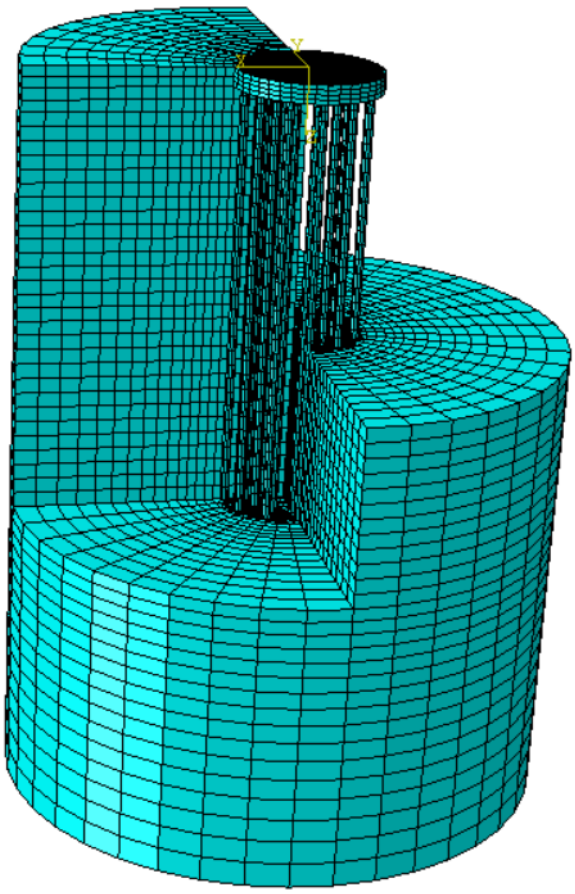

Figure 6.5. Mesh assembly with eight-noded hexahedral elements for soil (simulation domain V_1H_1)

6.1.3 Soil-structure interaction

One of the essential reasons for using the FE method in this study is to represent suitable interaction between the different surfaces of the piles, raft, and the soil. It is important to encapsulate the complex soil-structure interaction to derive realistic results. The soil, pile, and the raft are in contact with each other. The contact between pile skin and soil was defined by assigning the interaction properties. The contact between the soil and pile surfaces was defined in terms of the load transfer mechanism in normal and tangential

directions. The normal contact between the pile skin and soil was assigned using "hard" contact. "Hard" contact relationship eliminates the penetration of the slave surface into the master surface at constraint locations and does not allow the transfer of tensile stress across the interface. While defining the contact using a master-slave concept, one surface is defined as a master surface and the other as the slave surface. The general notion is to define the stiffer body as master and less stiff body as the slave surface. In the case of surfaces in contact with the same stiffness, the coarser surface is defined as master and finer surface as the slave surface. The stiffer body (pile) is defined as the master surface and the soil-skin as the slave surface in this interaction.

The friction formulation defined as "penalty" in ABAQUS was used to illustrate the tangential behavior. The tangential contact between the pile and soil was defined by the coefficient of friction (δ). The tangential behavior of the structure and soil surfaces in contact allow the slip to occur. The coefficient of friction value for the contact between concrete to soft clay was taken as 0.35, and between concrete and improved clay was taken as 0.45. The values of the coefficient of friction between the concrete (pile and raft) with the soil were obtained from NAVFAC DM 7.02 (1986). Figure 6.6 shows the normal and tangential contact between two elements.

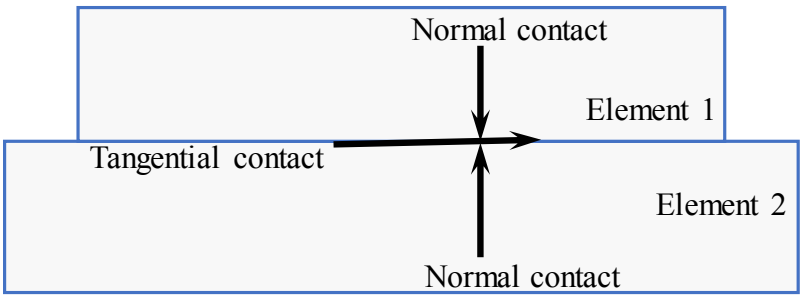

Figure 6.6. Interaction behavior of the elements in contact

The contacts between the top surface of the pile and bottom of the raft, pile toe and soil, and raft and soil were characterized by a surface to surface-based tie constraint. Such tie constraint also utilizes the master-slave concept. For surface contact between the pile top and raft bottom, the pile top was assigned as the master surface and raft bottom as the slave surface. Similarly, for the surface contact between pile toe and soil, pile toe was defined as master surface and soil as the slave surface. For the raft and soil contact, the raft surface was designated as the master surface and soil as the slave surface. The tie constraint binds the two surfaces in contact and thus enables equal translation and rotation between the surfaces in contact throughout the simulation. Several top nodes of the raft were connected to the center node by an MPC beam constraint. The MPC beam ties the raft's center node with the nodes on the surface of the raft and transfers the load from the center nodes to other nodes and eventually the piles.

6.2 Constitutive models

A linear elastic (LE) model and an elastoplastic (EP)-Drucker Prager constitutive models were used for the analysis. A LE model does not accurately represent the soil

continuum. The elastoplastic Drucker Prager (DP) model encompasses the non-linear behavior of the soil. A LE analysis is nevertheless carried out to make comparisons with analytical design results, as the analytical design is based on elastic theory. The EP model parameters were adjusted from the LE model parameters. The elastoplastic Drucker Prager hardening (DP-H) model was used for the analysis. The DP-H model better represents the soil undergoing large strain as the yield criterion is broader for the DP model compared to Mohr-Coulomb (MC). The following Figure 6.7 shows the yield surface criterion for DP and MC model. The DP-H soil model was used for the analysis to account for the stiffening of the soil under large loads. The LE and EP model parameters are shown in Table 6.1.

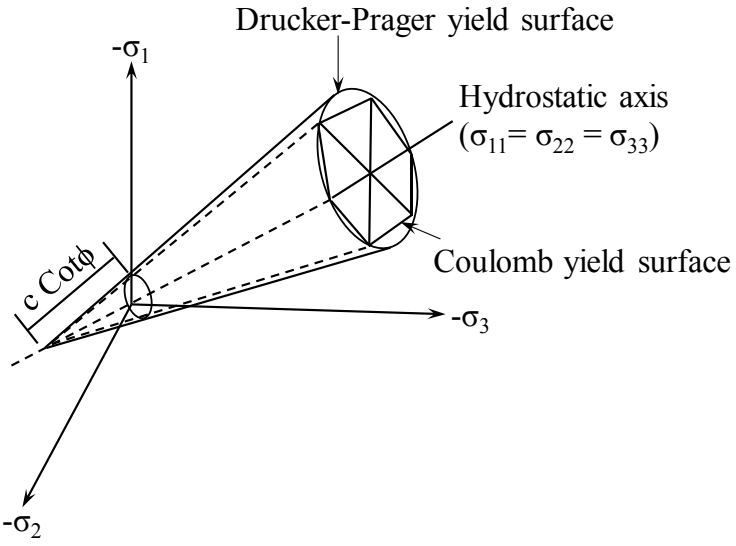

Figure 6.7.Yield surface criterion for DP and MC models

Table 6.1. Linear elastic and elastoplastic soil model parameters

Model	Parameter	Value
Linear elastic	Density (kg/m^3)	1835.5
	Young's modulus (N/m^2)	3.05 x 10^7
	Poisson's ratio	0.3
Elastoplastic DP	Shear criterion	Linear
	Flow potential eccentricity	0.1
	Friction angle (°)	0
	Flow stress ratio	1

The input parameter for the DP-H model was yield stress versus plastic strain curve. The yield stress needed to be determined first to obtain the yield stress ($\Delta\sigma$) versus the plastic strain (ε^p) curve. The yield stress was determined from the stress-strain curve (shown in Figure 4.1) as the deviator stress at which the soil started exhibiting non-linear behavior. For calculating the plastic strain, the elastic strain was determined first and then subtracted from the total strain. The elastic strain ε^e at different stresses was calculated by dividing yield stress $\Delta\sigma$ by the initial modulus of elasticity E_0 ($\varepsilon^e = \frac{\Delta\sigma}{E_0}$). The plastic strain ($\varepsilon^p$) was obtained by subtracting the elastic strain from the total vertical strain ε ($\varepsilon^p = \varepsilon - \varepsilon^e$). The yield stress versus plastic strain curve used in the study is shown in Figure 6.8.

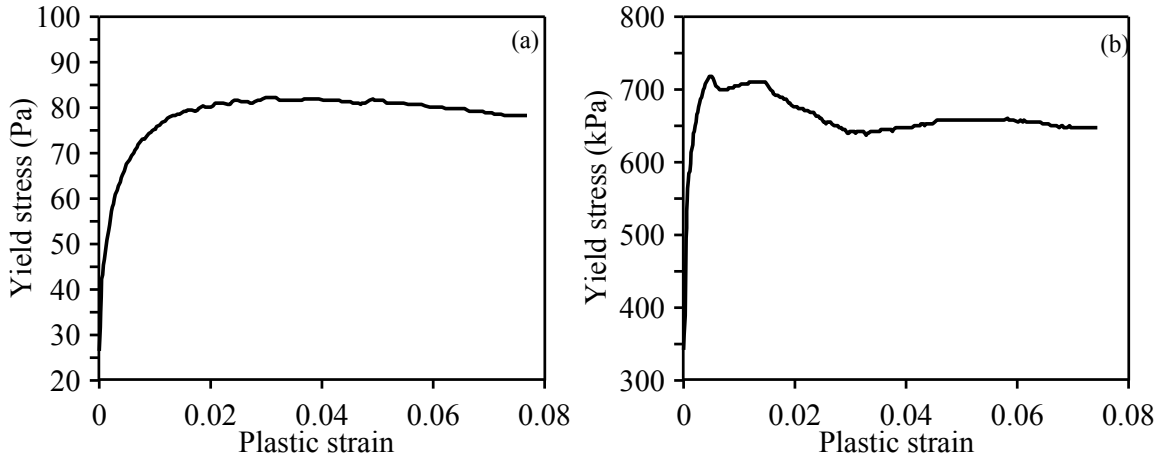

Figure 6.8. Elastoplastic DP-H model yield stress vs. plastic strain curve (a) soft clay and (b) CSM improved clay (calculated from Figure 4.1)

6.3 Finite element model development procedure

The development of the simulation domain (models) started with the creation of various individual components (parts), namely, piles, raft, and soil. The properties of the material used for each part were defined. The raft and piles were made of reinforced concrete. The density of the pile and raft was 2549.3 kg/m^3, the Poisson's ratio was 0.15, and Young's modulus of elasticity (E) was 3.0×10^{10} N/m^2. Since ABAQUS does not have a defined unit system, all the inputs made had consistent units. The parts were then assembled using the assembly module, and the cut instance was applied to the assembly to create space in the soil for adjusting piles and raft. The surfaces of the soil, pile, and raft to be in contact were specified, and the contact was generated using the interaction module. The properties of interaction have been discussed in the earlier sections. The piles, soil, and the raft were meshed using the meshing technique discussed earlier, and the boundary conditions were applied to the model.

The analysis consisted of three steps: initial step, geostatic step, and loading step. The initial step was automatically generated. The boundary conditions, contact constraints, and the interactions activated in the initial step circulate to the subsequent steps. The geostatic step enforces the gravitational load on the model. Automatic time step incrementation was applied to the geostatic step, and the maximum number of increments was limited to 100. In the loading step, the vertical, horizontal, and moment loads were applied in the desired location and direction. The loading step also had maximum increments set to 100, but the incrementation size was set to 10^{-5} or increased to 10^{-8} depending on the convergence. Following the creation of the 3D FE simulation domain, a job was created in ABAQUS. The job was submitted to the Clemson University Palmetto cluster, a network of high-performance computers. The runtime depended upon the availability of nodes and the processors in the cluster. The average time of completion of the smaller model domains was about 1.5 hours, and some of the larger models took a few hours to complete.

A total of 132 models were created and analyzed in this study under three different cases, as detailed below.

Case I: 60 models (30 LE and 30 EP) were created to analyze the effectiveness of ground improvement. In these models, the length of the pile varied with the variation in depth (V) of improvement. For each depth (V) of ground improvement, six horizontal radii of improvement (H) was applied to see the effect of improvement in the horizontal direction. The radius of horizontal improvement (H_i, i = 1 to 6) were 6.0, 6.4, 6.8, 7.2, 7.6

and 15 m respectively. The horizontal ground improvement radius (H_6 = 15 m) extends to the boundary of the model to emulate the analytical design condition. So, for each depth of improvement, six models with the same pile length and varying radius of improvement were obtained.

Case II: 60 models (30 LE and 30 EP) were created to analyze the performance enhancement of piled-raft foundation with ground improvement. In these models, the length of the pile was kept the same as in unimproved ground (L_p = 48.4 m) with the variation in depth (V) of improvement. For each ground improvement depth, six horizontal radii of improvement (H) was applied to see the influence of improvement in the horizontal direction. The radius of horizontal improvement (H) was the same as the case mentioned above. So, six models for each depth of improvement was obtained.

Case III: The parametric study was performed by changing the undrained shear strength (s_u) of unimproved and improved grounds. The variation was ±1σ, from the mean $s_u(\mu)$, where σ is the standard deviation in shear strength. The models created had radius of width of ground improvement stretching to the boundary of the model (H_6 = 15 m). This was done to make comparison with the analytical design. The case with the mean shear strength was already created for the determination of the effectiveness of ground improvement (*Case I*) mentioned earlier. Thus, 12 additional models were created, 6 with reduced shear strength (μ-1σ) and 6 with increased shear strength (μ+1σ). The following Figure 6.9 shows the outline of the simulation matrix created.

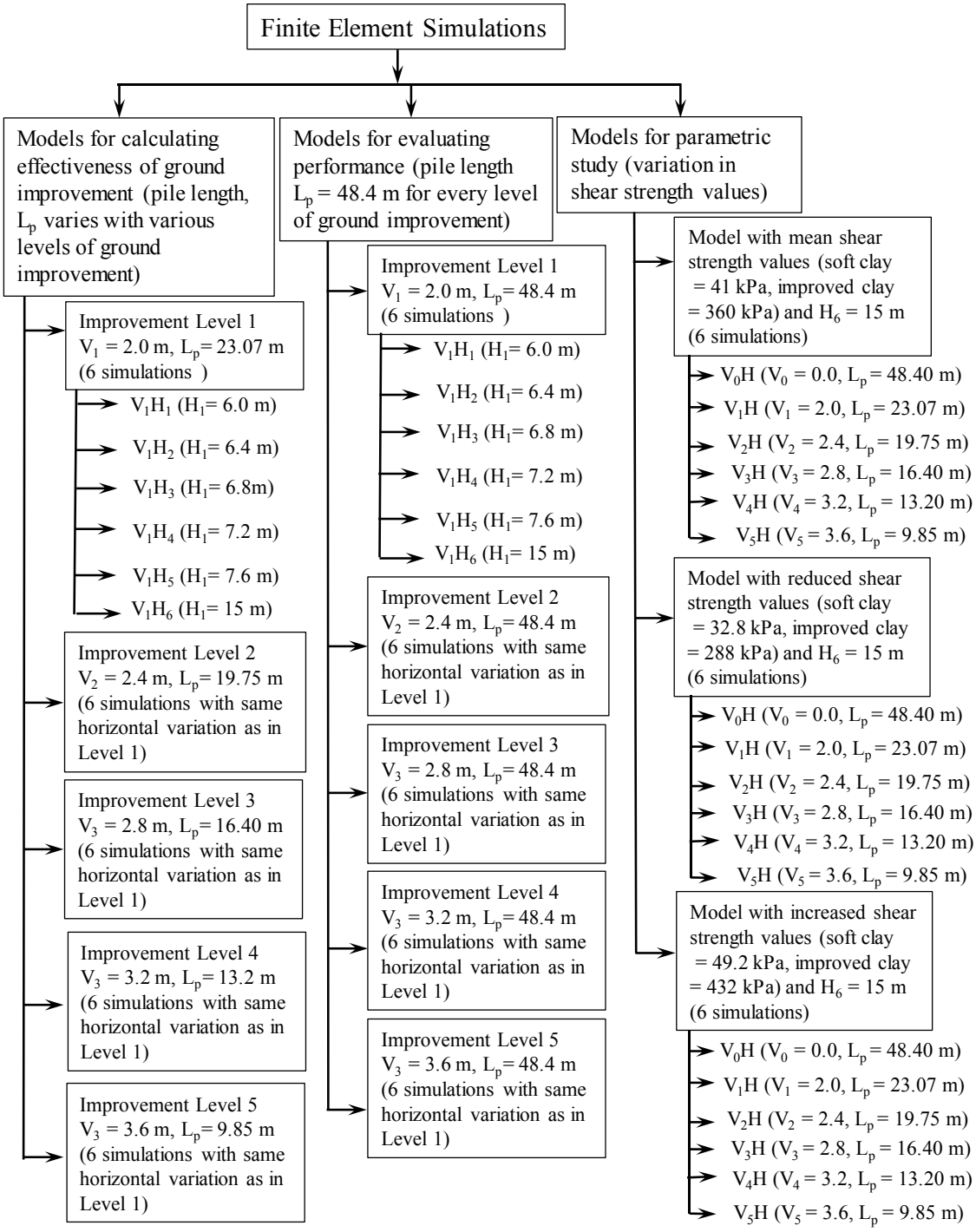

Figure 6.9. Outline of the simulation matrix

6.4 Finite element analysis results

The results on horizontal deflection and differential settlement of the LE and EP constitutive models were analyzed. Two different approaches were made to obtain the FE results. First, the analysis to determine the effectiveness of the ground improvement on the deformation behavior of a piled-raft foundation was carried out. It included the creation of FE models with ground improvement varying in both horizontal and vertical directions. It adopted the reduced length of the pile with ground improvement based on analytical design. The second approach was to evaluate the performance of the piled-raft foundation. The FE models were created for the improved ground with horizontal and vertical variations in ground improvement, meanwhile keeping the length of the pile (L_p) constant (equivalent to that of the unimproved ground). The following Figure 6.10 represents the deformed shape of a piled raft foundation of the EP model for an improved soil (V_1H_6). The deformation scale factor used was 200.

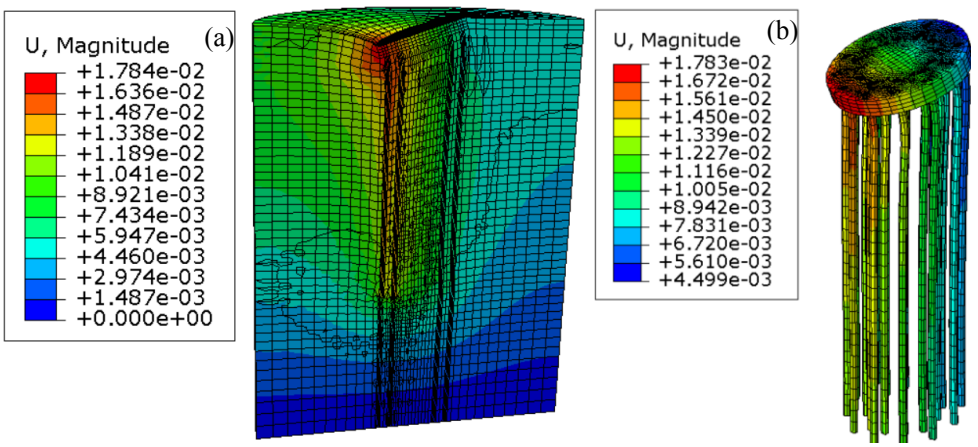

Figure 6.10. Deformed shape of the model with displacement contours (a) cross-section of the simulation domain and (b) piled-raft assembly (deformation scale factor = 200)

The following Figure 6.11 shows the stress-contour for the piled-raft foundation.

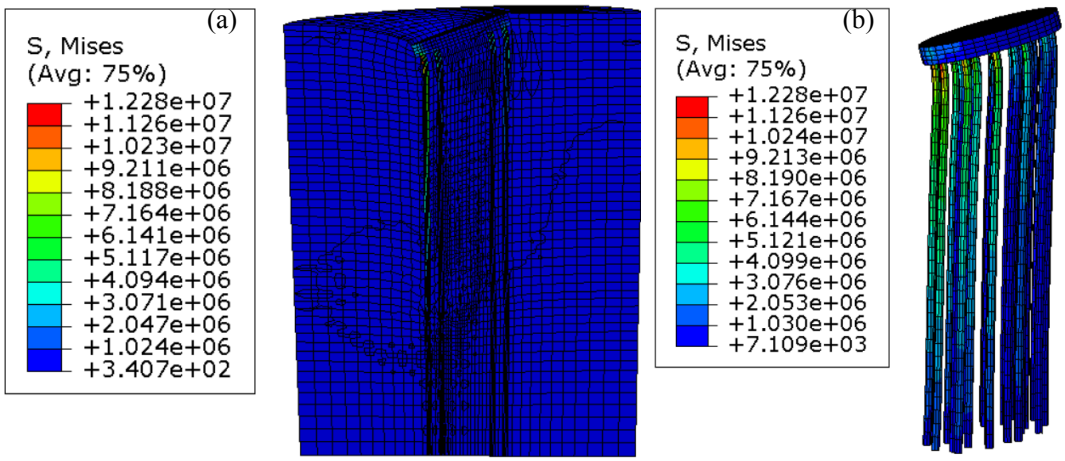

Figure 6.11. Von-Mises stress contours (a) cross-section of the simulation domain and (b) piled-raft assembly (deformation scale factor = 200)

The friction between the soil and piles (resisting the load and moment) induces shear between the surfaces in contact. Figure 6.12 shows the frictional shear in the soil and the piles. The shear between the piles and soil is essentially the same as seen from the figure.

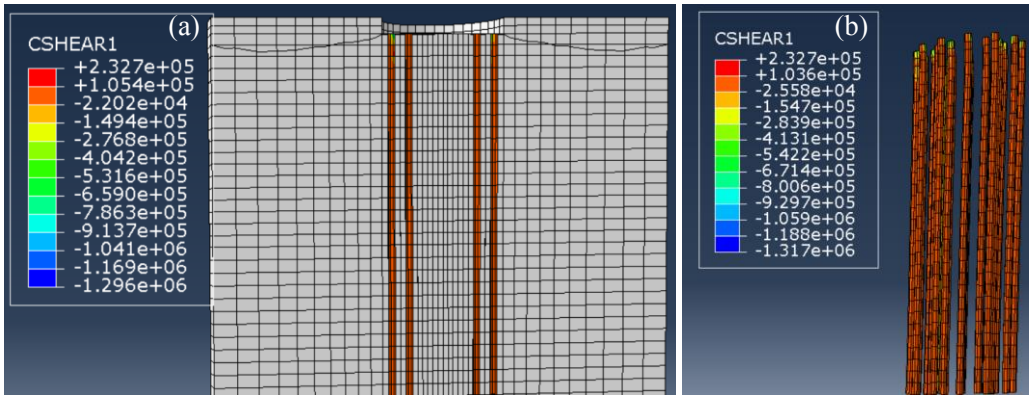

Figure 6.12. Frictional shear between piles and the soil (a) cross-section of the soil domain and (b) piles

6.4.1 Effectiveness of ground improvement on design outcomes

The results on the horizontal deflection and the differential settlement of the piled-raft have been discussed below. The analysis was performed by adopting the design outcome (length of the pile in this case) from the analytical design. The analytical designs only considered the vertical variation in ground improvement, but the FE designs incorporate both the horizontal and vertical variations. The analysis based on the FE models helps in the determination of the most effective design. The following Figure 6.13(a) and Figure 6.13(b) represent the horizontal deflection obtained from LE and EP FE models, respectively. Figure 6.13(a) reveals the increase in the horizontal deflection from the unimproved case to the first level of ground improvement. Though the horizontal deflection is expected to decrease with improvement, it increases in this case because of the massive reduction in length of the pile; 48.4 m in the unimproved ground to 23.07 m in improvement depth V_1. The horizontal deflection increased from 1.94 mm in the unimproved ground to 2.10 mm at V_1. The effect of the decrease in length outweighs the effect of improvement and thus leads to higher deflection. The trend of increase in horizontal deflection with each level of vertical improvement (V_i; i = 0 to 5) can be attributed to the reduction in length of the pile (48.4 to 9.85).

Keeping the depth of vertical improvement constant and increasing the radius of horizontal improvement led to a decrease in horizontal deflection. For the LE model, the vertical improvement V_5 (L_p = 9.85 m) led to a maximum deflection of 3.36 mm for the radius of horizontal improvement H_1 (6.0 m), and it decreased to 2.32 mm at H_5 (7.6 m). It shows the effect of horizontal improvement on the horizontal deflection. The EP model

results, as shown in Figure 6.13(b), also reveals a similar behavior to that of the LE model. The EP model, however, shows larger deflection values when compared to the LE models with the same case of improvement. In the unimproved case (L_p = 48.4 m), the EP model had a horizontal deflection of 2.08 mm compared to 1.94 mm in the LE model. For the EP model, the vertical improvement V_5 (L_p = 9.85 m) led to a maximum deflection of 4.17 mm at a radius of horizontal improvement H_1 (6.0 m), and it decreased to 2.58 mm at H_5 (7.6 m). It shows that the ground improvement yielded acceptable values of horizontal deflection for both EP and LE models, even with a huge reduction in the length of the pile.

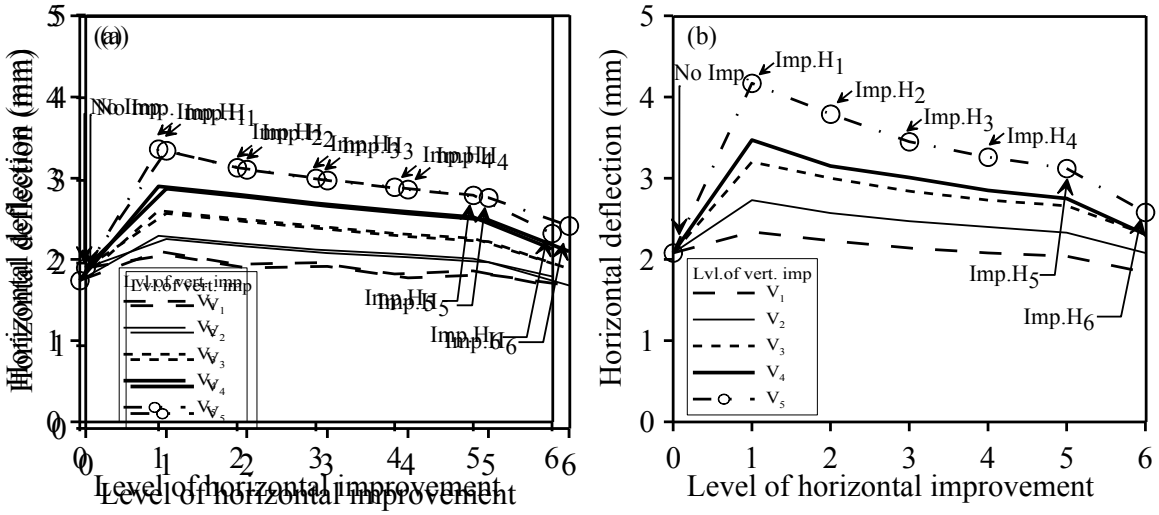

Figure 6.13. Horizontal deflection of piled-raft foundation (a) linear elastic model and elastoplastic model

The following Figure 6.14(a) and Figure 6.14(b) show the differential settlement of the piled raft foundation for LE and EP models, respectively. The differential settlement decreased with improvement owing to the substantial reduction in length of piles, which outweighed the effect of depth of improvement. The differential settlement of piled raft in

the unimproved ground (L_p = 48.4 m) for the LE model was 20.29 mm, and it increased with an increase in the level of vertical ground improvement. For ground improvement in horizontal direction H_1, the differential settlement increased from 22.31 mm at improvement V_1 to 32.40 mm at improvement V_5. The length of the pile in these two cases being 23.07 m and 9.85 m, respectively.

Unlike the case with horizontal deflection, the increase in the radius of horizontal ground improvement had little effect on differential settlement. The decrease in differential settlement upon an increase in the radius of ground improvement was small. For the LE model, the vertical ground improvement V_5 (L_p = 9.85 m) led to a maximum differential settlement of 32.40 mm for the radius of horizontal improvement H_1 (6.2 m). It decreased to 30.85 mm at H_6 (model boundary = 15 m). This shows that the effect of horizontal improvement on the differential settlement is minimal. Figure 6.14(b) shows the differential settlement behavior of the EP model with different levels of ground improvement and reveals a similar response to that of the LE model. The values of the differential settlement are higher for EP models than LE models with the same case of ground improvement. In the unimproved case (L_p = 48.4 m), the EP model had a differential settlement of 21.15 mm compared to 20.29 mm in the LE model. For the EP model, the vertical improvement V_5 (L_p = 9.85 m) led to a maximum differential settlement of 35.26 mm at the radius of horizontal improvement H_1 (6.2 m), and it decreased to 32.28 mm at H_6 (model boundary). Figure 6.14 shows that the ground improvement to level V_1 (L_p= 23.07 m) resulted in a differential settlement of 23.78 m, which is within the allowable

limit of 24 mm. Due to the significant reduction in the length of the pile, the other levels of improvement provide differential settlement higher than the permissible limit.

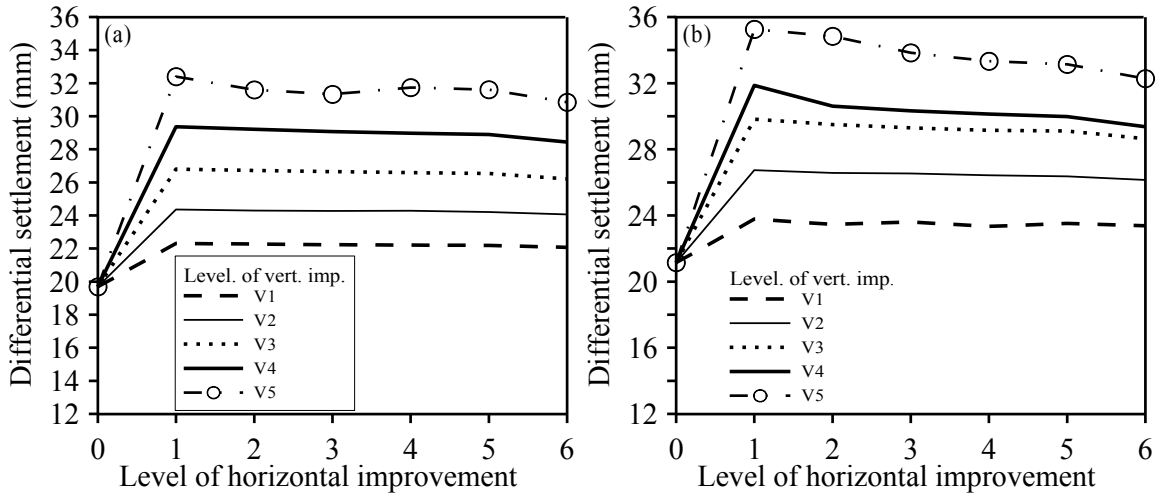

Figure 6.14. Differential settlement of piled raft (a) linear elastic model and (b) elastoplastic model

6.4.2 Performance evaluation of piled-raft

In the approach discussed earlier, the horizontal deflection and differential settlement was obtained by adopting the design outcome, i.e., varying length of pile upon variation of ground improvement depth. Since the length of the pile also changed along with the variation in ground improvement, this method does not represent the performance evaluation solely based on ground improvement. Thus, to understand the performance of the piled-raft foundation, 3D FE models were created by adopting the dimension of the piled-raft foundation in the unimproved ground. The dimensions of the piled-raft were fixed, and results on horizontal deflection and differential settlement were obtained by varying the level of ground improvement around the piled raft.

Figure 6.15(a) and Figure 6.15(b) show the horizontal deflection of the piled raft foundation for different levels of ground improvement when the length of the pile is fixed at 48.4 m (equivalent to that of the unimproved case). Figure 6.15 shows a very small decrease in horizontal deflection with variation in radius of ground improvement in the horizontal direction for the same depth of vertical ground improvement. For LE model, displacement decreases from 1.94 mm in unimproved case (L_p = 48.4 m) to 1.82 mm for improvement H_1 (6.0 m) and 1.37 mm at H_6 (model boundary = 15 m) when vertical improvement is V_5 (L_p = 48.4 m). Similarly, for the EP model, displacement decreases from 2.08 mm in the unimproved case (L_p = 48.4 m) to 1.85 mm for improvement H_1 (6.0 m) and 1.39 mm at H_6 (model boundary = 15 m) when vertical improvement is V_5 (L_p = 48.4 m). The horizontal deflection seems to increase slightly with the increase in depth of improvement. The increase is in the range of 10^{-2} mm. This unusual behavior can be due to the complex interaction between the soil-raft, raft-pile, and soil-pile. The length of the pile adopted from the analytical design was very conservative and yielded a minimal horizontal deflection of 1.94 mm in the unimproved ground. This value is minimal compared to the allowable horizontal deflection. Thus, improving the ground with the length of piles intact does not yield considerable improvement in the deformation behavior of the piled-raft as the deformation is already minimal.

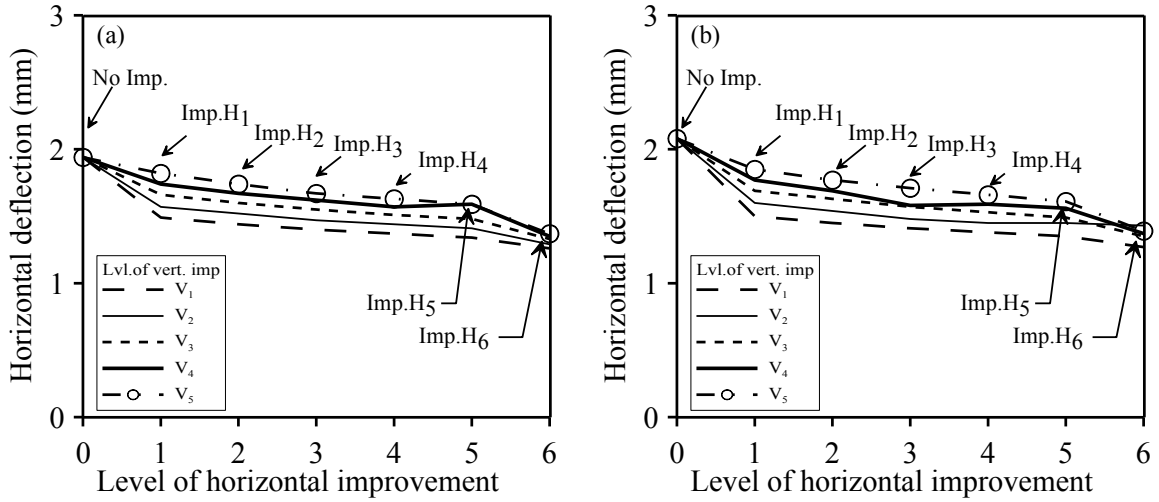

Figure 6.15. Horizontal deflection from FE models (pile length = length of the pile in the unimproved ground) (a) linear elastic model and (b) elastoplastic model

The differential settlement decreased with ground improvement, but the decrease was tiny. For LE model as shown in Figure 6.16(a), the differential settlement decreased from 20.29 mm in unimproved case (L_p = 48.4) m to a minimum deflection of 19.91 mm when improved to vertically to V_5 (L_p = 48.4 m) and horizontal improvement to the boundary of the model (H_6). There is minimal or no decrease in the differential settlement with the increase in horizontal improvement (H_1 to H_6) when the depth of vertical imp is kept constant. The case is similar in the case of the EP model. It is seen from Figure 6.16(b), the differential settlement decreases from 21.15 mm in the unimproved case (L_p = 48.4 m) to minimum deflection of 20.29 when improved to vertical level V_5 (L_p = 48.4 m) with the horizontal improvement extending to the boundary of the model (H_6). Also, the differential settlement decreases with the increase in the level of vertical improvement, but the decrease is very small.

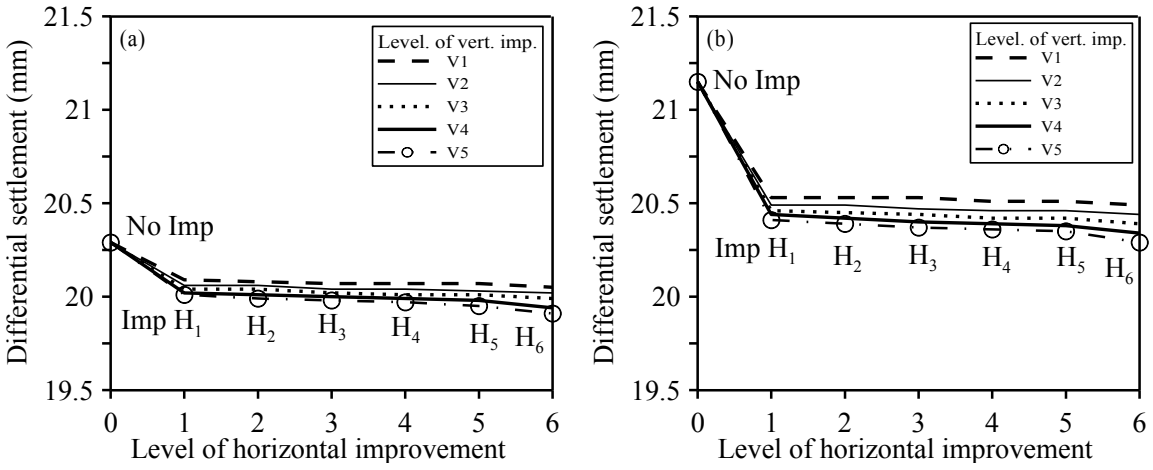

Figure 6.16. Differential settlement from FE models (pile length = length of the pile in the unimproved ground) (a) linear elastic and (b) elastoplastic

6.5 Comparison of analytical and finite element analyses results

The analytical design of the piled-raft foundation is based on simplified theory and lacks a concrete set of rules for the design. It is particularly true when the foundation is subjected to combined vertical, horizontal, and moment loads. Thus, analytical design can be inaccurate, conservative, and may under or overpredict the performance and the cost of the foundation. FE models are created adopting the design outcomes from the analytical design. The results obtained from the FE design can be compared to the results from the analytical designs. The FE design provides comparatively realistic results, and thus on the basis, FE results, the analytical design can be readjusted to obtain economic design.

The analytical design cannot incorporate the ground improvement variation in the horizontal direction, and the FE method can incorporate the variation in both horizontal and vertical directions. However, for one to one comparison between the analytical and FE

method, the FE models where the horizontal improvement extends to the boundary of the model (H_6) is only considered.

6.5.1 Effectiveness of ground improvement on the design outcome

The FE models were created by adopting the design outcomes from the analytical design, where the length of the pile was adjusted to meet the design requirements. The length of the pile varied from 48.4 m in the unimproved ground to 9.85 m for the vertical improvement V_5.

Figure 6.17(a) shows the comparison of horizontal deflections between the analytical and FE models for different levels of vertical variation. The analytical design predicts larger variation in the horizontal deflection with vertical improvement than both the EP and the LE FE models. For the unimproved case, the analytical design predicts the horizontal deflection to be 4.69 mm, and the EP and LE FE models predict lower values of 2.08 mm and 1.94 mm, respectively. The analytical design predicts a huge increase in the horizontal deflection with ground improvement (due to the massive reduction in pile length) compared to FE models. The FE models predict a slight increase in horizontal deflection compared to the analytical design. Also, the LE model showed lower deflections compared to the EP model. However, the difference is very small. It must be noted that the horizontal deflection was not the controlling factor for the design, and the design was governed by moment capacity for the unimproved case and differential settlement for the improved case.

Figure 6.17(b) shows the comparison of differential settlement between the analytical and FE models for different levels of vertical variation. The analytical design is governed by moment capacity for the unimproved case and differential settlement for the improved cases. It has resulted in a curve that starts at 13.80 for unimproved ground and flattens at 24 mm for all the improved cases. The FE models do not follow the pattern to that of the analytical design; rather, the differential settlement increases with an increase in improvement levels. It must be noted that FE models were created from the analytical design outcome where the length of the pile was reduced massively with ground improvement to obtain the critical differential settlement of 24 mm. Thus, FE models predict an increase in the differential settlement with ground improvement owing to the reduced length of the pile. The EP model predicts a differential settlement of 21.15 mm for the unimproved case (L_p= 48.4 m) and 32.28 mm for improvement level V_5 (L_p= 9.85 m). The LE model predicts a differential settlement of 20.29 mm for the unimproved case (L_p= 48.4 m) and 30.85 mm for improvement level V_5 (L_p= 9.85 m).

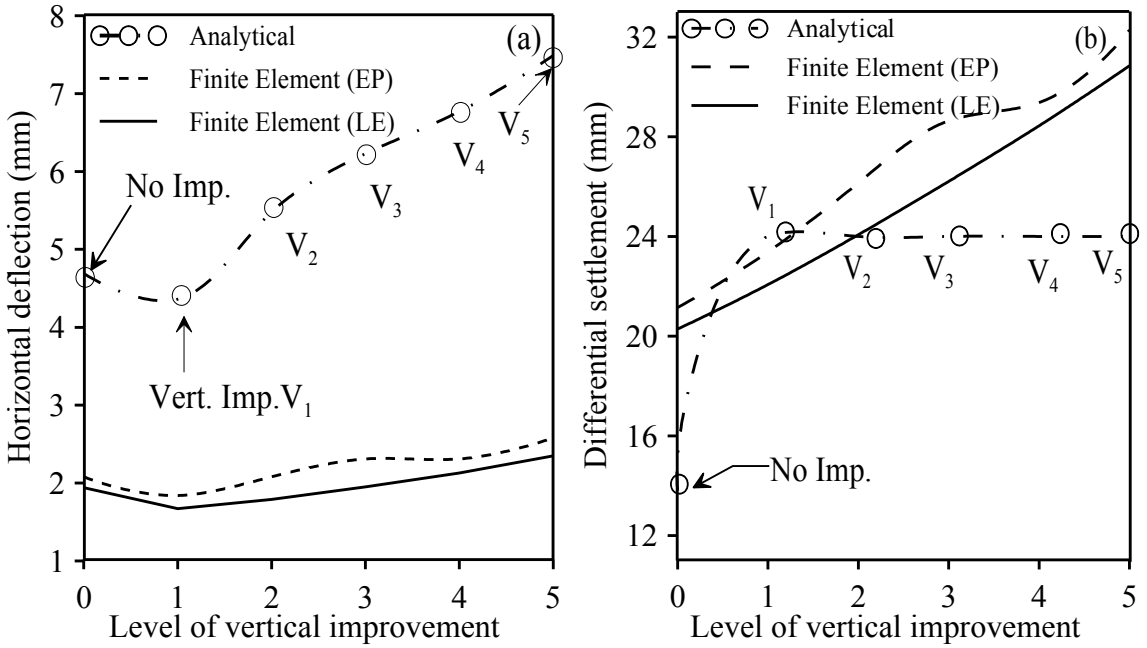

Figure 6.17. Analytical vs. FE comparison of models (varying pile length) (a) horizontal deflection and (b) differential settlement

6.5.2 Performance evaluation of piled-raft foundation

The analytical design was performed with the length of the pile equivalent to 48.4 m, and the same length of the pile was adopted for creating the FE models. Figure 6.18(a) shows the horizontal deflection comparison between the analytical design and the FE models with different levels of vertical improvement but with the same length of the pile. The analytical design predicts the horizontal deflection to decrease with ground improvement. The horizontal deflection decreases from 4.69 mm in the unimproved case to 3.10 mm for the improvement level V_5. However, for the FE models, the horizontal deflection decreased from unimproved ground to the first level of improvement, but the change in horizontal deflection was minimal with further levels of improvement. The EP and the LE models had a similar pattern and minimal horizontal deflection, and it could

well be because the length of the pile adopted (48.4 m) was conservative. It is evident that this length of the pile is not required for the improved case, as it can be seen from Figure 6.18(a) where the reduced pile length also yielded small (acceptable) horizontal deflection. The horizontal deflection has reached almost a saturation point, where even increasing the depth of improvement has very little effect.

Figure 6.18(b) shows the comparison of results on differential settlement from the analytical design and FE models. The analytical design predicted the decrease in the differential settlement with an increase in ground improvement. The analytical design predicted a differential settlement of 13.80 mm for the unimproved case, and it decreased to 12.80 with the level of improvement V_5. The differential settlement for the unimproved case for the EP-FE model was 21.15 mm, and it dropped to 20.29 mm for improvement level V_5. Similarly. The LE-FE model yielded a differential settlement of 20.29 mm, and it decreased to 19.97 mm. The decrease from unimproved to the improved case is minimal, and there is hardly any change with further improvement.

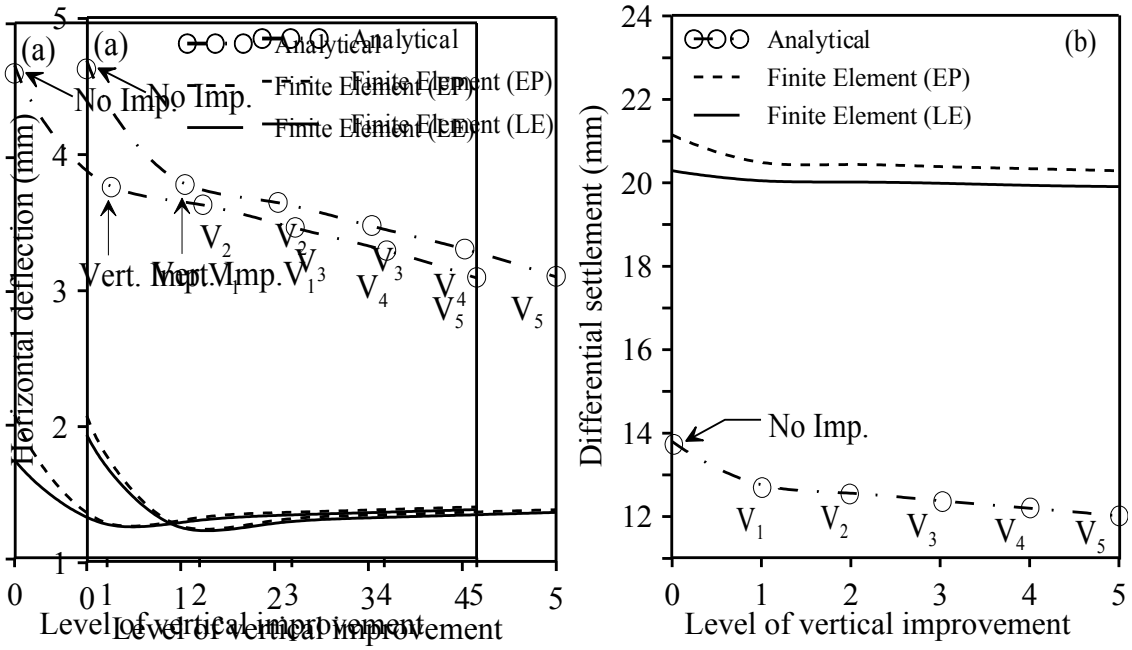

Figure 6.18.Comparison of analytical and FE analysis results (pile length = length of the pile in the unimproved ground) (a) horizontal deflection and (b) differential settlement

CHAPTER 7

PARAMETRIC STUDY

The results presented in the previous sections are based on the mean values. However, it is essential to conduct a parametric study considering a variation in properties of soil to cover a broad spectrum of properties of in-situ soil. For this reason, a parametric study in unimproved and improved soils was performed by changing the value of undrained shear strength (s_u). In both improved and unimproved soils, the undrained shear strength was varied using a coefficient of variance (COV) of 20 %. The mean undrained shear strength (μ) was 41 kPa with a standard deviation (σ) of 8.2 kPa in the case of unimproved soil. Likewise, for the improved soil, the mean shear strength was 360 kPa, and the standard deviation was 72 kPa. Though the full range of values in a normal distribution falls within the $\pm 3\sigma$ from the mean, in this study only a variation in $\pm 1\sigma$ was considered for both unimproved and improved soils. The variation of s_u for the soil profile improved to level V_5 is shown in Figure 7.1.

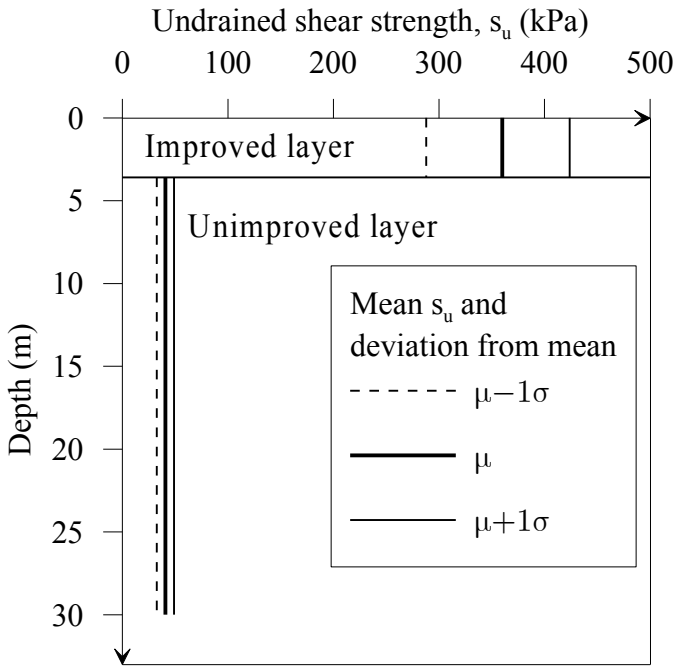

Figure 7.1. Variation of undrained shear strength for improved and unimproved soil profile for the level of improvement V_5

7.1 Pile length variation with variation in undrained shear strength

In this approach, the analytical design was performed to obtain the critical length of the piles (L_p) for each level of improvement with the variation in undrained shear strength. The foundation with the obtained pile length fulfilled the safety and serviceability requirements for considered levels of ground improvement. With the reduction in s_u, the L_p increased and vice-versa for both unimproved and various levels of improved cases. The L_p decreased to 40.0 m for s_u value equal to $\mu+1\sigma$ and increased to 60.2 m for s_u value equivalent to $\mu-1\sigma$, as compared to 48.4 m for the mean value(μ). Similar results were observed in case of improved ground. The variation in the length of piles with the variation in the s_u by $\pm1\sigma$ can be seen in Figure 7.2.

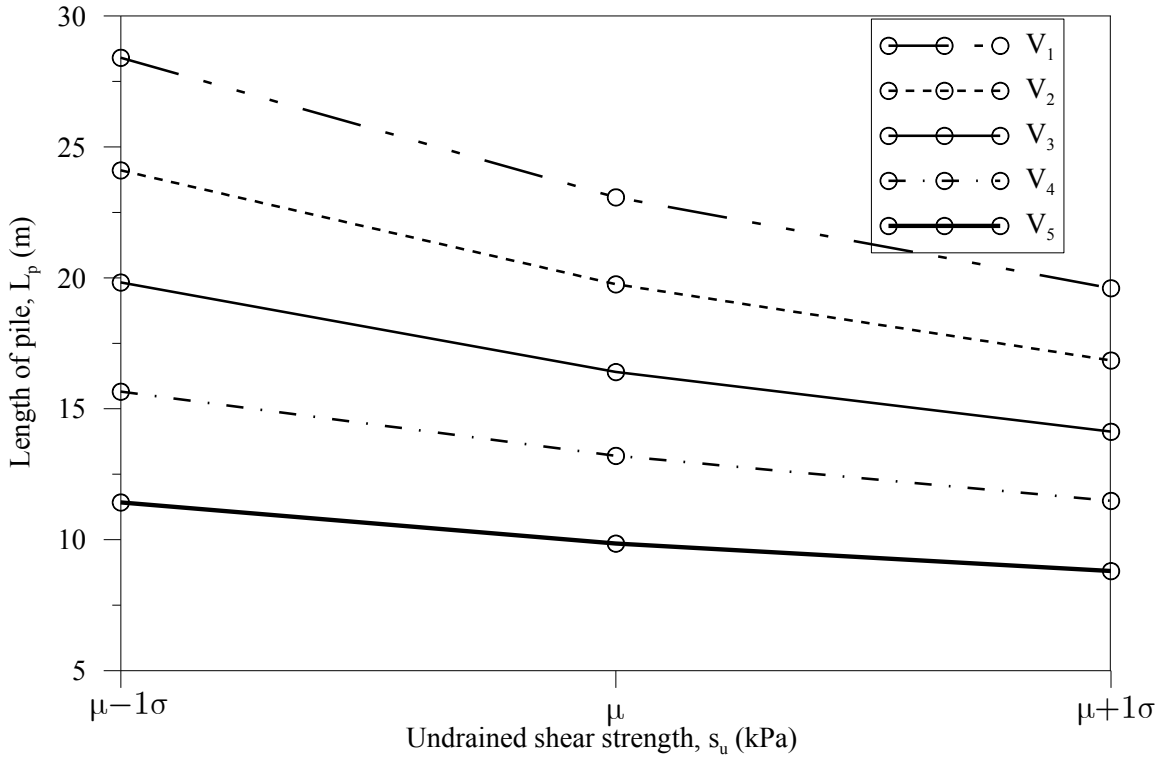

Figure 7.2. Change in the length of piles to meet the design requirement with varying undrained shear strength for different levels of ground improvement.

7.2 Performance evaluation of piled-raft foundation for varying undrained shear strength

For evaluating the performance of the piled-raft foundation under the variation of undrained shear strength (s_u), the length of the pile for each level of ground improvement was kept constant, and s_u varied by ±1σ. The length of the piles obtained from the analytical design (using mean s_u) as a design output for unimproved ground and the five levels of vertical improvement in increasing order were 48.4 m, 23.07 m, 19.75 m, 16.40 m, 13.20 m and 9.85 m, respectively. These pile lengths were kept constant for the respective level

of ground improvement, and the value of s_u was varied. The horizontal deflection and the differential settlement values for each of the cases were noted.

The analytical design showed that both the cases with positive and negative deviation from the mean had a similar pattern of the mean. For the unimproved case and each level of ground improvement, the horizontal deflection is higher for the case with a negative deviation from the mean s_u value (μ-1σ). Similarly, the horizontal deflection is lower for the case with a positive deviation from mean s_u value (μ+1σ). It can be seen in Figure 7.3, the horizontal deflection value for the unimproved ground with mean shear strength value is 4.69 mm. This value increased to 5.62 mm when the value of s_u decreases negatively by a single standard deviation (μ-1σ), and it declines to 4.33 mm when the s_u increases positively by a single standard deviation from the mean value (μ+1σ). The trend is similar for the other levels of ground improvement. The horizontal deflection values for improvement level V_5 were 7.49 mm, 8.66 mm, and 6.62 mm for cases with mean s_u values, negative deviation, and positive deviation from the mean, respectively.

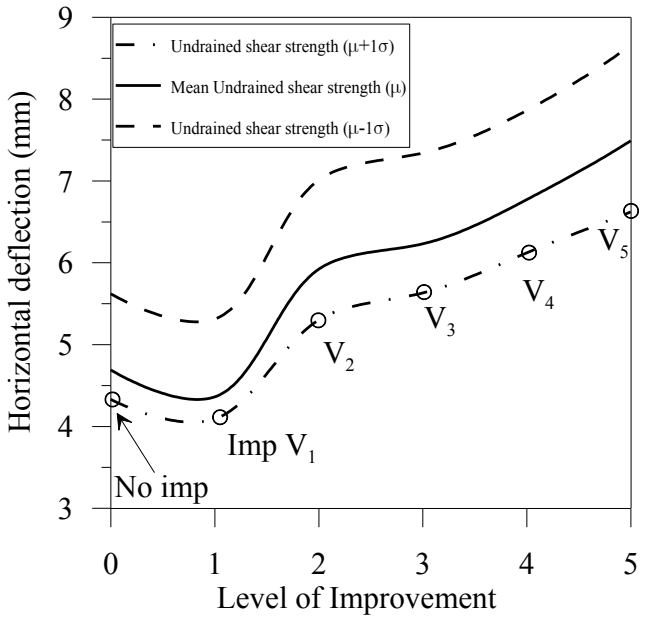

Figure 7.3. Effect of variation of undrained shear strength on horizontal deflection based on analytical design results

Figure 7.4 shows a similar variation discussed, but for the FE models. The FE analysis result shows that for the unimproved case, the variation of s_u did not influence the horizontal deflection. The horizontal deflection value is predominantly small (1.94 mm) for the mean cohesion value with the length (48.4 m). With the shear strength being the only variable, there is no significant change in the horizontal deflection. The result from the FE design also has the same pattern from that of the analytical design, but the magnitude of deflection obtained from the FE design results is slightly smaller than that predicted from the analytical design.

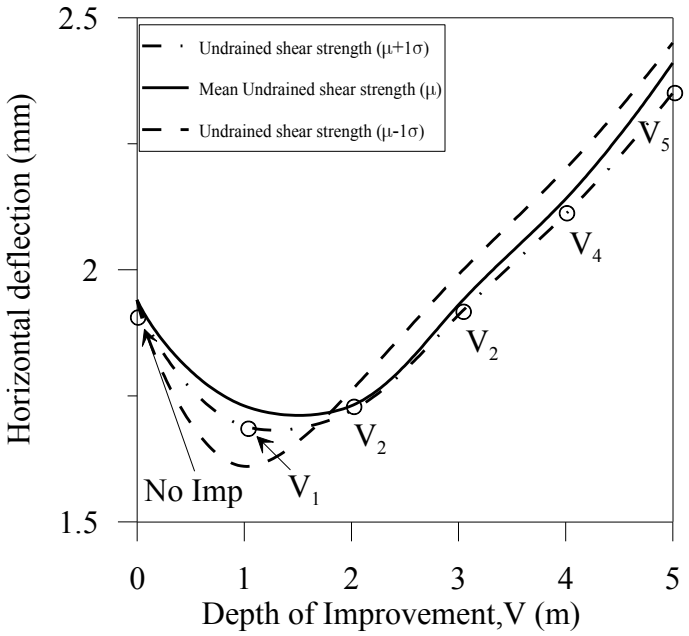

Figure 7.4. Effect of variation of undrained shear strength on the horizontal deflection for unimproved grounds based on FE analysis results

Similarly, the effect of variation of s_u on the differential settlement behavior for analytical design and FE models was investigated. Figure 7.5 shows the results from the analytical design on differential settlement due to variation in s_u. For the mean s_u, the differential settlement is 13.80 mm in the unimproved case and 24 mm for the improved cases (differential settlement controls for the design for improved cases). When the s_u decreased from the mean, the differential settlement increased and vice-versa. For negative deviation in s_u (μ-1σ), the differential settlement grew from 16.82 mm in the unimproved case (L_p = 48.4 m) to 30.28 mm for the first level of ground improvement V_1 (L_p = 19.75 m). It decreased with further improvement leading to a value of 25.54 mm for improvement V_5 (L_p = 9.85 m). For positive deviation in s_u (μ+1σ), the differential settlement curve was different from that of negative deviation in s_u (μ-1σ). The differential settlement increased

from 13.64 mm in the unimproved case (L_p = 48.4) to 17.73 mm for the first level of improvement V_1 (L_p = 19.75 m) and increased with further improvement leading to a value of 22.24 mm for the improvement V_5 (L_p = 9.85 m). The difference in the pattern for positive and negative deviations is due to the ground improvement having a profound effect in soil with lower strength and thus decreasing the settlement with ground improvement.

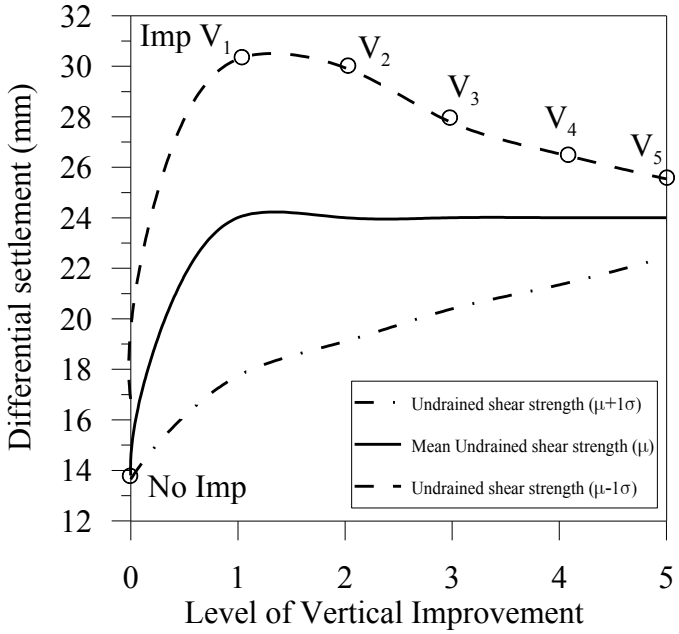

Figure 7.5. Effect of variation of undrained shear strength on the differential settlement for the unimproved and improved grounds based on analytical results

Figure 7.6 shows the results of differential settlement due to the variation in s_u for the FE models. The FE result shows that for the unimproved case, the variation of s_u did not influence the differential settlement. The horizontal deflection value is around 19.7 mm and does not change with the variation in mean cohesion, with the length of the pile kept constant at 48.4 m. The differential settlement increases with ground improvement due to the decrease in the length of pile outweighing the effect of ground improvement. For

different improvement levels, the models with higher s_u value have a lower differential settlement, as seen in Figure 7.6. The difference in the differential settlement between the mean, the negative and positive deviations from the mean is very small though. The differential settlement for improvement level V_5 for μ-1σ, μ, and μ+1σ values of s_u are 31.42, 30.97, and 30.73 mm, respectively.

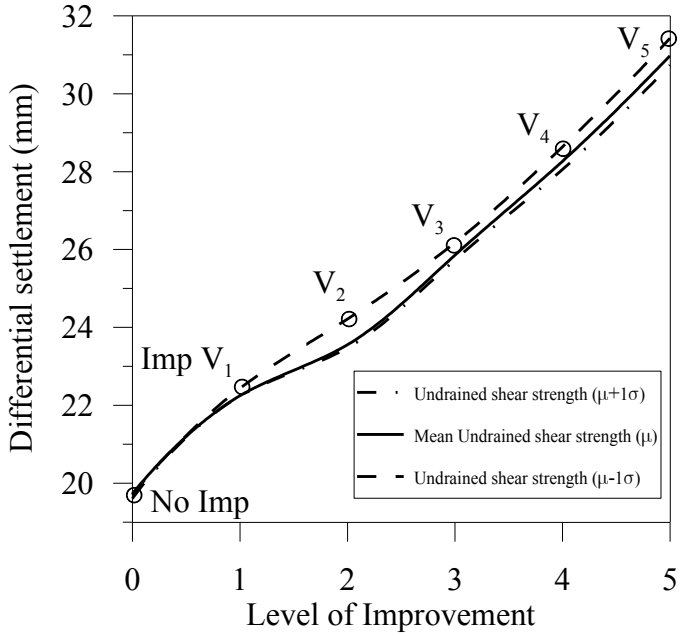

Figure 7.6. Effect of variation of undrained shear strength on the differential settlement for unimproved grounds based on FE results

CHAPTER 8

COST ANALYSIS AND EVALUATION OF ECONOMIC ADVANTAGE OF GROUND IMPROVEMENT

The feasibility of a construction project is massively reliant on the financial aspect. It is particularly true in the case of large-scale construction projects. Even a small cost reduction in the construction of a single wind turbine foundation could lead to a large decrease in the total cost of construction for wind farms with a large number of wind turbines. Cost analysis of piled-raft foundation construction in the unimproved ground and improved grounds was conducted in this study. The cost calculation was conducted by multiplying the dimension of the piles, the raft, and the volume of ground improvement to their corresponding unit cost of construction. The unit cost of foundation construction was obtained from RS Means Building construction cost data (Waier et al., 2013). The unit costs thus obtained consist of equipment, material, and labor costs.

In the case of the unimproved foundation, the total cost of the foundation was the cost of the piled-raft alone. The unit cost of the raft was \$268.00 per $yd^{3,}$ and that of auger-cast piles was \$46.50 per ft^3. The cost of the raft was calculated by multiplying the volume of the raft by its unit cost. The total cost of the piles was calculated by multiplying the number of piles, the length of piles, and the unit cost per unit volume. The total cost of piled-raft assembly (24 numbers of auger cast piles, 48.4 m long and 0.457 m diameter and a raft 8 m in diameter and 1 m in thickness) was calculated to be \$194,774.

For the improved cases, the total cost of piled-raft construction was calculated using a similar procedure as in the unimproved case. However, for improved cases, the total cost calculation also included the cost of ground improvement along with the cost of piles and the raft. It must be noted that the cost of piles decreases due to the decrease in the length of the pile in improved ground. The cost of the ground improvement was estimated by multiplying the unit cost of cement soil mixing with the volume of ground improvement. The unit cost of ground improvement using mass mixing was $97.00. The unit cost of mass stabilization varied within the industry. U.S Department of Transportation, Federal Highway Administration, suggested the range of mass mixing to $15-$75 (FHWA-NHI, 2017). A mark up of around 30 % of the suggested cost was considered to adjust for inflation and market variability. The adjustment was also made to make a conservative approximation of the total cost calculation. The ground improvement around the piled raft was considered to be cylindrical. The height of the cylinder was equal to the extent of improvement (V_i, where i is the improvement layer; i = 1 to 5). Similarly, the radius of the cylinder was equivalent to the sum of the radius of the raft and the extent of improvement ($H_i = R + V_i$, i =1 to 5).

The total cost of foundation in the unimproved ground was found to be higher than the total cost of foundation in the improved ground. This is because of the longer length of piles in case of the unimproved ground and the cost of ground improvement being less than the cost of piles. The cost reduced upon integrating ground improvement was determined by taking the discrepancy in the cost of the foundation for the unimproved case with longer piles to that for improved case (cost of the raft, piles with reduced length and ground

improvement). The maximum cost benefited was by applying the depth of improvement to 2.4 m, where L_p was 19.75 m. The cost benefited reduced with a further increase in ground improvement levels. Though improvement to depth V_5 had a highly reduced pile length, it came at the expense of a higher volume of improvement, thereby increasing the total cost of the foundation. The increase in cost shows that improving ground does not necessarily mean the cost would be saved instead suggests a need for optimum depth of improvement. Figure 8.1 shows the cost reduced by incorporating ground improvement compared to the unimproved ground. The cost-benefit will be highly significant for a wind farm with a large number of wind turbines.

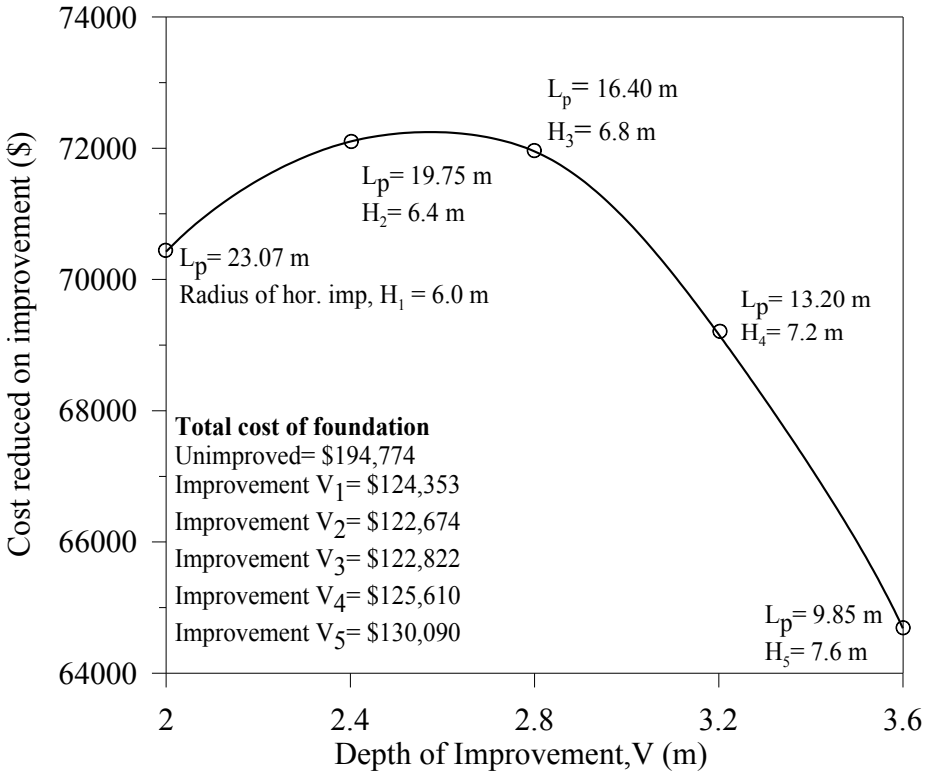

Figure 8.1. Cost-benefit for various depths (levels) of ground improvement and corresponding horizontal distance (radius) of ground improvement

The study on variation in the total cost due to the variation in undrained shear strength was also performed. The variation in s_u brings about the change in the length of piles, which results in the alteration in the cost of the foundation. The results of the cost analysis for various s_u values are summarized in Figure 8.2 which includes the total cost of foundation in unimproved and improved grounds for all the instances of the parametric study, i.e., $s_{u(\mu)}$, $s_{u(\mu-1\sigma)}$, and $s_{u(\mu+1\sigma)}$. It was observed from the analysis the instance with higher undrained shear strength ($\mu+1\sigma$) had minimum costs and the instance with lower undrained shear strength ($\mu-1\sigma$) had maximum cost for the improved and unimproved cases. With ground improvement to level 1, the cost of foundation reduced drastically, but upon further improvement, the tendency of variation in cost was inconsistent for different s_u values. For the mean s_u, the variation in the cost is almost constant till Imp3, and with further improvement, it increased slightly. For higher s_u ($\mu+1\sigma$), the total cost was minimum for Imp1, and it increased past Imp1. In the case of the lowest s_u ($\mu-1\sigma$), the cost decreased slightly from Imp1 to Imp 3, and on further improvements, the total cost is nearly equal. From the results, it is seen that for mean s_u value (μ), Imp2 was the least costly. Similarly, for higher s_u value ($\mu+1\sigma$), Imp1 was the least expensive and for lower s_u value ($\mu-1\sigma$), Imp4 was least expensive.

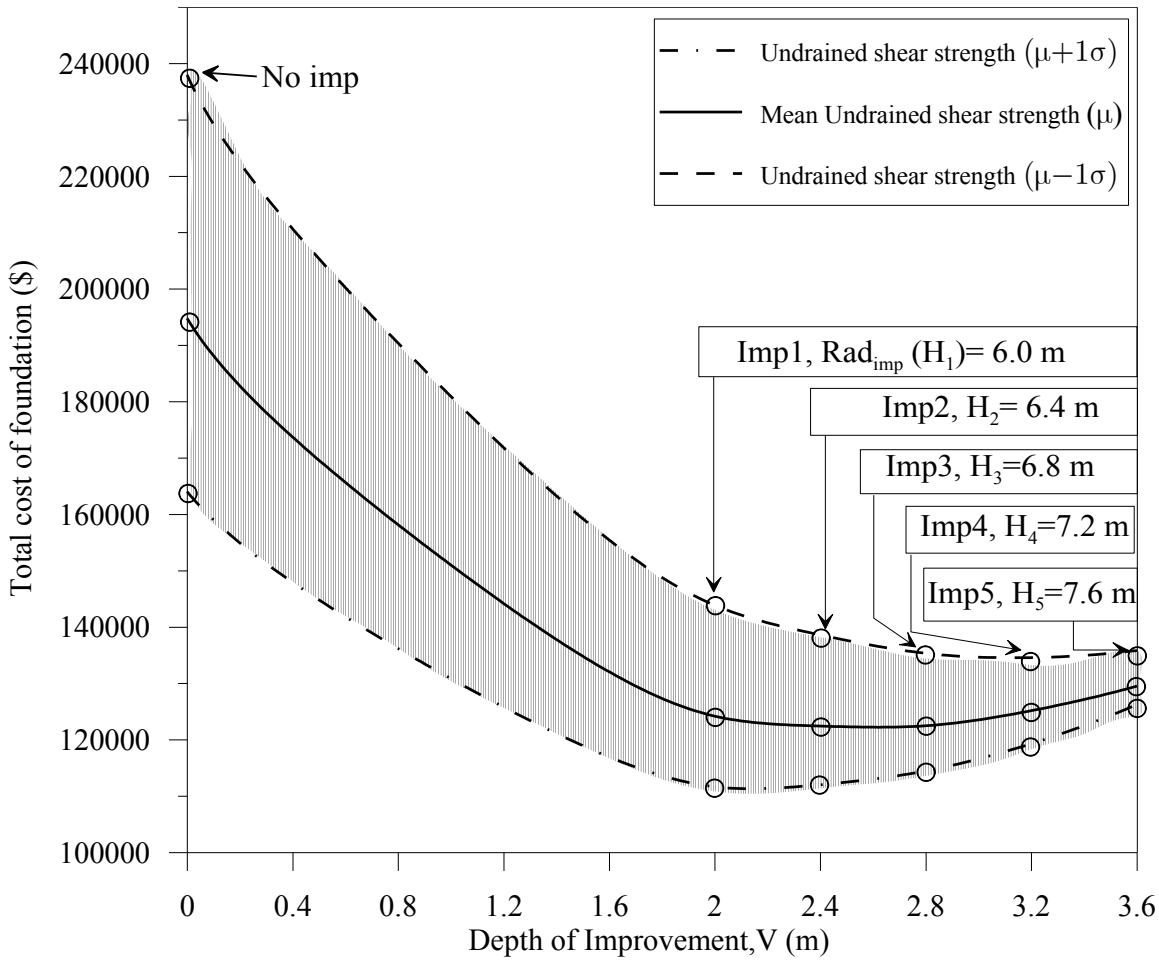

Figure 8.2. Effect of variation of undrained shear strength on the total cost of the foundation for unimproved and improved grounds.

CHAPTER 9

CONCLUSION AND RECOMMENDATIONS

9.1 Conclusions

The wind has been gaining popularity as one of the most important sources of renewable energy. The cost of foundation construction for tall wind turbines in wind farm sites with poor subsurface properties is huge. In this study, the effectiveness of ground improvement around the piled-raft foundation and the cost analysis to evaluate the economic benefit of incorporating ground improvement were performed. The following conclusions have been made based on the study conducted for the given conditions.

- The analytical design of the piled-raft foundation in the unimproved ground was governed by the safety criterion (moment capacity). The design in the improved ground was governed by the serviceability criterion (differential settlement).
- The analytical design of the piled-raft foundation showed a significant reduction in the length of the pile can be achieved by incorporating ground improvement while still satisfying the safety and serviceability criteria.
- The analytical design results on the performance of the piled-raft foundation showed the increase in factor of safety of vertical, moment, and horizontal capacities with ground improvement.
- The FE analysis performed on the models with reduced pile length for improved ground showed an increase in horizontal deflection and differential settlement. The decrease is most likely because the analytical design adopted to prepare FE

models had under-predicted the length of piles for each level of ground improvement. Thus, the length of the pile reduced was not entirely compensated by the ground improvement, resulting in higher deformation. It shows the analytical design by itself is not the appropriate tool to design a piled-raft foundation and requires comprehensive finite element analysis.

- From the cost analysis on the foundation in unimproved and improved ground improvement, it can be concluded that the ground improvement reduces net foundation cost.
- The study also shows that ground improvement can be beneficial only up to a specific level, and a larger volume of ground improvement does not necessarily yield economic gain. Instead, an optimum depth of improvement needs to be calculated to gain the maximum advantage of ground improvement.
- From the parametric study conducted by varying the undrained shear strength of soil, it was observed that for the identical depth of improvement, the cost of piled-raft foundation on soil with higher undrained shear strength was less than that of lower undrained shear strength.
- Finally, from the study, it was concluded that wind energy can be economically harvested from wind farms in geotechnically weak soils by proper use of ground improvement.

9.2 Limitations

- The pile capacity calculation is based on methods designed for clays and not applicable for granular soils.

- The method of ground improvement (CSM using mass stabilization) adopted in the study is not particularly suitable for granular soils.
- The parametric study considering the variation in loads from the tower, and the wind pressure is not performed in the study.
- The parametric study conducted on the undrained shear strength considers the variation of only one standard deviation from mean ($\mu \pm 1\sigma$) and does not cover the full spectrum/range of a normal distribution ($\mu \pm 3\sigma$).

9.3 Recommendations and future work

- A full scale or scaled-down model tests of piled-raft foundation with ground improvement is recommended for analytical design and FE model validation.
- It is recommended to develop a coupled FE model with a tower and other above-ground components resting on the piled-raft foundation with a realistic representation of load transfer from the tower to the piled-raft foundation.
- The loads considered in this study are static, but the wind load is dynamic. Thus, a dynamic analysis of a piled-raft foundation is advocated to obtain more realistic results.
- A parametric study with the variation in load can be conducted to suggest the foundation configuration and performance for different sizes of towers or for different wind conditions.
- Ground improvement methods other than cement soil mixing can be performed to compare the results to devise with a better solution.

APPENDICES

APPENDIX A

DESIGN LOAD CALCULATION

A.1 Vertical load calculation

Dead load calculation of wind turbine (Lyrner et al., 2010)		
Weight of tower	666	tons
Weight of nacelle	120	tons
Weight of blade	31.5	tons
Weight of rotor	56.5	tons
Hub weight	25	tons
Total weight	899	tons
Dead load (P)	8819.19	kN

A.2 Wind load Calculation

A. 2.1 Wind load parameters from ASCE 7-10

Wind load parameters (using ACSE 7-10)	
Location	Hypothetical
Risk category	III
Wind speed, V	80 mph (35.8 m/s)
Wind directionality factor (K_d)	0.95
Exposure category	C
Topographic factor (K_{zt})	1
Gust effect factor, G	0.85

A.2.2 Topographic constants

Exposure	z_g (ft/m)	a	z_{min} (ft/m)
C	900	9.5	15

For 15 ft $\leq z \leq z_g$: $K_z = 2.01\ (z/z_g)^{2/a}$

For $z \leq 15$ ft: $K_z = 2.01\ (15/z_g)^{2/a}$

Internal pressure coefficients, $GC_{pi} = 0$

Calculation of wind load

Wind pressure, $q_z = 0.613 K_z K_{zt} K_d V^2$ (Vin m/s)

$q_z = 744.829 K_z$ (N/m^2)

Wind load, $F = q_z G C_f A_f$, $C_f = 0.8$ and A_f is the area exposed to the wind

Drag force on wind

No of blade (n)= 3

Length of blade (l) = 40 m

Chord length (b) = 3

Area of airfoil (A)= $l \times b = 360\ m^2$

Drag coefficient for blade, $C_d = 0.07$

Density of air(d) = $0.01201725\ kN/m^3$

Drag force on blade (Fd) = $0.5 \times C_d \times A \times d \times V^2 = 193.67\ kN$

Moment due to drag on turbine = 15493.10 kNm

A.3.3 Horizontal load and moment (M) calculations

Outer dia. (m)	Height range (m)		Ht. of sect. (m)	z (m)	K_z	q_z (N/m^2)	C_f	A_f (m^2)	F (kN)	Lever arm from tower base (m)	Moment at base of tower (kNm/m)
6.75	0	5	5	2.50	0.85	633.09	0.80	53.01	22.82	2.50	57.06
6.5	5	10	5	7.50	0.94	701.71	0.80	51.05	24.36	7.50	182.70
6.25	10	15	5	12.50	1.05	781.38	0.80	49.09	26.08	12.50	326.03
6	15	20	5	17.50	1.13	838.74	0.80	47.12	26.88	17.50	470.34
5.75	20	25	5	22.50	1.19	884.31	0.80	45.16	27.16	22.50	611.02
5.5	25	30	5	27.50	1.24	922.47	0.80	43.20	27.10	27.50	745.16
5.25	30	35	5	32.50	1.28	955.49	0.80	41.23	26.79	32.50	870.70
5	35	40	5	37.50	1.32	984.71	0.80	39.27	26.30	37.50	986.08
4.75	40	45	5	42.50	1.36	1011.01	0.80	37.31	25.65	42.50	1090.02
4.5	45	50	5	47.50	1.39	1034.96	0.80	35.34	24.87	47.50	1181.49
4.25	50	55	5	52.50	1.42	1057.00	0.80	33.38	23.99	52.50	1259.57
4	55	60	5	57.50	1.45	1077.44	0.80	31.42	23.02	57.50	1323.48
3.75	60	65	5	62.50	1.47	1096.52	0.80	29.45	21.96	62.50	1372.54
3.5	65	70	5	67.50	1.50	1114.43	0.80	27.49	20.83	67.50	1406.12
3.25	70	75	5	72.50	1.52	1131.32	0.80	25.53	19.64	72.50	1423.66
3	75	80	5	77.50	1.54	1147.32	0.80	23.56	18.38	77.50	1424.64
Total:			80						385.82		14730.60

Total horizontal load (L) = 385.82+193.67 = 579.49 kN

Total Moment (M) = 14730.60+15493.10 = 30223.70 kNm

APPENDIX B

CALCULATION OF PILED-RAFT CAPACITY

B.1 Calculation of pile capacity

B.1.1 Dimensions of the pile

Diameter (D)	0.457 m
Length (L)	48.4 m
Area (A)	0.164 m^2
Depth (D_f)	1.0 m
Unit Wt. (Υ)	25. 0 kN/m^3
Weight of pile (W_f)	198.48 kN

B.1.2 Skin resistance from clay layer for a single pile (API method)

For S_u <150 kPa, $\alpha = 0.55$

For 150<S_u<250 kPa, linearly interpolate

For S_u>250, $\alpha = 0.45$

S_u = 41.00 kPa, $\alpha = 0.55$

$P_s = \alpha S_u \times \pi D \times (L - 1.5)$

P_s = 1486.02 kN

B.1.3 Toe resistance (O'Neil and Reese method)

$q_t' = N_c \times S_u$

For S_u = 41 (Interpolate between N_c= 6.5 at S_u= 25kPa and N_c= 8.0 at S_u= 50kPa)

N_c= 7.7

q_t' = 338.8 kN/m^2

$P_t' = q_t' \times A$ = 1541.60 kN

Allowable upward and downward capacity

P_{ult-dn} = 30383.19 kN

P_{ult-up} = 3360.00 kN

P_{all-dn} = 440.46 kN

P_{all-up} = 280.75 kN

Total number of piles = 24 (2 concentric circles of 12 piles each)

B.2 Piled-raft capacity

B.2.1 Vertical load capacity

Ultimate bearing capacity of raft $(q_{ult})_{raft} = K_1 \times N_r = 94.97$

Total raft capacity $(P_{ult})_{raft} = 4773.93$ kN

Total downward capacity of piles $(P_{ult})_{piles} = 36998.29$ kN

Capacity of piles and raft $(P_{ult})_{pr} = 41772.22$ kN

Calculation of piled- raft capacity as a block

Radius of pile group block = 3.60 m

Skin resistance of pile group in block $(P)_{gs} = 24177.27$ kN

Toe resistance of pile group in block $(P)_{gt} = 313.51$ kN

Capacity of pile group block $(P_{ult})_g = 24490.78$ kN

Capacity of raft around the perimeter of pile group $(P_u)_{rg} = 907.05$ kN

Total capacity of block $(P_{ult})_{block} = 25397.82$ kN

Ultimate vertical capacity $(P_{ult}) = \min [(P_{ult})_{block}, (P_{ult})_{pr}] = 25937.82$ kN

Factor of safety for vertical load $(FOS)_{vertical} = (P_{ult})_{pr} / P = 2.88$ (okay)

B.2.1 Moment load capacity

Maximum possible moment that soil can support $(M_m) = 5495.63$ kN (from equation 5.11)

Ultimate moment capacity contributed by outer piles $(M_{ult})_{p\text{-}o} = 42390.76$ kNm

Ultimate moment capacity contributed by inner piles $(M_{ult})_{p\text{-}i} = 28025.81$ kNm

Ultimate moment capacity of raft $(M_{ult})_{raft} = 5290.62$ kNm

Total moment capacity of pile and raft $(M_{ult})_{pr} = 75707.20$ kNm

Moment capacity of block $(M_{ult})_{block} = 55530741.62$ kNm (from equation 5.12)

Ultimate moment capacity $(M_{ult}) = \min [(M_{ult})_{block}, (M_{ult})_{pr}] = 75707.20$ kN

Factor of safety for vertical load $(FOS)_{moment} = (M_{ult})_{pr} / M = 2.50$ (Critical FOS; governs the design)

B.2.1 Horizontal load capacity

Brom's method to determine the horizontal capacity of pile

Soil type: Cohesive

Cohesion $(c_u) = 41$ kPa

Horizontal coefficient of subgrade reaction $k_h = n_1 n_2 80 q_u / B$

$n_1 = 0.4$

$n_2 = 1.15$

Unconfined Compressive strength (q_u) = 82 kPa

Width of the pile (B) = 0.457 m

k_h = 6603.063 kN/m^3

Adjust k_h for loading and soil conditions

$k_h^{adj} = (1/3) \times k_h$ = 2201.021 kN/m^3

Pile Parameters

Young's Modulus of elasticity (E) = 3×10^7

Embedment length of pile (L) = 48.4 m

Diameter (D) = 0.457 m

Second moment of Inertia (I) = 0.0021411m^4

Section modulus (S) = 0.093702 m^3

Compressive strength of pile ($f_c^{'}$) = 40000 kPa

Resisting moment (M_y) = 374.8076 kNm

Determine factor β

$\beta = (k_h B/4EI)^{1/4}$ = 0.3292

βL = 15.93339

If βL> 2.5; Long pile

If βL<2.0; Short pile

If 2< βL < 2.5; Intermediate pile

Ultimate load for single pile

$M_y/c_u B^3$ = 95.78026

$P_u/c_u B^2$ = 40 (from Figure B.1)

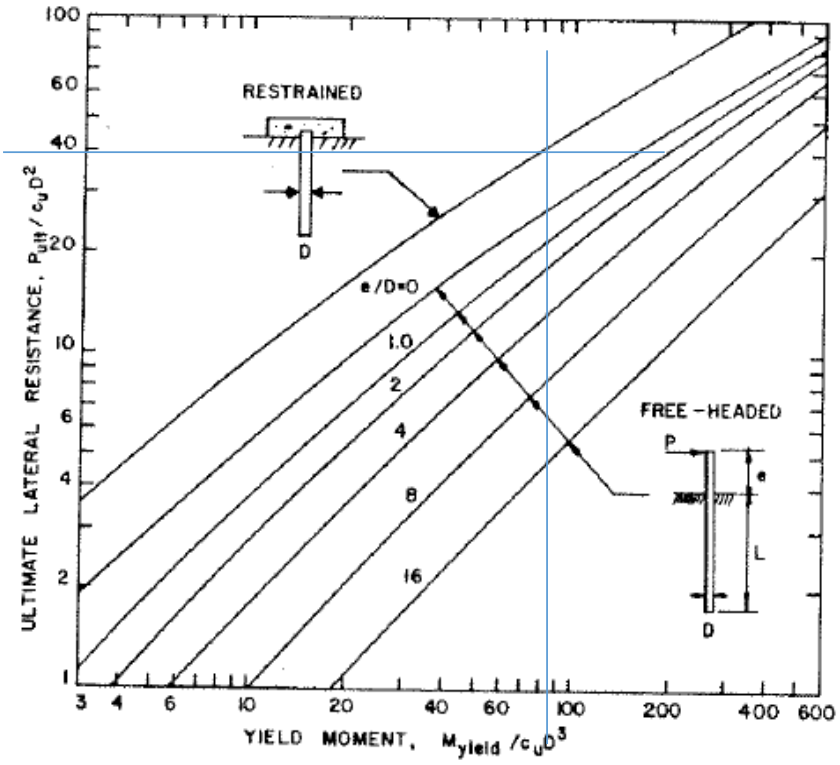

Figure B.1 Ultimate horizontal resistance of piles in cohesive soil (Brom's, 1964a)

P_u = 341.51236 kN

Maximum allowable load (P_m) = 137.00494 kN (with FOS of 2.5)

Working load for a single pile P_a corresponding design deflection y_m at the ground,

If P_a and y are not given, using Figure B.2 to find the following

$y_m k_h DL/ P_a = 5$

y_m = 4.69 mm

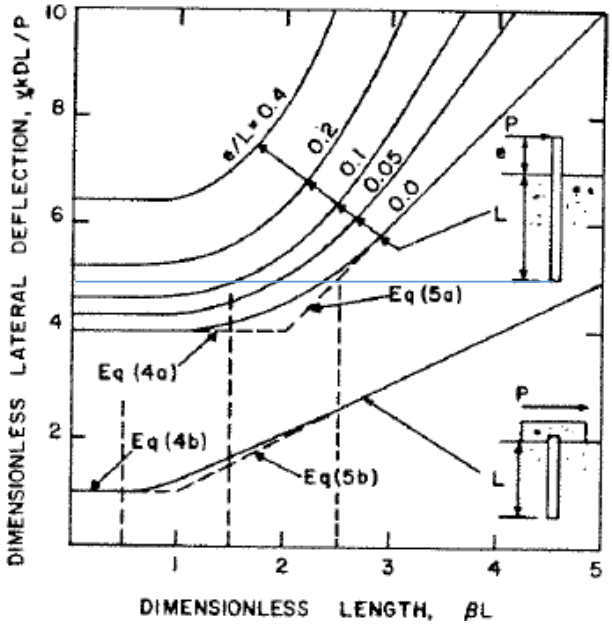

Figure B.2 Horizontal deflection at the ground surface (Brom's 1964a)

From Brom's method

Ultimate horizontal load for one pile (P_{lat}) = 342.51 kN

Deflection of pile (y_m) = 4.69 mm

Ultimate horizontal load for all piles [(P_{lat}) × n] = 8220.30 kN

Factor of safety for load capacity ($FOS_{horizontal}$) = 14.19

B.3 Calculation of total settlement for piled-raft foundation

B.3.1 Load sharing calculation between piles and raft

Modulus of Elasticity (E)	30500.00 kN/m^2
Poisson's ratio (ν)	0.30
Equivalent width of circular raft (B)	7.09 m
Stiffness of raft (K_r) (using equation 5.16)	267.33 kN/mm
Allowable settlement ($S_{allowable}$)	30.00 mm
Required stiffness of the system (K_{cd})	293.97 kN/mm
Stiffness of pile group (K_p) (using equation 5.15)	263.48 kN/mm
Interaction factor (α_{rp})	0.8

Stiffness of piled-raft (K_{pr})	293.97 kN/mm
Load shared by raft (P_r/P_t = X) (using equation 5.19)	40.03 %
Load shared by piles (P_p/P_t =1- X)	59.97 %

a =	1.078
β_p = 1/(1+a) =	0.48
$P_p = \beta_p * P$ =	4.24 MN
$P_r = P - P_p$ =	4.57 MN
P =	8.82 MN

where a = $[0.2/\{1-0.8(k_r/k_p)\}]$ (k_r/k_p)

B.3.2 Secant stiffness calculation (Using equation 5.19)

Hyperbolic factor for pile group (R_{fp})	0.2
Hyperbolic factor for raft (R_{fr})	0.1
Ultimate capacity of piles $(P_{ult})_{piles}$	24.49 MN
Ultimate capacity of raft $(P_{ult})_{raft}$	4.77 MN

B.3.3 Vertical load settlement curve generation

P (MN)	X	a	β_p	P_p (MN)	P_r (MN)	K_r (MN/mm)	K_p (MN/mm)	K_{pr} (MN/mm)	P_M (MN)	$P > P_A$	S (mm)
0	1.116	1.078	0.481	0.00	0.00	0.27	0.26	0.29	50.88	NO	0.00
5	1.116	1.078	0.481	2.41	2.59	0.25	0.26	0.29	50.88	NO	17.35
10	1.105	0.902	0.526	5.26	4.74	0.24	0.25	0.28	46.58	NO	35.90
15	1.098	0.809	0.553	8.29	6.71	0.23	0.25	0.27	44.30	NO	55.61
20	1.093	0.743	0.574	11.47	8.53	0.22	0.24	0.26	42.70	NO	76.61
25	1.089	0.696	0.590	14.74	10.26	0.21	0.23	0.25	41.53	NO	99.02
30	1.086	0.658	0.603	18.10	11.90	0.20	0.22	0.24	40.60	NO	123.01
35	1.084	0.627	0.615	24.49	10.51	0.21	0.21	0.23	39.85	NO	152.87
40	1.108	0.948	0.513	24.49	15.51	0.18	0.21	0.23	39.85	YES	174.89
45	1.076	0.544	0.648	24.49	20.51	0.15	0.21	0.23	39.85	YES	207.83
50	1.054	0.343	0.744	24.49	25.51	0.12	0.21	0.23	39.85	YES	255.59
51	1.038	0.224	0.817	24.49	26.51	0.12	0.21	0.23	39.85	YES	267.84
52	1.035	0.206	0.829	24.49	27.51	0.11	0.21	0.23	39.85	YES	281.31
53	1.033	0.189	0.841	24.49	28.51	0.11	0.21	0.23	39.85	YES	296.17
54	1.030	0.173	0.853	24.49	29.51	0.10	0.21	0.23	39.85	YES	312.66
55	1.028	0.158	0.863	24.49	30.51	0.10	0.21	0.23	39.85	YES	331.07
56	1.026	0.144	0.874	24.49	31.51	0.09	0.21	0.23	39.85	YES	351.75
57	1.024	0.132	0.884	24.49	32.51	0.09	0.21	0.23	39.85	YES	375.14
58	1.022	0.120	0.893	24.49	33.51	0.08	0.21	0.23	39.85	YES	401.82
59	1.020	0.108	0.902	24.49	34.51	0.07	0.21	0.23	39.85	YES	432.53
60	1.018	0.098	0.911	24.49	35.51	0.07	0.21	0.23	39.85	YES	468.27
61	1.016	0.088	0.919	24.49	36.51	0.06	0.21	0.23	39.85	YES	510.37

B.4 Calculation of resultant of vertical load and bending moment on each pile

B.4.1 Pile arrangement

Radius (m)	n	Spacing (m)	Angle (deg)	Moment contribution (kNm)
3.3715	12	1.77	30	42390.76
2.23	12	1.17	30	28025.81
	24			**70416.57**

B.4.2 Calculation of resultant of vertical load and bending moment on each pile

Pile no.	$(P_i)_a$ (kN)	x (m)	x^2 (m^2)	$(P_i)_m$ (kN)	P_i (kN)	Type
1	367.47	2.23	4.97	564.74	932.21	C
2	367.47	1.93	3.73	489.08	856.55	C
3	367.47	1.11	1.24	282.37	649.84	C
4	367.47	0.00	0.00	0.00	367.47	C
5	367.47	1.11	1.24	282.37	649.84	C
6	367.47	1.93	3.73	489.08	-121.62	T
7	367.47	2.23	4.97	564.74	-197.28	T
8	367.47	1.93	3.73	489.08	-121.62	T
9	367.47	1.11	1.24	282.37	85.09	C
10	367.47	0.00	0.00	0.00	367.47	C
11	367.47	1.11	1.24	282.37	85.09	C
12	367.47	1.93	3.73	489.08	-121.62	T
13	367.47	3.37	11.37	854.21	-486.74	T
14	367.47	2.92	8.53	739.77	-372.30	T
15	367.47	1.69	2.84	427.10	-59.64	T
16	367.47	0.00	0.00	0.00	367.47	C
17	367.47	1.69	2.84	427.10	794.57	C
18	367.47	2.92	8.53	739.77	1107.23	C
19	367.47	3.37	11.37	854.21	1221.68	C
20	367.47	2.92	8.53	739.77	1107.23	C
21	367.47	1.69	2.84	427.10	794.57	C
22	367.47	0.00	0.00	0.00	367.47	C
23	367.47	1.69	2.84	427.10	794.57	C
24	367.47	2.92	8.53	739.77	1107.23	C
	8819.19		$\sum x^2 =$ **98.01**		**10174.77**	

Note: C represents pile in compression and T represents pile in tension

Vertical load acting on i^{th} pile due to dead load $(P_i)_a = P_t/n$

Vertical load acting on i^{th} pile due to moment $(P_i)_m = Mx/\sum x^2$

Resultant vertical load acting on i^{th} pile $(P_i) = (P_i)_a + (P_i)_m$

B.5 Calculation of rotation of foundation

Radius of raft = 4 m

Thickness of raft = 1 m

Moment applied at the base of foundation ($M_{applied}$) = 30803.18 kNm

Portion of moment taken by raft (M_r) = 5790.50 kNm

Portion of moment taken by piles (M_p) = 24382.68 kNm

Second moment of area for area of foundation (I_{found})	201.06 m^4
Elastic modulus of compressibility ($E_{s,stat}$)	30500.00 kN/m^2
Shape factor for overturning (f')	0.25
Area of foundation (A_{found})	50.27 m^2
Effective depth for antisymmetric action effect (t_{found})	1.77 m
Foundation modulus (c_s)	17207.78 kN/m^3
Rotation of tower (θ) (using equation 5.20)	0.098873 degree
Horizontal displacement at the top of tower (ΔH)	138.05 mm

B.5 Calculation of Differential settlement of foundation (for single pile)

Using Fellenius method:

$(P_m) = (P_t)\,' (\delta/\delta_{ut})^g + (P_s) (\delta/\delta_{us})^h$

Skin resistance $(P_s) = A_s f_s' = 1486.02$ kN

Toe resistance $(P_t)\,' = A_t q_t' = 55.57$ kN

Factor of safety (FOS) = 3

Allowable load $(P_a) = 513.87$ kN

$\delta_{ut} = 45.7$ mm

$\delta_{us} = 10$ mm

g = 0.5 for clay

h = 0.02 (assumed for clay)

$z_c = 0.75D$, where D is the length of pile

δ (mm)	$(P_t')_m$ (kN)	Actual $(P_t)_m$ (kN)	$(P_s)_m$ (kN) clay	Actual $(P_s)_m$ (kN)	$(P)_m$ (kN)	δ_e (mm)	δ_{adj} (mm)
0	0.00	0.00	0.00	0.00	0.00	0.00	0.00
1	1.22	1.22	1419.14	1419.14	1420.36	10.48	11.48
2	2.43	2.43	1438.95	1438.95	1441.38	10.63	12.63
3	3.65	3.65	1450.67	1450.67	1454.32	10.73	13.73
4	4.86	4.86	1459.04	1459.04	1463.90	10.80	14.80
5	6.08	6.08	1465.56	1465.56	1471.64	10.86	15.86
6	7.30	7.30	1470.92	1470.92	1478.21	10.90	16.90
7	8.51	8.51	1475.46	1475.46	1483.97	10.95	17.95
8	9.73	9.73	1479.41	1479.41	1489.13	10.98	18.98
9	10.94	10.94	1482.89	1482.89	1493.84	11.02	20.02
10	12.16	12.16	1486.02	1486.02	1498.18	11.05	21.05
11	13.38	13.38	1488.86	1486.02	1499.40	11.06	22.06
12	14.59	14.59	1491.45	1486.02	1500.61	11.07	23.07
13	15.81	15.81	1493.84	1486.02	1501.83	11.08	24.08
14	17.02	17.02	1496.06	1486.02	1503.05	11.09	25.09
15	18.24	18.24	1498.12	1486.02	1504.26	11.10	26.10
16	19.46	19.46	1500.06	1486.02	1505.48	11.11	27.11
17	20.67	20.67	1501.88	1486.02	1506.69	11.11	28.11
18	21.89	21.89	1503.59	1486.02	1507.91	11.12	29.12
19	23.10	23.10	1505.22	1486.02	1509.13	11.13	30.13
20	24.32	24.32	1506.77	1486.02	1510.34	11.14	31.14
21	25.54	25.54	1508.24	1486.02	1511.56	11.15	32.15
22	26.75	26.75	1509.64	1486.02	1512.78	11.16	33.16
23	27.97	27.97	1510.98	1486.02	1513.99	11.17	34.17
24	29.19	29.19	1512.27	1486.02	1515.21	11.18	35.18
25	30.40	30.40	1513.51	1486.02	1516.42	11.19	36.19
26	31.62	31.62	1514.69	1486.02	1517.64	11.20	37.20
27	32.83	32.83	1515.84	1486.02	1518.86	11.20	38.20
28	34.05	34.05	1516.94	1486.02	1520.07	11.21	39.21
29	35.27	35.27	1518.01	1486.02	1521.29	11.22	40.22
30	36.48	36.48	1519.03	1486.02	1522.50	11.23	41.23

Percentage of moment carried by raft = 19.383 %

Differential settlement of raft = Different settlement of pile = 13.80 mm

Maximum load on a pile = 1221.68 kN

Maximum vertical settlement = 9.87 mm

APPENDIX C

COST CALCULATION OF PILED-RAFT FOUNDATION

Table C.1: Cost calculation of piled-raft for mean shear strength value (μ)

Level. of imp.	Unimproved	Improv.1	Improv.2	Improv.3	Improv.4	Improv.5
Len. of Pile (m)	48.40	23.07	19.75	16.4	13.2	9.85
Radius. of imp. (m)	-	6.00	6.40	6.80	7.20	7.60
Dep. of imp. (m)	-	2.00	2.40	2.80	3.20	3.60
Vol. of raft (m^3)	50.27					
Vol. of imp. (m^3)		175.93	258.57	356.48	470.89	602.98
Unit cost of pile (per ft^3)		46.50				
Unit cost of raft (per yd^3)		268.00				
Unit cost of CDSM (per yd^3)		97.50				
Cost before imp. ($)	194,774.02					
Total cost of CDSM ($)	-	22,299.02	32,773.20	45,184.20	59,684.93	76,428.31
Cost saved ($)	-	70,420.93	72,099.56	71,951.16	69,163.96	64,683.19
Total Cost (S)	194,774.02	124,353.09	122,674.5	122,822.86	125,610.06	130,090.83

Table C.2: Cost calculation of piled-raft for mean shear strength value (μ-1σ)

Level. of imp.	Unimproved	Improv.1	Improv.2	Improv.3	Improv.4	Improv.5
Len. of Pile (m)	48.40	28.40	24.10	19.82	15.65	11.42
Radius. of imp. (m)	-	6.00	6.40	6.80	7.20	7.60
Dep. of imp. (m)	-	2.00	2.40	2.80	3.20	3.60
Vol. of raft (m^3)	50.27					
Vol. of imp. (m^3)		175.93	258.57	356.48	470.89	602.98
Unit cost of pile (per ft^3)		46.50				
Unit cost of raft (per yd^3)		268.00				
Unit cost of CDSM (per yd^3)		97.50				
Cost before imp. ($)	237967.69					
Total cost of CDSM ($)	-	22,299.02	32,773.20	45,184.20	59,684.93	76,428.31
Total Cost (S)	237,967.69	143,863.449	138,597.60	135,341.7	134,578.24	135,837.8

Table C.3: Cost calculation of piled-raft for mean shear strength value ($\mu + 1\sigma$)

Level. of imp.	Unimproved	Improv.1	Improv.2	Improv.3	Improv.4	Improv.5
Len. of Pile (m)	48.40	19.60	16.84	14.12	11.48	8.8
Radius. of imp. (m)	-	6.00	6.40	6.80	7.20	7.60
Dep. of imp. (m)	-	2.00	2.40	2.80	3.20	3.60
Vol. of raft (m^3)	50.27					
Vol. of imp. (m^3)		175.93	258.57	356.48	470.89	602.98
Unit cost of pile (per ft^3)		46.50				
Unit cost of raft (per yd^3)		268.00				
Unit cost of CDSM (per yd^3)		97.50				
Cost before imp. ($)	164,025.99					
Total cost of CDSM ($)	-	22,299.02	32,773.20	45,184.20	59,684.93	76,428.31
Total Cost (S)	164,025.99	111,615.22	112,022.47	114,476.96	119,314.03	126,247.33

APPENDIX D

PUBLISHED WORK (ANALYTICAL AND NUMERICAL INVESTIGATION OF EFFECTIVENESS OF GROUND IMPROVEMENT AROUND PILED-RAFT FOUNDATION FOR TALL WIND TURBINES IN WEAK SOILS)

(Ravichandran, N., Phuyal, S., and Shrestha, S. "Analytical and Numerical Investigation of Effectiveness of Ground Improvement Around Piled-Raft Foundation for Tall Wind Turbines in Weak Soils" *Geo-Congress 2020 GSP 317*, Minneapolis, MN)

The work presented herein Appendix D is similar to the study discussed in earlier chapters. The essential difference is the study presented herein Appendix D deals with three levels of vertical and horizontal improvement, but the study in previous chapters dealt with five levels of ground improvement. The soil profile investigated in this Appendix D also has a layer of sand under the clay layer, while the study discussed earlier comprised of clay layer only. Thus, it was justified for the study presented in Appendix D not to be included in the main body of the thesis.

Analytical and Numerical Investigation of Effectiveness of Ground Modification Around Piled-Raft Foundation for Tall Wind Turbine in Weak Soil

Nadarajah Ravichandran[1], Saphal Phuyal[2], and Shweta Shrestha[3]

[1]Associate Professor, Glenn Department of Civil Engineering, Clemson University, 202 Lowry Hall, Clemson, SC, 29634; email: nravic@clemson.edu
[2]Graduate Student, Glenn Department of Civil Engineering, Clemson University, 139 Lowry Hall, Clemson, SC, 29634; email: sphuyal@clemson.edu
[3]Graduate Student, Glenn Department of Civil Engineering, Clemson University, 123 Lowry Hall, Clemson, SC, 29634; email: shwetas@clemson.edu

ABSTRACT

A site with favorable wind condition may not have suitable subsurface condition for building wind turbines. In such situations, it may be economical to improve the subsurface properties to gain net economic advantage. In this study, the effectiveness of ground improvement to support 80 m tall wind turbine on a piled-raft foundation using analytical and 3D finite element methods. First, analytical designs were conducted to determine the length of the piles for assumed raft and pile size and number of piles to meet the safety and serviceability requirements. Three different depths of improvements were considered in the design. Then, 3D FE models of the piled-raft foundations and the supporting soils were created and analyzed using ABAQUS. In the FE modeling, the lateral distance was varied in addition to the depth of improvement. Both methods show that significant economic advantage can be achieved by improving the ground.

INTRODUCTION

Generation of energy from the wind provides a sustainable and clean alternative to fossil fuels and nuclear energy. There are many wind farms in the USA and around the world and the number is keep growing with new design and construction procedures for tall wind turbines. The site selection for constructing wind farm may depend on many factors including wind speed, real-estate value, availability of construction materials, and suitability of subsurface condition to support large loads. In some situations, the wind condition may be favorable, but the subsurface condition may not be suitable for transferring large vertical and lateral loads. The construction of wind turbine in such areas may result in a very large foundation that may be uneconomical. In such a situation, the subsurface soil may be modified to improve the strength and deformation properties and to gain a net economic advantage. The ground modification may not only improve the axial capacity but also the lateral capacity that is important for the foundation of a tall wind turbine.

Taghavi et al. (2015) investigated the effectiveness of ground improvement on lateral capacity of pile groups using centrifuge model tests. In their tests, the ground was modified using Cement Deep Soil Mixing (CDSM) method. Yamashita et al. (2012) conducted field tests to investigate the seismic behavior of a building supported on a piled-raft foundation with ground improvement. In their study, ground was modified in a grid-form deep using cement mixing walls. Shrestha and Ravichandran (2016) have shown through analytical, finite element modeling, multi-objective optimization that a piled-raft

foundation is economical to support tall wind turbines in clayey soil compared to a raft foundation or pile groups. Among the many different ground improvement techniques used in practice, the CDSM technique was considered in this study to investigate the effectiveness of the ground improvement for supporting tall wind turbine. It should be noted that other ground improvement techniques may be economical for a given site depending on the availability of the materials, contractors and the expected improvement in the properties and performance. However, the analytical and numerical procedures presented in this paper can be used for other ground improvement techniques.

The major objectives of the study are **(i)** to design and analyze the piled-raft foundation to support an 80 m tall wind turbine in soft clay with and without ground improvement and investigate the effectiveness of ground improvement and **(ii)** to develop a 3D FE models of a pile-raft-soil system in a coupled manner (considering soil-pile-raft interaction) and to investigate the effective depth and width of ground improvement on the performance of the foundation. Initially, a piled-raft foundation was designed in soft clay and improved clay with three levels of vertical improvement using a simplified method developed by Hemsley (2000). Then, 3D FE models were created for each case using ABAQUS and analyzed. It should be noted that the analytical design procedure available in the literature can incorporate only the variation in depth of ground improvement. But, for practical application, the width (radius in the case of wind turbine) must also be considered. In such situation, 3D FE analysis can be performed to gain a better understanding of the performance of the foundation and the effectiveness of the ground

improvement. The sample problem considered in this study and the procedure followed are detailed in the following sections.

WIND TURBINE AND SUBSURFACE CONDITION

An 80 m tall wind turbine tower made of prestressed concrete with a base diameter of 6.75 m and top diameter of 3 m was considered in this study. The wind turbine tower specifications (diameter, height, and material) were obtained from Vindforsk III project report by Lyrner et al. (2010). The wind turbine had rotor diameter of 80 m and a rated power of 3 MW. The lateral load on the foundation was calculated using a mean survival wind speed of 80 mph at the site. A piled-raft foundation (circular raft supported by several auger cast piles) was considered as foundation to support this wind turbine.

Soil profile and properties

The soil profile used in the study was obtained from Taghavi et al. (2015) in results of a series of centrifuge tests conducted on pile groups with and without ground improvement. The soil profile consisted of 9.6 m clayey layer on top of dense sand as shown in Figure 1. The properties of the clay and sand are listed in the Table 1. The properties of the improved clay were obtained from Quiroga et al. (2017). The value of Young's modulus and undrained shear strength for CDSM improved clay obtained from the plot were 120,000 kPa and 360 kPa respectively. The stress-strain relationship obtained from the tests conducted for improved soil sample by Quiroga et al. (2017) was used in this study and is shown in Figure 2(b).

In the analytical design, the depth of ground improvement was varied and in the FE modeling both the depth and the width of ground improvement was varied to investigate effect of depth and width of improvement on the performance of piled-raft foundation. Depths of 2.4, 2.8 and 3.2 meters which are equivalent to 0.3, 0.35 and 0.4 times the diameter of the raft, respectively. Figure 1 shows the different levels of ground improvement for analytical design and finite element simulation. The analytical design was performed by considering improvement in the vertical direction only and for each improvement in the vertical direction (V), horizontal improvement (H) extends to infinity. Improvement in the vertical direction, V_1, V_2, and V_3 are shown in Figure 2. The FE analysis was performed by considering three vertical improvements (V_1, V_2, and V_3) and three lateral improvements (H_1, H_2, and H_3) in addition to the infinite extension used for analytical design.

Table 2. Properties of clay (Quiroga et al., 2017) and Nevada sand (Taghavi et al., 2015)

Clay		Sand	
Properties	Values	Properties	Values
Saturated unit weight (kN/m^3)	19.20	Saturated unit weight (kN/m^3)	22.4
Liquid limit (%)	32	Friction angle (°)	38
Plastic limit (%)	17	Specific gravity	2.67
Specific gravity	2.69	Void ratio	0.57
Average water content (%)	0.22	Relative density (%)	84
Young's modulus (kPa)	30,500	Young's modulus (kPa)	45,575
Undrained shear strength (kPa)	41	Poisson's ratio	0.3

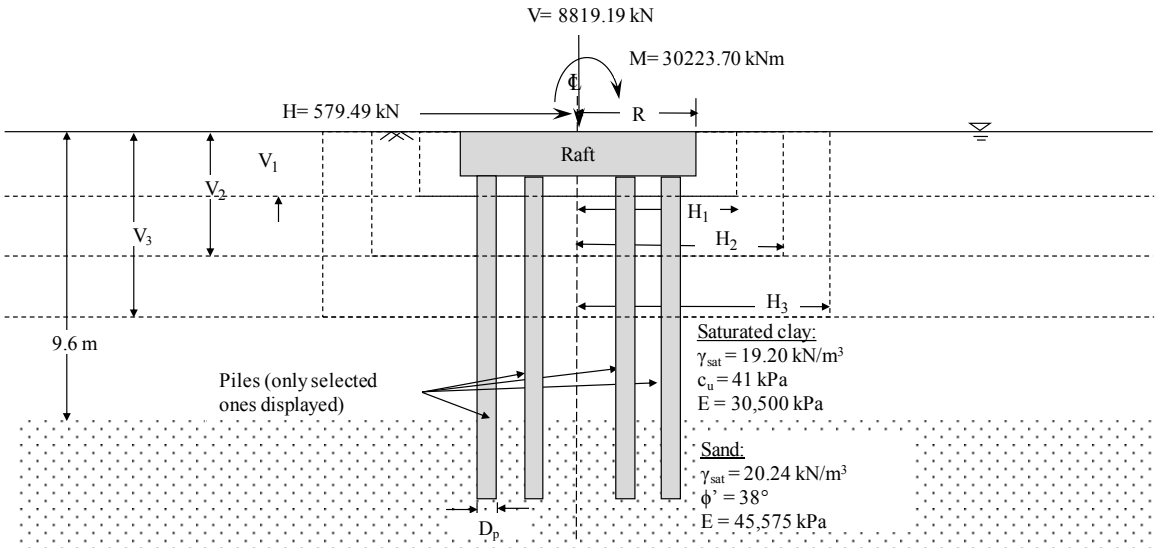

Figure 1. Soil profile with different levels of ground improvement (not to scale)

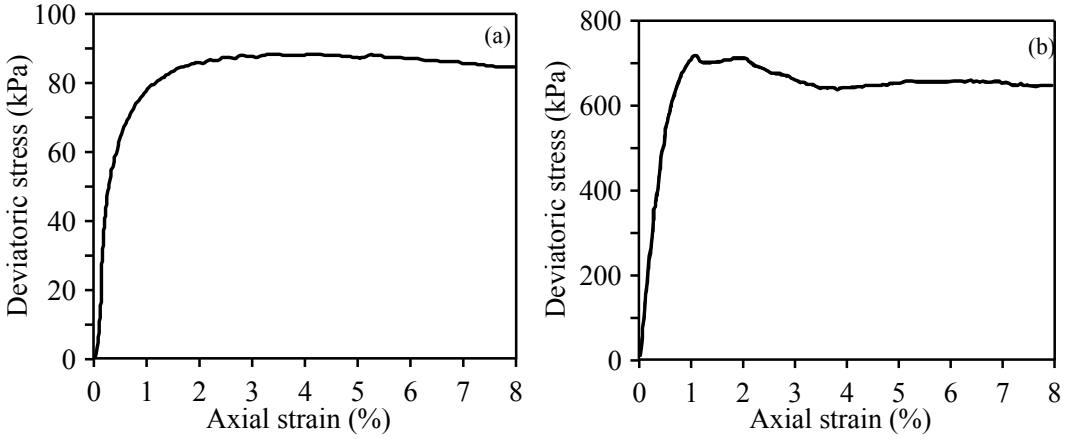

Figure 2. Stress-strain diagram from consolidated undrained compression test (recreated from Quiroga et al., 2017) (a) soft clay and (b) CDSM improved clay

Design loads:

The foundation is subjected to an axial load due to the self-weight of the tower and the turbine components. The weight of the individual components like nacelle, rotor, and the weight of the tower was obtained from Vindforsk III project report by Lyrner et al. (2010). The final dead load was calculated to be 8819.19 kN. The wind on the above ground components induces lateral load and bending moment at the base of the tower. The wind load was calculated following the procedure described in ASCE/SEI 7-10 (2010). The total horizontal load and bending moment at the base of the tower were calculated to be 579.49 kN and 30223.70 kNm, respectively.

ANALYTICAL DESIGN AND ANALYSIS OF PILED-RAFT FOUNDATION

The dimensions of the raft and number and size of the piles were determined by performing safety and serviceability checks. The stability checks included the checks for vertical load, lateral load, and bending moment capacities. The serviceability checks included total and differential settlements and the rotation of the raft. In this study, the raft diameter was assumed based on the size of the bottom of the tower and the number and length of piles were adjusted until both the safety and serviceability requirements are met for all the in situ and improved ground conditions. A factor of safety of 2.5 was assumed to be adequate for all the safety checks. Allowable rotation and differential settlement of the foundation were calculated to be 0.172° and 24 mm respectively considering a vertical misalignment within 3 mm/m of the tower height (Grunberg and Gohlmann, 2013).

Safety Check

The vertical capacity of the raft was determined as the product of the raft area and bearing capacity of the soil. The vertical load capacity of the piles was obtained by using O'Neil and Reese (1999) method for the clay layer and the β-method for the skin friction and Neely's (1991) method for toe resistance calculation for the sand layer. The calculated vertical load capacity was compared with the design vertical load to obtain the factor of safety. This exercise resulted in a factor of safety of 8.16 for the assumed foundation size and number of piles which satisfies the factor of safety requirement of 2.5. The moment capacity of the individual components and the block were calculated using the method presented by Hemsley (2000). It should be noted that the moment load capacity controlled the design and therefore the size and the length of the pile were adjusted to obtain a factor of safety of 2.5 which is the minimum required for the design. The method presented by Brom's (1964) was used to calculate the horizontal load capacity. The horizontal capacity for single pile was calculated to be 342.51 kN and multiplied by the number of piles to get the horizontal capacity of the piled-raft. The horizontal load capacity of the piled-raft was compared with the design horizontal load and the factor of safety was found to be 15.40.

Serviceability check

Vertical settlement: Randolph (1994) suggested a simple method of load sharing between the raft and the pile in the piled-raft foundation. Equation (1) was used to calculate the stiffness of the piled-raft foundation and the proportion of the load carried by the raft.

$$K_{pr} = \frac{K_p + \left(1 - 2\alpha_{rp}\right)K_r}{1 - \alpha_{rp}^2\left(K_r / K_p\right)}\ ;\ \frac{P_r}{P_r + P_p} = \frac{(1 - \alpha_{rp})K_r}{K_p + (1 - 2\alpha_{rp})K_r} = X \tag{22}$$

where K_r is the stiffness of raft, K_p is the stiffness of the pile group, and α_{rp} is the piled-raft interaction factor. The value of K_r was calculated using the equation suggested by Randolph (1994). α_{rp} depends on the slenderness ratio, pile spacing and the value ranges from 0.65 to 0.8. When the foundation is subjected to the vertical load, the stiffness of the piled-raft will remain operative until the load-bearing capacity of pile is fully mobilized at load P_A. It was calculated that the vertical settlement of the piled-raft foundation for a design vertical load of 8.81 MN was 9.77 mm. The piles carried 59.97% and the raft carried 40.03% of the vertical load.

Differential settlement and rotation: The differential settlement of the piled-raft foundation was calculated following the procedure outlined by Shrestha et al. (2017). It was calculated that the raft carried 17.90% and piles carried 82.1% of the total bending moment to yield equal differential settlement. The differential settlement of the piled-raft was calculated to be 12.75 mm which gives a rotation θ of 0.091°. For 80 m high tower, this θ of 0.091° induces a horizontal displacement of 127.55 mm at the top of the tower which is within the acceptable limit.

The final design comprises of a 1 m thick raft having a diameter of 8 m with top of the raft flushed with the ground surface. For the in-situ soil (without improvement), a total of twenty-four 29.3 m long auger cast piles of the diameter of 457 mm were used. The piles

are arranged in two concentric circles with the radii of 3.37 m and 2.23 m from the center of the circle. The arrangement of the pile can be seen in Figure 3.

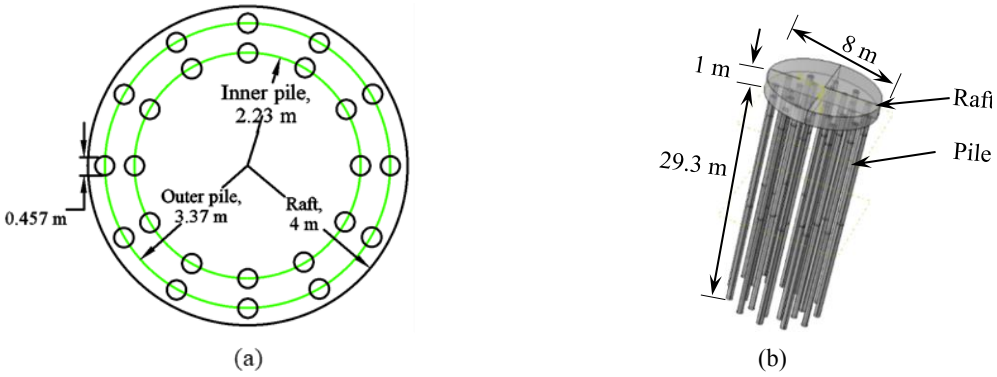

Figure 3. Arrangement of piles in piled-raft foundation (a) plan view and (b) 3D view

Result and Discussion

Figure 4 shows the variation of required pile length to meet the design requirements and the computed horizontal deflection, differential settlement, and rotation with depth of ground improvement. From the figure, with the increase in the depth of ground improvement, the factor of safety for axial capacity increased. Further, it was observed that the differential settlement and rotation of piled-raft foundation decreased with increase in ground improvement depth. On the other hand, the horizontal deflection decreased for the first ground improvement (shallow depth) and increased when the depth of improvement increased. This is only because the length of the pile decreased with the increase vertical improvement depth.

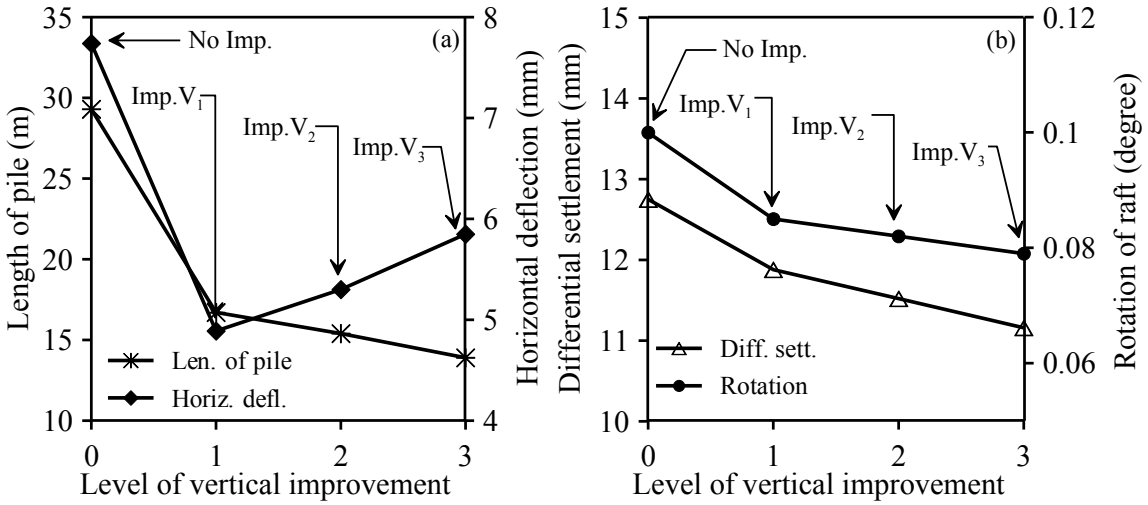

Figure 4. Analytical design results (a) length of pile and horizontal deflection and (b) differential settlement and rotation of piled-raft for different level of ground improvement

Figure 4(a) reveals the decrease in the length of piles with ground improvement and shows the reduction from 29.3 m in the unimproved ground to 13.9 m after improvement to depth V_3. The horizontal deflection decreases from unimproved case (7.74 mm) to the first level of improvement (4.88 mm) but increases slightly for further levels of improvement. This can be because of the reduction in length of pile being greater than the corresponding increase in depth of improvement. Figure 4(b) shows the decrease in differential settlement and rotation of piled-raft with ground improvement in the vertical direction. The differential settlement decreased from 12.74 mm in the unimproved ground to 11.16 mm for vertical improvement of depth V_3. Even with the reduction of the pile length from 29.3 m to 13.9 m, the differential settlement still decreased due to the effect of ground improvement.

The horizontal variation in ground improvement along with vertical variation must be incorporated in the design to replicate real-world scenario. Analysis of models with both

horizontal and vertical variations is necessary for developing the most effective and economical ground improvement configuration. The analytical design results are only based on vertical variation and hence, to get further insight into the behavior of piled-raft foundation with both horizontal and vertical variations, 3D FE models need to be created and analyzed.

FINITE ELEMENT ANALYSIS OF PILED-RAFT FOUNDATION

Finite Element Model:

3D finite element models of the piled-raft and subsurface soil with different levels of ground improvement were created using ABAQUS which can model the soil-pile-raft interaction more accurately and has nonlinear stress-strain models suitable for representing soil behavior under large deformation. The diameter and thickness of the raft were 8 m and 1 m, respectively. The model for each analysis was created by first developing a separate 3D model of the individual components namely, raft, piles, and soil. The size of the simulation domain was determined to be 40 m high and 30 m in diameter after performing the size sensitivity analysis. Then, a soil-piled-raft assembly was created. While assembling each component, cut instance technique was used to create spaces for piles and raft in the soil body. This created a new soil component model with spaces for the pile and raft. The base of the model was fixed in all directions whereas the sides were fixed in x and y directions and free to move along the z-direction. Figure 5(a) shows a 3D FE model for the unimproved case used in the analysis.

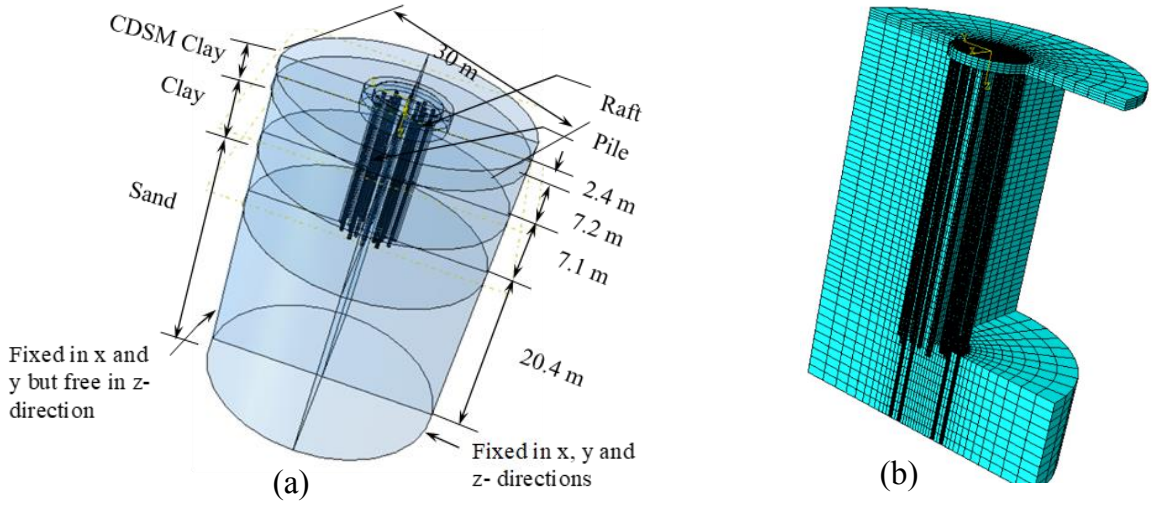

Figure 5. (a) 3D simulation domain of piled-raft foundation and (b) mesh assembly

The contact between pile skin and soil was defined by assigning the interaction properties. The interaction between the soil and pile surfaces was defined in terms of load transfer mechanism in the normal and tangential direction. The normal contact between the pile skin and soil was modeled by "hard" contact whereas the tangential contact between the pile and soil was defined as the interface friction angle (δ). Value of δ was 0.35 for soft clay, 0.48 for sand and 0.45 for improved clay. The contacts between the pile top and raft bottom, pile toe and soil, and raft and soil were defined by a surface to surface based tie constraint which uses the master-slave concept in ABAQUS. An MPC beam constraint was applied between the top nodes of the raft and the center node of the raft which ties the center node with all the nodes on the surface and transfers the load from the raft to the piles. Partition technique was used to divide the component into smaller parts to generate a quality mesh. Meshing was done with areas exposed to higher stress concentration

receiving a finer mesh and areas with lower stress concentration receiving coarser mesh using the bias feature available in ABAQUS. Each component was discretized using 8-noded hexahedral elements. The partition of the model and the FE mesh generated with the internal mesh view is shown in Figure 5(b). The total number of nodes were 371,006 and the total number of elements were 333,889 in the generated mesh.

Constitutive Model and Model Parameters

The stress-strain behavior of the improved and unimproved ground was represented by an elastoplastic Drucker Prager (DP) model with hardening DP-H feature. The key parameters of DP-H model parameters are shown in Table 2. The other key input, yield stress versus plastic strain curve is graphically represented in Figure 6. The yield stress was determined from the stress-strain curve as the stress at which the soil started demonstrating non-linear behavior. The elastic strain at different stresses was calculated by dividing stress by the initial modulus of elasticity and the plastic strain was obtained by subtracting the elastic strain from the total axial strain. The yield stress versus plastic strain curve is shown in Figure 6.

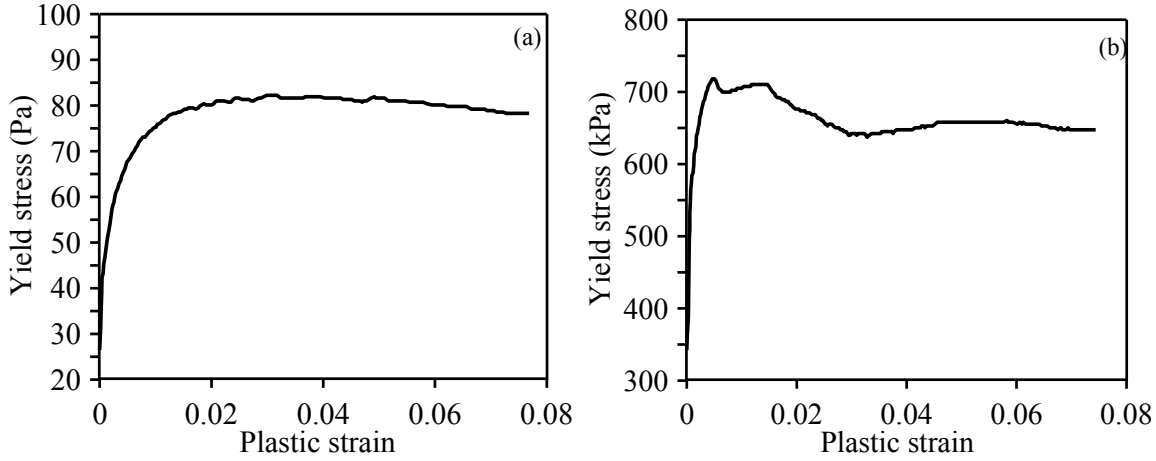

Figure 6. DP-H input yield stress vs. plastic strain curve (a) soft clay and (b) for CDSM improved clay (calculated from stress strain curve shown in Figure 2)

Table 3. Elastoplastic soil model parameters

Shear Criterion	Flow Potential eccentricity	Friction angle (°)	Flow stress ratio	Dilation angle (°)
Linear	0.1	0	1	0

Results and Discussion

The computed horizontal deflection and differential settlement for different levels of ground improvement obtained from FE analysis are presented in Figure 7. Figure 7(a) shows a reduction in horizontal deflection with ground improvement. The horizontal deflection decreases from 5.60 mm in the unimproved ground to a minimum value of 0.87 mm. The decrease in lateral deflection is large from unimproved case to the first level of improvement and the decrease is small with further improvement. Figure 7(b) shows the differential settlement decreases from 37.01 mm to a minimum value of 12.5 mm with ground improvement. The differential settlement also reduces with the first level of improvement but the change for the consecutive levels is small. The differential settlement

in unimproved soil is greater than the allowable differential settlement of 24 mm but with the improvement the differential settlement decreases to the allowable limit.

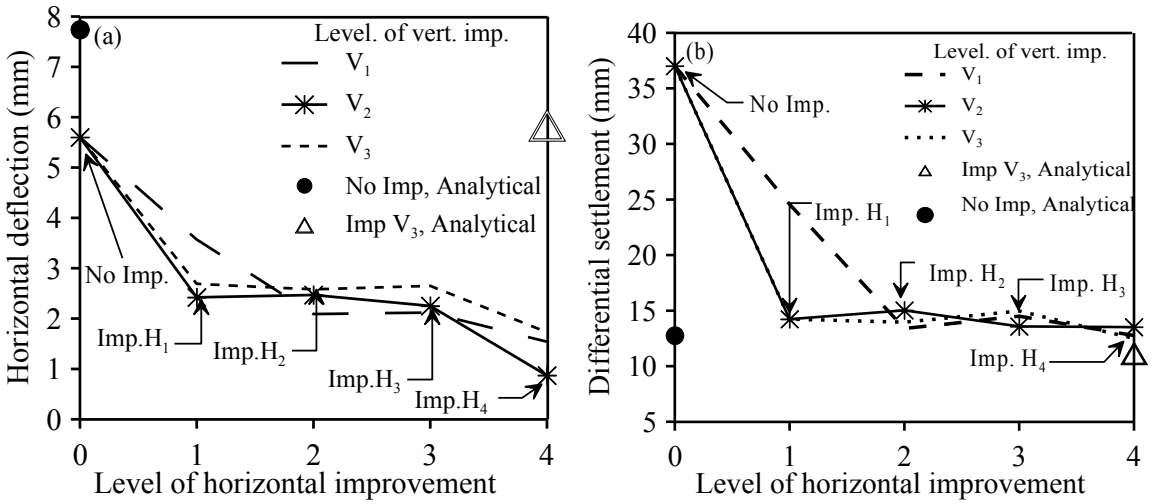

Figure 7. Comparison of Finite element results and analytical design results (a) horizontal deflection and (b) differential settlement for various levels of ground improvement

The results from FE model with no improvement and with the horizontal improvement extending to the boundary of the model (Imp H_4) was compared with the analytical design results. The analytical design resulted a horizontal deflection of 7.74 mm and the FE model resulted in a deflection of 5.6 mm. Direct comparison between analytical design and improvement level 4 of FE analysis for all three levels of vertical improvement resulted in lower deflection for FE analysis.

CONCLUSION

The analytical designs and FE analyses of the piled-raft foundation with and without ground improvement were carried and the results were compared to determine the effectiveness of ground improvement on the performance of the piled-raft foundation.

From the analytical design results, it was found that the length of the pile can be significantly reduced with ground improvement. The horizontal deflection decreased with improvement even after a large reduction in pile length which supports that the ground improvement enhances the lateral resistance of the soil. The FE analyses conducted on the same size of the piled-raft foundation with different levels of ground improvements showed that the horizontal deflection, differential settlement, and rotation decreased significantly from unimproved case to the first level of improvement. However, the reduction was negligible for further improvement. Therefore, it can be concluded that the improvement in the performance of the piled-raft foundation plateaus after a certain level of improvement. Such results can be used by the engineer to decide the optimum or the desired level of ground improvement based on the requirements.

REFERENCES

ASCE. (2010*). Minimum Design Loads for Buildings and Other Structures.* ASCE/SEI Standard 7-10.

Broms, B. B., "Lateral Resistance of Piles in Cohesive Soils," *Journal of the Soil Mechanics and Foundation Division, American Society of Civil Engineers*, Vol 90, 1964, pp 27-63.

Hemsley, J. A. (2000). *Design applications of raft foundations*. Thomas Telford Ltd., Heron Quay, London, ISBN 0727727656.

Lyrner, T., Hassanzadeh, M., Stalin, T., and Johansson, J. (2010). *Tall towers for large wind turbines Tall towers for large wind turbines.* Vindforsk project V-342, 2010.

Quiroga, A. J., Thompson, Z. M., Muraleetharan, K. K., Miller, G. A., and Cerato, A. B. (2017). "Stress–strain behavior of cement-improved clays: testing and modeling." *Acta Geotechnica*, Springer Berlin Heidelberg, 12(5), 1003–1020

Randolph, M. F. (1994). "Design methods for pile groups and piled-rafts." *13th International Conference on Soil Mechanics and Foundation Engineering*, New Delhi, India, 61-82.

Shrestha, S., and Ravichandran, N. (2016). "Design and Analysis of Foundation for Onshore Tall Wind Turbines." *Geo-Chicago 2016 GSP 270*, Chicago, IL, 217-226.

Shrestha, S., Ravichandran, N., and Rahbari, P. (2017). "Geotechnical Design and Design Optimization of a Pile-Raft Foundation for Tall Onshore Wind Turbines in Multilayered Clay." *International Journal of Geomechanics*, 18(2), 04017143.

Taghavi, A. (2015). *Seismic and Quasi-Static Lateral Load Behavior of Pile Groups in Improved Soft Clay: Centrifuge and Numerical Modeling*. [Doctoral Dissertation, University of Oklahoma], Norman, Oklahoma.

Taghavi, A., Muraleetharan, K. K., Miller, G. A., and Cerato, A. B. (2015). "Centrifuge Modeling of Laterally Loaded Pile Groups in Improved Soft Clay." *Journal of Geotechnical and Geoenvironmental Engineering*, 142(4), 04015099.

Yamashita, K., Hamada, J., Onimaru, S., and Higashino, M. (2012). "Seismic behavior of piled-raft with ground improvement supporting a base-isolated building on soft ground in Tokyo." *Soils and Foundations*, Elsevier, 52(5), 1000–1015.

REFERENCES

ASCE. (2010). *Minimum Design Loads for Buildings and Other Structures*. ASCE/SEI Standard 7-10. American Society of Civil Engineers, pp 187-297.

BP (2019). *BP Energy Outlook*, 2019 edition. https://www.bp.com/energyoutlook

Bilal, M., Talib, A. (2016). "A study on advances in ground techniques." *National Conference on Advances in Geotechnical Engineering*. Aligarh, India. doi:10.13140/RG.2.1.4865.4965

Brom's, B. B. (1964a). "Lateral Resistance of Piles in Cohesive Soils," *Journal of the Soil Mechanics and Foundation Division, American Society of Civil Engineers*, 90, 27-63.

Clancy, P., and Randolph, M. F. (1993). "An approximate analysis procedure for analysis of piled raft foundations." *Int. J. Num. & Anal. Methods in Geomechanics.* https://doi.org/10.1002/nag.1610171203.

Coduto, D. P. (2001). *Foundation Design: Principles and Practices*. (2nd Ed.). Prentice-Hall, NJ, USA, ISBN: 0-13-589706-8.

CNMB International. (2020). *Wind turbine foundations: 5 foundation types explained for onshore wind turbine.* http://www.steelwindtower.com/wind-turbine-foundation-5-foundation-types-explained-for-onshore-wind-turbine/

DOE/EIA (2018). *International Energy Outlook 2018*. Washington, DC, USA: US Energy Information Administration, US Department of Energy; 2018.

Eurostat (2018). *Renewable energy statistics, 2018*. https://ec.europa.eu/eurostat/statistics-explained/index.php/Renewable_ energy_ statistics

Falling costs and tech innovations will drive offshore windpower boom. (2017, January 27). CPH World Media. Retrieved March 15, 2020, from https://cph.world/2017/01/27/falling-costs-tech-innovations-will-drive-offshore-wind-power-boom/

Fellenius, B. H. (1999). *Basics of foundation design* (2nd ed.). BiTech Publishers, Richmond, British Columbia.

Grunbeg, J., and Gohlmann, J. (2013). *Concrete Structures for Wind Turbines*. Wilhelm Ernst & Sohn, Berlin, Germany, ISBN 978-3-433-03041-7.

Grzyb-Faddoul, A. M. (2014). *Numerical analysis of the reinforcement of existing foundation by the soil mixing technique.* [Doctoral Dissertaton, L'Institut National des Sciences Appliquées de Lyon], Lyon, France.

History of wind power. (2020). Wikipedia. Retrieved March 10, 2020, from https://en.wikipedia.org/w/index.php?title=History_of_wind_power

Katzenbach, R., and Reul, O. (1997b). "Design and Performance of Piled Rafts." *Proceedings of XIV International Conference of Soil Mechanics and Foundation Engineering*, Hamburg. 4, 2253-2256.

Lantz, E., Roberts, O., Nunemaker, J., Demeo, E., Dykes, K., and Scott, G. (2019). *Increasing wind turbine tower heights: Opportunities and challenges*. National Renewable Energy Laboratory, Golden, CO, May 2019. NREL/TP-5000-73629.

Lyrner, T., Hassanzadeh, M., Stalin, T., and Johansson, J. (2010). *Tall towers for large wind turbines: Report from Vindforsk project V-342 Höga*. July 2010.

Maharaj, D. K. (2003), "Three Dimensional Nonlinear Finite Element Analysis to study the effect of Raft and Pile Stiffness on the Load-Settlement Behaviour of Piled RaftFoundations." *Electronic Journal of Geotechnical Engineering. Geotechnical Engineering.* 3, 107-113

Mahara, D. K., and Gandhi, S. R. (2004). "Non-linear finite element analysis of piled-raft foundations." *Proceedings of the Institutions of Civil Engineering.*

Mass Soil Stabilization. (2020). Ground Developments Ltd. Retrieved on March 15, 2020, from https://grounddevelopments.co.uk/ground-improvement/deep-soil-mixing/mass/

Masuka, G. P. (2013). *Soil stabilization methods and materials in engineering practice: State of the art review.* Lueala University of Technology, Luela, Sewden

Moulas, D., Shafiee, M., and Mehmanparast, A. (2017). "*Damage analysis of ship collision with offshore wind turbine foundations.* " Ocean Engineering, Elsevier, 143, 149-162.

Mohammad. (2019, June 30). *Pile cap.* Civil Engineering diary. http://www.mocivilengineering.com/2019/06/pile-cap.html

Mokhtari, M., and Kalantari, B. (2012). " Soft soil stabilization using stone columns- A Review." *Electronic Journal of Geotechnical Engineering.*17 (2012).

Muhammad, N. (2014). *The effects of temperature and kaolin mixture on plasticity characteristics and shear strength behaviour of natural soil.* [Masters Thesis, Universiti Malasiya], Pahang, Malaysia.

Naval Facilities Engineering Command. (1986). *DM-7.02 Foundation and Earth Structures.* Alexandria, VA.

Norwegian Geotechnical Institute. (2017, December 11). *Rock-solid anchoring for design pylons at Lysefjorden.* http://www.mynewsdesk.com/ngi/pressreleases/rock-solid-anchoring-for-design-pylons-at-lysefjorden-2325779.

O'Neill, M. W., and Reese, L. C. (1999). *Drilled shafts: Construction procedures and design methods*. Publication FHwA-IF-99-025, FHwA, Washington, DC.

Poulous, H. G., and Davis, E. H. (1980). *Pile foundation analysis and design*. John Wiley and Sons, New York. ISBN: 0471020842.

Poulous, H. G. (2001). "Piled raft foundation design and applictions" *Géotechnique.* 51(2), 95-113.

Quiroga, A. J., Thompson, Z. M., Muraleetharan, K. K., Miller, G. A., and Cerato, A. B. (2017). "Stress-strain behavior of cement-improved clays: testing and modeling." *Acta Geotechnica*, Springer Berlin Heidelberg, 12(5), 1003–1020.

Rahman, M. R. (2016). *Horizontal Infiltration of Grouts and its effects on shear strength of sandy soil*. [Masters Thesis, Bangladesh University of Engineering and Technology]

Randolph, M. F. (1994). "Design methods for pile groups and piled-rafts." *13th International Conference on Soil Mechanics and Foundation Engineering*, New Delhi, India, 61-82.

Ravichandran, N., and Shrestha, S. (2018). "Performance and cost-based robust design optimization procedure for typical foundations for wind turbine." *International Journal of Geotechnical Engineering*. 1-14.

Reul, O. and Randolph, M. F (2003), "Piled rafts in overconsolidated clay: comparison of in-situ measurements and numerical analysis" *Géotechnique*, 53(3), 301-315.

Righter, R. W. (1996). *Wind energy in America: A History*, University of Oklahoma Press, pp 44, ISBN: 0806128127.

Rollins, K. M., Adsero, M. E., Herbst, M. A., and Lemme, N. (2010). "Ground Improvement for Increasing Lateral Pile Group Resistance." *International Conference on Recent Advances in Geotechnical Earthquake Engineering and Soil Dynamics,* Missouri; https://scholarsmine.mst.edu/icrageesd/05icrageesd/session12/3.

Roshan, A., and Shoodhpasha, I. (2013). "Numerical analysis of piled raft foundation in soft clay." *Electronic Journal of Geotechnical Engineering*. 19, 4541-4554

Soil Improvement: Methods to Enhance Soft Ground Conditions. (2017, January 10). Pilebuck. Retrieved on March 15, 2020, from https://www.pilebuck.com/foundation/soil-improvement-methods-enhance-soft-ground-conditions/

Sayehvand, S., and Kalantari, B. (2012). " Use of Grouting Method to Improve Soil Stability Against Liquefaction- A Review." *Electronic Journal of Geotechnical Engineering.* 17(2012), 1559-1566.

Sinha, A. and Hanna, A. M (2016). "3D Numerical Model for Piled-Raft Foundation". *International Journal of Geomechanics*. 17(2), 04016055-1-9.

Shrestha, S., and Ravichandran, N. (2016). "Design and Analysis of Foundation for Onshore Tall Wind Turbines." *Geo-Chicago 2016 GSP 270*, Chicago, IL, 217-226.

Shrestha, S., Ravichandran, N., and Rahbari, P. (2017). "Geotechnical Design and Design Optimization of a Pile-Raft Foundation for Tall Onshore Wind Turbines in Multilayered Clay." *International Journal of Geomechanics*, 18(2), 04017143.

Taghavi, A., Muraleetharan, K. K., Miller, G. A., and Cerato, A. B. (2015). "Centrifuge Modeling of Laterally Loaded Pile Groups in Improved Soft Clay." *Journal of Geotechnical and Geoenvironmental Engineering*, 142(4), 04015099.

UN Environment Programme (2019). *Emissions Gap Report 2019*. UNEP, Nairobi, ISBN 978-92-807-3766-0.

Varpe, P. (2018, February 20). *Geosynthetics Industry outlook, regional growth & industry share by 2024*. Market News Wire. https://marketnewswire.wordpress.com /2018/02/20/geosynthetics-industry-outlook-regional-growth-industry-share-by-2024/

Vibro-Compaction or Vibro-Flotation for Ground Improvement. (2016, November 3). Civildigital. Retrieved on March 10, 2020, from https://civildigital.com/vibro-compaction-vibro-flotation-ground-improvement-principle-images/

Various vertical drain methods. (2020). Wackachiku construction. Retrieved on March 10, 2020 from https://www.wakachiku.co.jp/en /technologies/various _vertical_drain _methods

Waire, P. R., and Charest, A. (2013). *RS Means building construction cost data* (71st Ed.). Construction Publishers and Consultants, Norwalk, MA, ISBN 978-1936335565.

Weaver, J. F. (2017, November 2). *World's tallest wind turbine built in Germany*. Electrek. https://electrek.co/2017/11/02/worlds-tallest-wind-turbine-built-in-germany/